Using Layered Division Multiplexing for Mixed Unicast-Broadcast Service Delivery in 5G-MBMS

by

Yu Xue

A thesis submitted in conformity with the requirements
for the degree of Master of Applied Science
Graduate Department of The Edward S. Rogers Sr. Department of
Electrical & Computer Engineering
University of Toronto

Abstract

Using Layered Division Multiplexing for Mixed Unicast-Broadcast Service Delivery in 5G-MBMS

Yu Xue

Master of Applied Science

Graduate Department of The Edward S. Rogers Sr. Department of Electrical & Computer Engineering

University of Toronto

2019

Point-to-multipoint (PTM) transmission is a key enabler for emerging 5G New Radio (NR) applications. For more efficient use of spectrum, 3GPP is working on a 5G multimedia broadcast multicast service (5G-MBMS) subsystem to provide effective mixed services on a unified platform. This thesis shows in many cases, capacity of the current multi-cell unicast service is limited by co-channel interference. Using a reduced transmission power will not impact the system performance. Meanwhile, for broadcast services using single frequency network (SFN), there is no co-channel interference. Slightly reducing the broadcast service emission power will not impact the system quality of service (QoS). This provides a good opportunity to apply layered division multiplexing (LDM) to combine broadcast and unicast services in one RF channel by power sharing. This work demonstrates that, in a 5G-MBMS with two-layer P-NOM/LDM, broadcast and unicast services can be efficiently and effectively delivered using the same spectrum resource.

I dedicate this to my parents,

whose unconditional support, both tangible and intangible,

laid an indispensable foundation for this work.

Acknowledgements

First and foremost, I would like to convey my gratitude to Professor E. S. Sousa, as my supervisor, for providing me a permissive environment which allowed me to pursue the path of my interest. His suggestions and support kept me moving forward. This work would have been impossible without him.

I would like to thank the research scientists at CRC, Dr. Li, Dr. Zhang and Dr. Wu for letting me be a part of their team. They efforts in equipping me with the necessary technical background and continuous technical support during the project ensured this successful outcome. I also appreciate their kindness deeply for inviting me to CRC over the summer of 2018, as well as all their help during my first ever conference.

I would like to thank Ahmed Alsohaily for arranging this opportunity for me. He was always there to listen to my concerns and offer advice. He is truly a great mentor.

Thanks to all my colleagues in the laboratory, for their help and friendships.

And lastly, I extend my warmest thanks to my parents. They've made so much sacrifices in their life for my development. Their unconditional support was always there and kept me going even during the darkest of times.

Contents

List of Tables

List of Figures

Chapter 1

Introduction

It has been forecasted that between the years 2017 and 2022, global mobile data traffic will grow by 7 folds, reaching 77.5 exabytes per month. Nearly 80% will be generated by high definition mobile videos, while the remaining 20% will be generated by other bandwidth thirsty applications such as augmented reality, extended reality, virtual reality, and Internet of Things (IoT)[1]. One way to address this demand is to incorporate multimedia broadcast multicast service (MBMS) transmission modes into the unicast-based mobile broadband systems to more efficiently deliver desired multimedia content to large groups of interested user equipment (UE).

1.1 Motivation

Evolved MBMS (eMBMS) was added to the Long-Term Evolution (LTE) system specification as a supplementary system in the 3rd Generation Partnership Project (3GPP) Release 9 (Rel-9) and then further enhanced in Rel-11 to achieve higher spectral efficiency when delivering multicast/broadcast video traffic [2]. eMBMS utilizes Time-Division-Multiplexing (TDM), where up to 60% of the available time resources are allocated for multicasting/broadcasting services; while the remaining time resources are allocated for unicast services to provide high-throughput broadcast services and efficient co-existence

with unicast services. 3GPP Rel-14 [3] provides significant eMBMS system and architecture improvements to better support broadcast service delivery. The improved system, called further evolved MBMS (feMBMS), introduces many new enhancements for delivering broadcast services. The system now supports larger inter-site distance (ISD) of up to 15 km for single frequency networks (SFNs) and the ability to operate in broadcast mode by allocating 100% of the time resource to the broadcast service. New features including shared broadcast among operators and receive-only mode for free-to-air (FTA) reception are also included [4]. In the 5G New Radio (NR) systems, broadcast and multicast services will find their ways to use cases spanning virtual and augmented reality (VR/AR) delivery, infotainment and safety applications in connected vehicles, software updates for IoT applications as well as public warning and alert systems [5].

3GPP technical report TR 38.913 [6] focuses on two main MBMS requirements for 5G, which are the ability to deliver broadcast services to fixed, portable and handheld receivers; and be able to deliver mixed unicast, multicast and broadcast services within the same radio frequency (RF) channel. Since new system operating parameters are introduced in feMBMS to enhance its broadcasting capabilities using existing infrastructure, it is able to meet these requirements. However, its legacy transmission technologies still suffers from low performance and limited flexibility. feMBMS is expected to lag behind the next generation digital TV broadcasting systems in terms of efficiency and capability. For the next generation 5G-MBMS systems, it is reasonable to expect a performance that is similar to or better than the next generation digital TV broadcasting systems, and to have flexibility in radio resource allocation among unicast, multicast and broadcast services similar to or better than feMBMS.

1.2 Contribution

This work investigates the possibility of a more spectrum efficient solution in mixed unicast-broadcast service delivery in 5G-MBMS using a power-based non-orthogonal multiplexing (P-NOM) such as layered division multiplexing (LDM) [7]. While the capacity gains from using non-orthogonal multiplexing (NOM) over OM for delivering mixed mobile and fixed broadcast services is well understood, the capacity gain of NOM for mixed broadcast and unicast services has never been investigated. Investigating the potential capacity gains from using NOM over OM in broadband systems (such as LTE and 5G NR) to deliver mixed broadcast and unicast services over the same frequency and time resources is the problem of interest.

1.3 Research Collaboration with CRC

This work is the result of a collaborated research project between the University of Toronto Wireless Communication Laboratory and Communication Research Centre Canada (CRC). The project goal is to explore the impact of Non-orthogonal Multiplexing and Multiple Access (NOMA) on the next generation broadband system. Previous research from CRC has shown that using two layered power-domain NOMA, digital television broadcasting can deliver robust high-definition TV and ultra-HDTV in one channel with a higher spectral efficiency than traditional systems. This two-layer structure has been accepted by the Advanced Television Systems Committee (ATSC) as a baseline physical-layer technology for the new ATSC 3.0 standard[8]. The research has been divided into two parts, the University of Toronto is responsible for evaluating the performance of broadband unicast services, while CRC is responsible for evaluating the performance of broadband broadcast services. The result of this work, [7] and [9], was presented at the 2019 IEEE International Symposium on Broadband Multimedia Systems and Broadcasting, held in Jeju, Korea, from June 5^{th}-June 7^{th}, 2019. Reference [7], which presented

selected results from this thesis, received "2019 Best Student Paper Award" from the conference.

1.4 Two-Layer LDM for 5G-MBMS

Contrary to the traditional TDM-based eMBMS system, where the total transmission capacity is split proportionally between the broadcast and unicast services according to the time allocation, this paper explores the additional opportunistic network capacity gain that is offered by using a two-layer LDM in a broadcast-priority network, which can be either future eMBMS or 5G applications. In this scenario, we assume a SFN broadcast service, with all transmitters emitting a two-layer LDM signal. The higher power core layer (CL) is used to deliver broadcast services and the lower power enhanced layer (EL) is used for unicast supplementary services, as shown in Figure 1.1.

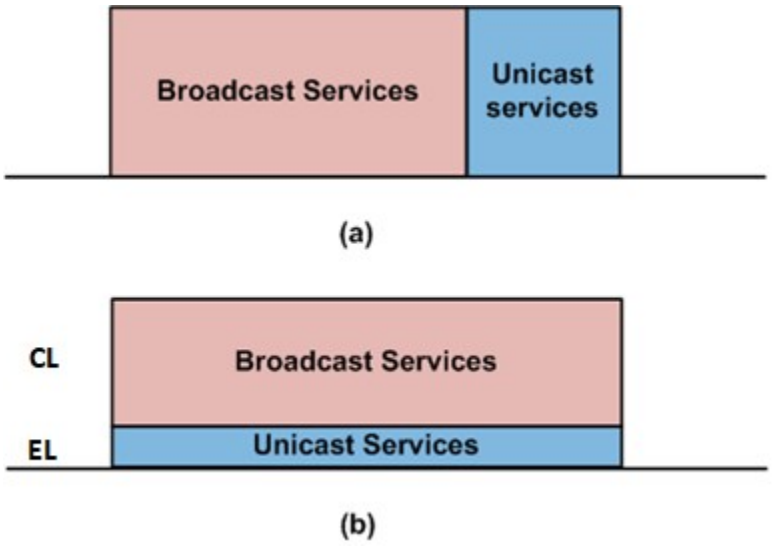

Figure 1.1: Mixed unicast-broadcast service delivery: (a) TDM; (b) LDM.

Simulation results from CRC [9] shows that in a broadcast SFN environment, the CL is still able to meet a full broadcast network's required quality of service. This thesis will focus on the performance of the EL, which will provide an additional opportunistic

unicast service to the network.

1.5 Organization

The rest of the thesis is organized as follows. Chapter 2 provides an overview of LDM and its capacity advantage over current systems, its complexity will be discussed, and the next generation digital TV broadcasting system, which incorporates LDM as one of its baseline technologies will be introduced. Chapter 3 details the process of validating the simulators. Chapter 4 presents the benchmark simulation results of a single layer unicast network. Chapter 5 and Chapter 6 presents and analyzes the simulation results of the enhanced layer. Finally, Chapter 7 concludes the thesis.

Chapter 2

Background on LDM, Complexity Analysis, and NG-DTV standards

2.1 Layered Division Multiplexing

LDM is a power-based NOM technique, it was proposed in [10] as one of the new physical layer baseline technologies used in the next generation digital TV (NG-DTV) broadcasting system, ATSC 3.0 [8], to achieve more efficient spectrum utilization and to provide more versatile broadcasting services[11]. LDM is different from traditional orthogonal multiplexing schemes such as TDM and frequency-division-multiplexing (FDM). As Figure 2.1 shows, in an LDM system, different services are multiplexed to different signal layers within a single RF channel using a power allocation scheme, with each layer occupying the full frequency and time resources of the channel, providing full frequency and time diversity to the signals in all layers.

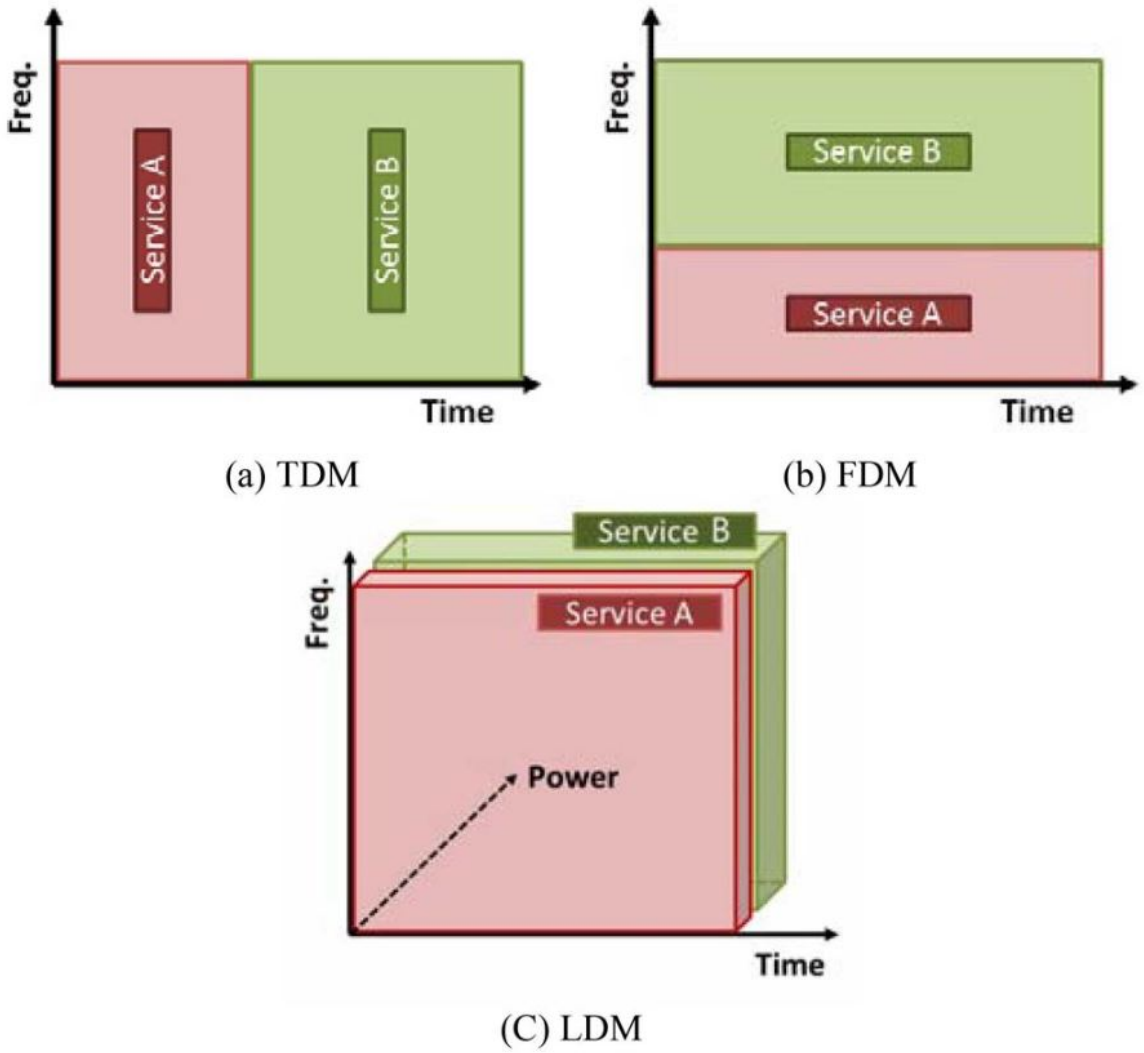

Figure 2.1: Multiplexing strategies for multiple services.

These different services are multiplexed using superposition coding techniques at the transmitter, and then decoded using successive interference cancellation at the receiver [12]. On the receiver side, the CL signal can be decoded while treating the EL signal as additional interference, while the EL signal must be decoded with highly accurate successive signal cancellation. Figure 2.2, taken from [8], shows the block diagrams of the transmitter and receiver of a two-layer LDM system. It has been shown in [8] that since transmission in different layers have different characteristics for the delivery of different services, LDM is especially advantageous for delivering services with different

robustness and throughput requirements to achieve more efficient spectrum utilization and higher transmission capacity. As an example, in a two-layer LDM system for Ultra-HDTV broadcasting, the CL with higher power allocation is used to deliver 720p or 1080p HDTV robust mobile broadcasting services to portable or hand held receivers, whereas the lower powered EL with lower power allocation is designed to deliver high data rate services, such as UHDTV or multiple HDTV services, to fixed reception terminals with high gain antenna.

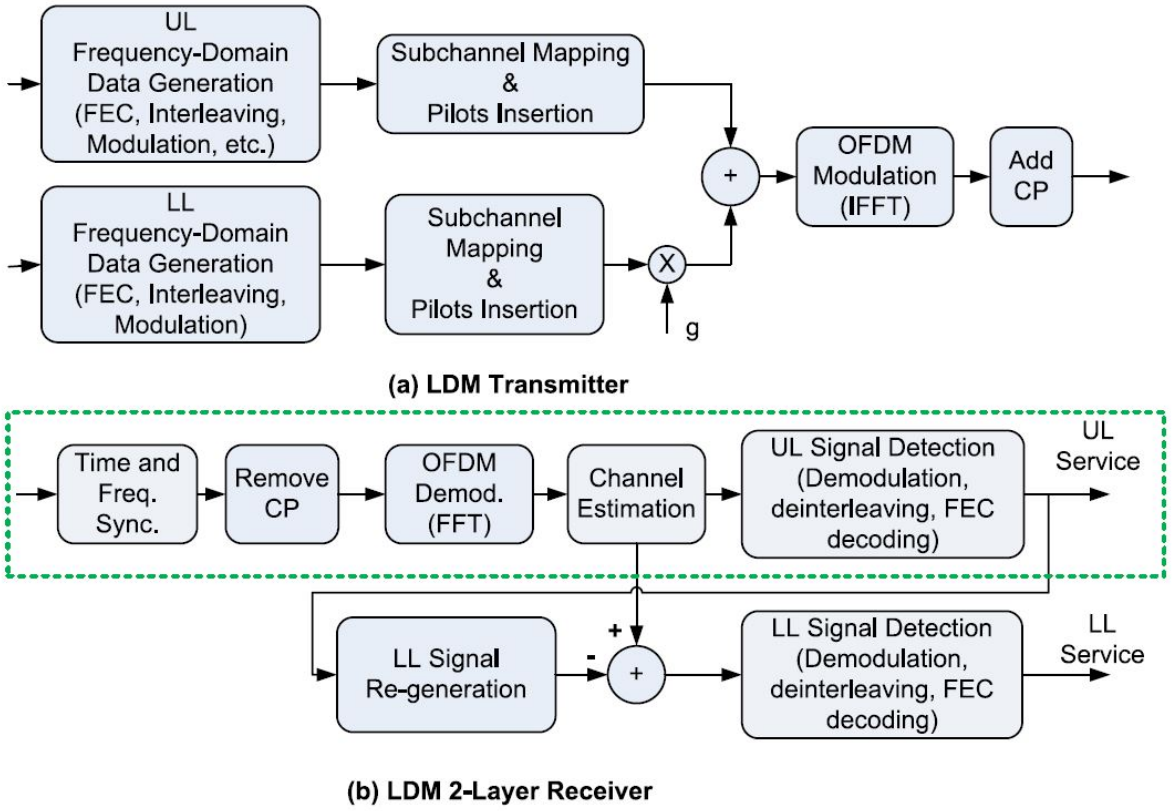

Figure 2.2: Two-layer LDM transmitter and receiver.

To deliver robust mobile services with high throughput and large coverage area, the CL signal in an LDM system is designed to have higher transmission power and use very strong channel coding and modulation, e.g., rate 1/4 Low-Density-Parity-Check (LDPC) code with QPSK modulation. The signal is optimized for robustness in hash wireless channel environments and it is expected to have low data rates around 2-4 Mbps

with very low signal-to-noise ratio (SNR) thresholds around 0-5 dB. On the other hand, the fixed receivers intended for the EL usually requires high operational SNR due to large antennas or directional antennas that are capable of providing significantly higher antenna gain as compared to mobile devices. The EL is expected to have data rates around 15-30 Mbps with SNR threshold around 15-25 dB, therefore it is usually designed to have lower transmission power, weaker channel coding, higher rate LDPC codes, and larger signal constellation.

LDM is able to co-exist with all the other emerging technologies such as multiple input multiple output (MIMO) transmission, non-uniform constellations (NU-QAM), bit-interleaved-coded-modulation (BICM), and Peak-to-Average-Power-Ratio (PAPR) reduction techniques for enhanced performance.

2.2 LDM Injection Levels

The power allocation of the two-layer LDM system is controlled by the injection level, often denoted by g, which defines the power level of the EL signal relative to the CL signal. Since by design the CL signal has higher power, the injection level will have a real value between 0 and 1, where setting $g = 0$ results in a single layer system as the EL is not allocated with any power. Assuming a total transmission power of P_T, and let P_{CL} and P_{EL} be the average powers of the CL and EL signals, respectively, then the total power is $P_T = P_{CL} + P_{EL}$. Thus, the injection level is defined as $g = P_{EL}/P_{CL}$, or alternatively, $P_{EL} = g \cdot P_{CL}$.

In practical systems, the injection level needs to be properly configured so that the EL can provide the desired service throughput with strong robustness, at the same time, the injection level needs to be low enough in order to limit cross-layer-interference (CLI) to achieve accurate successive signal cancellation. For practical LDM systems, [8] suggests that the injection levels should range from 0.1 to 0.4 based on the extensive simulation

results.

2.3 LDM Signal Generation and Detection

Going back to the block diagram of a two-layer LDM transmitter in Figure 2.2(a), the data of each layer is first processed into QPSK/mQAM symbols by its own signal processing modules. The frequency domain (FD) LDM signal is then generated as the superposition of the two individual FD signal from each layer as

$$X(k) = X_{CL}(k) + g \cdot X_{EL}(k), \tag{2.1}$$

Where $X(k)$ is the LDM symbol in the k^{th} sub-channel; $X_{CL}(K)$ and $X_{EL}(k)$ are FD symbols from the CL and EL respectively, and g is the injection level.

The block diagram of a two-layer LDM receiver is shown in Figure 2.2(b), in which the received LDM signal can be expressed as

$$Y(k) = X_{CL}(k) \cdot H(k) + g \cdot X_{EL}(k) \cdot H(k) + N(k), \tag{2.2}$$

Where $Y(k)$ is the received symbol in the k^{th} sub-channel, $H(k)$ is the channel response, and $N(k)$ contains additive white Gaussian noise and other interference.

To decode the CL signal, the received signal goes through regular signal detection to generating an accurate decision bit sequence while the lower power EL signal is treated as additional interference. To decode the EL signal, the receiver first cancels the CL signal, then obtaining the decision symbol by

$$\hat{Y}_{EL}(k) = \frac{1}{g}(Y(k) - \hat{X}_{CL}(k) \cdot \hat{H}(k)), \tag{2.3}$$

Where $\hat{X}_{CL}(k)$ is the estimated CL transmission symbol, and $\hat{H}(k)$ is the channel esti-

mate.

To perform successive interference cancellation, the receiver first obtains the estimates of the CL transmission symbols, $\hat{X}_{CL}(k)$, then performs channel encoding, interleaving and modulation to reconstruct the CL transmission symbols. Assuming perfect CL signal detection, i.e. $\hat{X}_{CL}(k) = X_{CL}(k)$ the receiver cancels the CL signal component from the received signal and then perform the EL signal detection.

2.4 The LDM Advantage

It has also been shown in many literatures including [8] that LDM can strictly outperform FDM/TDM in delivering multiple broadcast services with different reception conditions (mobile, portable, handheld) using a single RF channel. This section presents an information theoretical analysis on the achievable transmission capacity of a two layered LDM system, as well as a traditional TDM/FDM system delivering the same two services. The results will be used to show the advantage associated with LDM over TDM/FDM in delivering multiple services using the same frequency, time and power resource.

For a selective fading channel, with signal power P_s, noise power P_n, and channel response H, the SNR of the system can be expressed as

$$SNR = \left(\frac{P_s \cdot |H|^2}{P_n} \right), \tag{2.4}$$

Therefore, the total channel capacity can be calculated as

$$C = E\left[\log_2(1 + \left(\frac{P_s \cdot |H|^2}{P_n} \right)) \right], \tag{2.5}$$

Assuming perfect CL signal cancellation, the two layers of an LDM system where the CL delivers mobile services and the EL delivers fixed services, can be modeled as two parallel independent transmissions, the SNR values of the two layers can be expressed as

the following, respectively

$$SNR_{CL} = \frac{P_{CL} \cdot |H|^2}{P_{EL} \cdot |H|^2 + P_n}, \tag{2.6}$$

$$SNR_{EL} = \frac{P_{EL} \cdot |H|^2}{P_n}, \tag{2.7}$$

where P_{CL} and P_{EL} are the CL and EL transmission powers.

Then, the theoretical achievable capacities in a two-layer LDM can be expressed as the following, respectively

$$C_{CL} = E\left[\log_2\left(1 + \left(\frac{P_{CL} \cdot |H|^2}{P_{EL} \cdot |H|^2 + P_n}\right)\right)\right], \tag{2.8}$$

$$C_{EL} = E\left[\log_2\left(1 + \left(\frac{P_{EL} \cdot |H|^2}{P_n}\right)\right)\right], \tag{2.9}$$

In comparison, for a TDM or FDM system, the channel capacity available for one service is directly proportional to its time or frequency allocation. For a TDM system with total transmission interval of T_t to provide mobile and fixed services, the corresponding available capacities for the mobile and fixed services C_m and C_f, will be directly proportional to its time allocation T_m and T_f, given respectively, by

$$C_m = C \cdot \frac{T_m}{T_t}, \tag{2.10}$$

$$C_f = C \cdot \frac{T_f}{T_t}, \tag{2.11}$$

Similarly for a FDM system with total spectrum F_t, providing mobile and fixed services with spectrum allocation F_m and F_f, the capacity allocated for the two services are, respectively

$$C_m = C \cdot \frac{F_m}{F_t}, \tag{2.12}$$

$$C_f = C \cdot \frac{F_f}{F_t}, \tag{2.13}$$

Equations 2.10 and 2.11, as well as Equations 2.12 and 2.13 show that the achievable capacities of the two services in a TDM system and FDM system are linearly dependent on the time or frequency allocation between the two services. On the other hand, Equations 2.9 and 2.8 show that the achievable capacities of the two layers in an LDM system are non-linearly dependent on the power allocation. Therefore, when properly configured, an LDM system is capable of outperforming TDM/FDM systems.

To illustrate this further, assuming a system that is simultaneously delivering mobile and fixed services in one RF channel, where the mobile service is configured to have robust performance with a low SNR threshold of 0 dB, while the fixed service is configured to have a high SNR threshold of 20 dB. Figure 2.3, taken from [8], plots the achievable transmission capacities for the mobile and fixed services for both LDM and TDM/FDM systems. In this LDM system, the total transmission power P_s is kept constant and shared between the two services with different power allocations. The leftmost point of each curve represents a single-service transmission where all the resource is allocated for the mobile service, while the rightmost point is for delivering fixed service only. Comparing the curves for LDM and TDM/FDM, it is clearly shown that LDM always provides higher transmission capacities over TDM/FDM. As an example, when the required mobile service throughput is 0.7 b/s/Hz, using LDM can provide an additional capacity 2.5 b/s/Hz of transmission capacity for the fixed service over the TDM/FDM system.

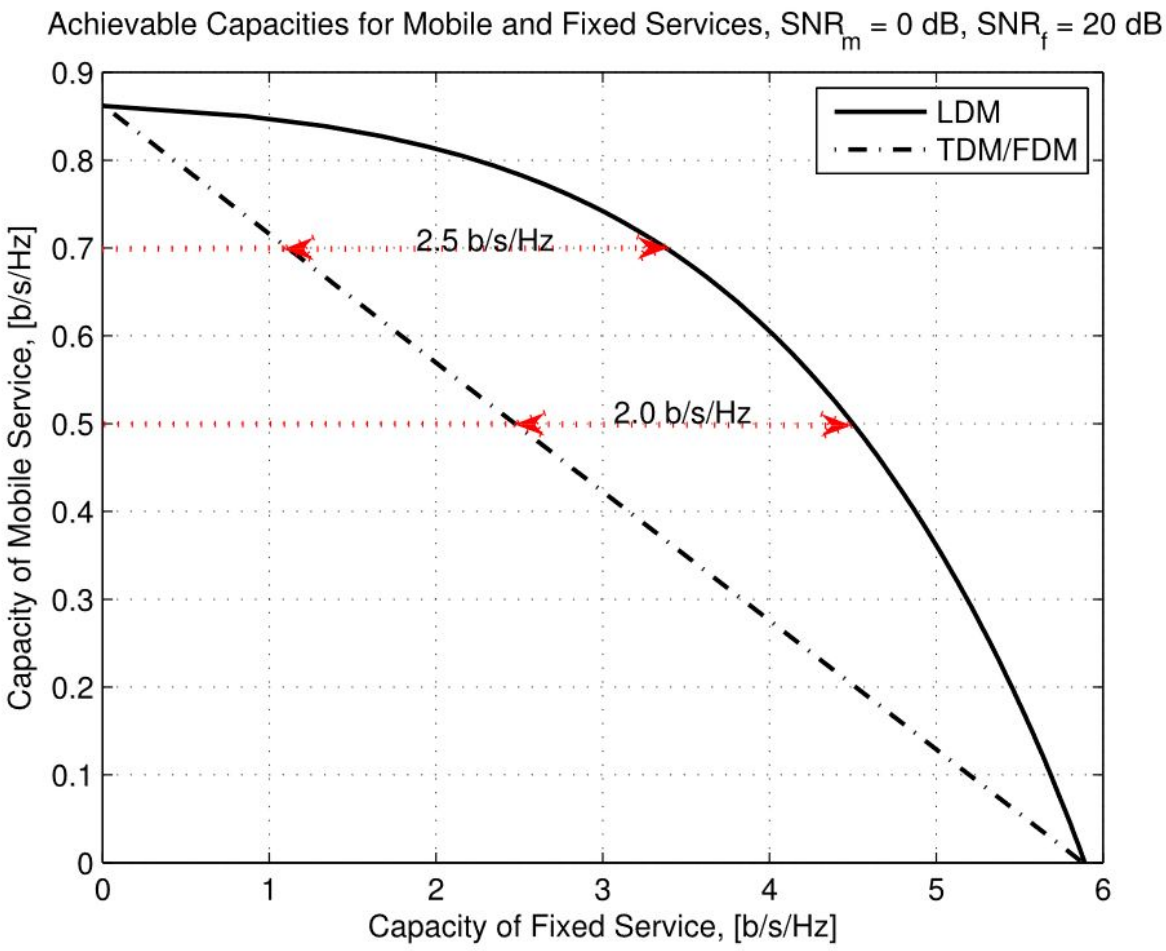

Figure 2.3: Achievable service capacities for LDM versus TDM/FDM.

2.5 Complexity Analysis of LDM Systems

2.5.1 Low Complexity Transmitter and Receiver

In [13], the authors propose a novel transmitter and receiver architectures for low complexity LDM systems for ATSC 3.0 and other NG-DTV broadcasting systems. The proposed architecture is already adopted as a baseline technology for the ATSC 3.0 standard.

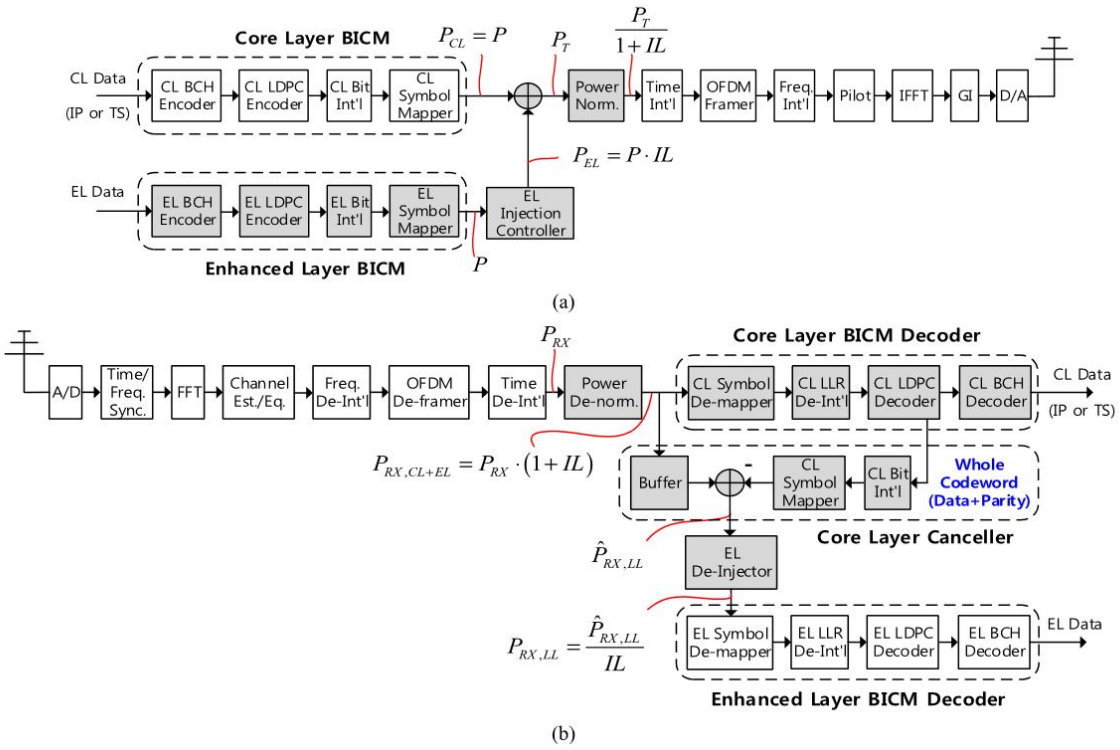

Figure 2.4: Architectures for LDM system: (a) Transmitter (b) Receiver.

Figure 2.4 shows the proposed low complexity LDM system transmitter and receiver architectures. In this architecture, the transmission signals in both layers use orthogonal frequency-division multiplexing (OFDM) based physical-layer waveforms, and both layers share the same OFDM signal structure and related chain such as fast Fourier transform (FFT), pilot patterns, time and frequency interleavers, guard interval, and preamble. Although it is not mandatory, sharing the same OFDM structure simplify the signal detection process at the LDM receiver and therefore allowing for a low complexity, low memory use and power-efficient physical layer implementation.

Figure 2.4(a) shows the low complexity LDM transmitter. The blocks coloured in gray are additional components needed to create the EL symbols including the EL bit-interleaved coded modulation (BICM) encoder, EL injection controller, adder, and power normalizer. After superimposing the CL and EL symbols, the time and frequency inter-

leavers, pilot patterns, inverse FFT (IFFT), GI, preamble, bootstrap can be shared by the CL and EL to reduce the complexity of the LDM transmitter.

Figure 2.4(b) shows the low complexity LDM receiver. Similar to the transmitter, a large number of components including the tuner, ADC, time and frequency synchronizer, FFT, channel estimator, equalizer, and frequency and time de-interleavers can be shared by the both layers. The blocks coloured in grey are the additional components needed for successive interference cancellation and detection, these components include the power de-normalizer, CL BICM decoder, UL canceler and EL de-injector.

2.5.2 Complexity Analysis

This section discusses the complexity increase of the CL and EL of LDM receiver as compared to a single layer receiver. The complexity increase of a LDM transmitter is not a big concern in practical deployments since they are usually fixed commercial equipment owned by operators. A transmitter of this kind is not as sensitive to the increase in components, memory usage, power consumption or weight. However, for the receivers, which are most likely devices owned by consumers, increase in complexity and power consumption becomes more of an important matter.

The remainder of this section will show that compared to a conventional single layer receiver, an LDM receiver can be implemented with low complexity and low memory usage, causing no more than 10% complexity increase as a trade off for the significant performance gain.

For a receiver detecting the CL service, only the CL needs to be decoded while the EL is treated as additional noise, therefore the complexity is the same as a traditional single layer receiver. On the other hand, if the receiver is detecting the EL service, then as mentioned before, additional BICM decoder and canceler for the CL, as well as power de-normalizer and EL de-injector are needed for successive interference cancellation, while the other parts of the receiver can be shared. Since the power de-normalizer and EL

de-injector are simple scaling operations and therefore have negligible complexity, the two major complexity increase sources are the CL BICM decoder and CL canceler.

CL BICM Decoder

In practical receivers, the CL and EL can share one BICM decoder because CL BICM decoding, CL canceling, and EL BICM decoding are performed sequentially. Within the BICM decoder, the complexity increase of sharing the LDPC decoder is of the most interest since it occupies the largest part of the LDM receiver.

Extensive simulations from [13] shows that if the CL is working under relatively high SNR environment of 15-25 dB, using QPSK constellation and 4/15 rate LDPC code with 64800 length; while the EL is working under relatively low SNR environment of 0-5 dB, using 64QAM and 10/15 rate LDPC code with 64800 length, and lastly the injection level is set to -4 dB. If the EL requires 50 iterations in the LDPC decoder, then the extra CL decoding can be performed with less than 5 iterations at the target SNR range since CL is 10-20 dB more robust than EL. Since both the CL and EL share the same LDPC decoder, then the pure complexity increase approximately $5/50 = 10\%$ compared to a generic single layer scenario. In an ASIC chip point of view, since almost 50% chip area in AISC is occupied by the LDPC decoder, the total complexity increase of a receiver is less than 5%.

CL Canceler

In the CL canceler, the most prominent complexity increase comes from the memory buffer to store time de-interleaver (TDI) outputs as well as the regeneration of CL symbols. Since components including the subtractor, bit re-interleaver, and symbol re-mapper require very minimal logic and memory, their complexity can be neglected, only the memory increase compared to a single layer should be investigated in depth.

Memory buffer size requirement is highly dependent on constellation order and LDPC

length of each layer. Assuming that the CL uses 16200 length LDPC code and QPSK constellation, while the EL uses 64800 LDPC code and 64QAM, the the simulations and analysis presented in [13] show that the required maximum memory buffer size is 32400 cells. On the other hand, for worst case memory considerations and potential use case for mobile reception, if CL uses 64800 length LDPC code, the maximum buffer size increases to 64800 cells. Assume TDI memory size is $512 \cdot 10^3$ cells, then the worst case memory increase is $64800/(512 \cdot 10^3) = 12.4\%$. If desired, adopting smart scheduling can further reduce the required memory size to about 8%.

2.6 ATSC 3.0

The Advanced Television Systems Committee (ATSC) is a Standard Development Organization (SDO) that developed ATSC 3.0, which is the next generation Digital Terrestrial Television (DTT) broadcasting standard. The ATSC 3.0 standard provides a complete technical specification for broadcasting, including physical, management and transport protocol as well as application layers. Moreover, ATSC 3.0 is designed to have improvements in performance, functionality, flexibility and efficiency compared to existing systems for the aim of leverage recent research into the new digital terrestrial broadcasting system, outperform existing terrestrial broadcast standards [14] [15], and become the reference terrestrial broadcasting technology worldwide.

The ATSC's call for proposals (CfP) was issued in March 2013 to other SDO's, industry organizations and universities around the world. Twelve proposals with technology elements or full physical layer system descriptions were received in October 2013. After selecting the most suitable technologies then determining how to combine them into a coherent system, the ATSC 3.0 physical layer specification passed Technology and Standard Group 3 Candidate Standard ballot in September 2015. By 2016, the first experimental systems have been successfully deployed at multiple countries around the world [16].

The primary goal of ATSC 3.0 is to offer higher system capacity and efficiency to provide emerging ultra high definition (UHD) television broadcast services simultaneously to both fixed and mobile receivers, including but not limited to traditional household television, handheld portable devices, and vehicles. ATSC 3.0 utilizes the latest technology and offers a wide range of tools to let the broadcasters and service providers taylor the operating modes to the needs of the consumers and the targeted devices for an optimal trade-off between robustness and throughput.

The ATSC 3.0 physical layer uses OFDM based wave forms and LDPC forward error correction codes similar to existing state of the art systems. It supports uniform QPSK modulation and five non-uniform constellation sizes: 16-QAM, 64-QAM, 256-QAM, 1024-QAM, and 4096-QAM [17], as well as two code lengths (16200 and 64800 bits) and twelve code rates (from 2/15 up to 13/15)[18]. In addition to the traditional TDM and FDM multiplexing modes, a third two-layered LDM mode is also added. These multiplexing modes can be combined with three frame types: SISO (Single-Input-Single-Output), MISO (Multiple-Input-Single-Output), and MIMO. Lastly, ATSC 3.0 provides great flexibility in terms of configuration parameters with 12 guard interval lengths from $27\mu s$ to $700\mu s$, and 3 FFT sizes of 8K, 16K, and 32K, 16 pilot patterns, and 2 time interleavers.

Compared to the ATSC A/53 DTT television broadcast standard[19] that it replaces, ATSC 3.0 improves the spectral efficiency and robustness to improve the capacity at the same SNR operating point by more than 30%. ATSC 3.0 also allows combining two RF channels to double the maximum service peak data rate and to exploit the additional inter-RF channel frequency diversity as well as improved statistical multiplexing. In addition, the inclusion of a 2x2 MIMO antenna system [20] improves the transmission robustness via additional spatial diversity or increases the system capacity by sending two independent data streams using dual polarization in the same RF channel without increasing the total transmission power [21]. Additionally, ATSC 3.0 will include

a dedicated wireless return link as an optional connection or interactive service. This service is very important in all kinds of usage scenarios such as multi-view/multi-screen, where users can chat with each other during a television broadcast show, choose one or more preferred viewing angles of a program, and obtain additional information on their devices such as background information of actors [22]. Another scenario is adaptivity robustness, where the return channel can help broadcasters collect and analyze user data, allowing them to perform dynamic advertisement insertion, and adaptively adjust the transmission parameters [23].

The ATSC 3.0 is intended to evolve with technology over time without having to develop a new standard every time new technologies becomes available. Therefore, not only does the standard have no backward compatibility constraints with existing standards, the standard also removes many constraints of using future systems that are yet to be developed to allow including new technologies in the future without disrupting ATSC 3.0 services.

Chapter 3

Simulator Validation

3.1 Introduction

In the field of telecommunication research, simulation tools are essential in the development of new techniques for LTE and 5G. However, there are only a few open-source simulators available to the general public for research purposes, while the vast majority of the simulators are built by the industry and not available to the public. The most popular open-source simulators are the Vienna LTE-A simulators [24]and the ns-3 LTE module [25]. There are also a number of 5G simulators being developed, however they were not released at the time when this project was started.

Open-source simulation tools are beneficial in a number of ways. First, compared to hardware experiments, software simulations are generally less expensive and more readily accessible while maintaining an accurate modeling of real-world phenomena. Second, since these simulators are developed by academic research institutions and the open-source community, they can be modified by other researchers to develop custom systems to better fit their own needs. Lastly, due to the open-source availability, the simulators enable reproducible research along with comparison and validation of novel algorithms.

This chapter introduces the Vienna LTE-A simulator and the ns-3 LTE module. The

simulators are configured according to a 3GPP reference scenario and their results are gathered and compared. Lastly, the performance of each simulator is discussed and used to choose the most suitable simulator for the project.

3.2 Vienna LTE-A Downlink System Level Simulator

The Vienna LTE-A simulators are a set of MATLAB-based, open source, publicly available simulation environments that support link and system level simulations of the Universal Mobile Telecommunications System (UMTS) Long-Term Evolution (LTE) System. These simulators are developed by the Institute of Telecommunications, Vienna University of Technology, Austria.

The Vienna LTE-A simulators come with three separate components: LTE-A Downlink/Uplink Link Level Simulators, and LTE-A Downlink System Level Simulator. The link level simulators are used to investigate channel estimation, tracking, prediction and synchronization algorithms, as well as MIMO gains, Adaptive Modulation and Coding (AMC), feedback techniques, receiver structures, modeling of channel encoding and decoding. On the other hand, system level simulations focus more on network related issues, such as resource allocation, scheduling, multi-user handling, mobility management, admission control, interference management, and network planning optimization.

Unlike the link level simulators that investigate individual physical layer links, the system level simulator analyzes the performance of a whole network. A typical network would be made up of several Evolved Node B (eNodeBs) that cover an area in which mobile terminals are located. For such a large-scale system level investigation, simply performing physical layer simulations on each link between dozens of eNodeBs and hundreds or thousands of users would require too much computational power to be feasible. Thus, the Vienna LTE-A Downlink System Level Simulator abstracts the physical layer

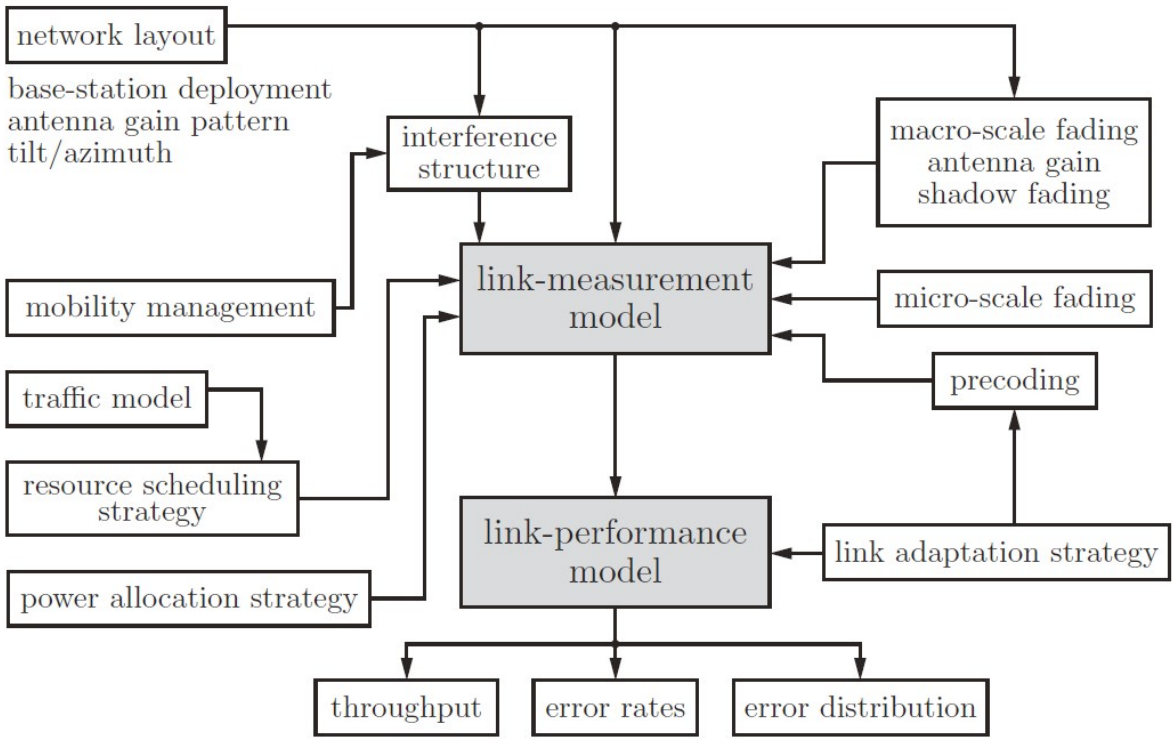

Figure 3.1: Interactions between the link measurement and performance model.

by simplifying the models to capture its essential dynamics with high accuracy at low complexity.

The core of the Vienna LTE-A Downlink System Level Simulator consists of two parts, a link measurement model, and a link performance model, as shown in Figure 3.1. The link measurement model outputs the link quality measure based on the calculated Signal to Interference and Noise Ratio (SINR) and the UE feedback of a given link. This model also carries out link adaptation and resource allocation to users to optimize the performance of the system, in terms of throughput. Based on the link measurement model, as well as the receiver SINR and the transmission parameters, the link performance model then maps the information to block error rate (BLER) and outputs the throughput and errors of the link.

In terms of the actual implementation, the simulator is made up of a number of class objects, each of which represents a corresponding network element. Their interactions

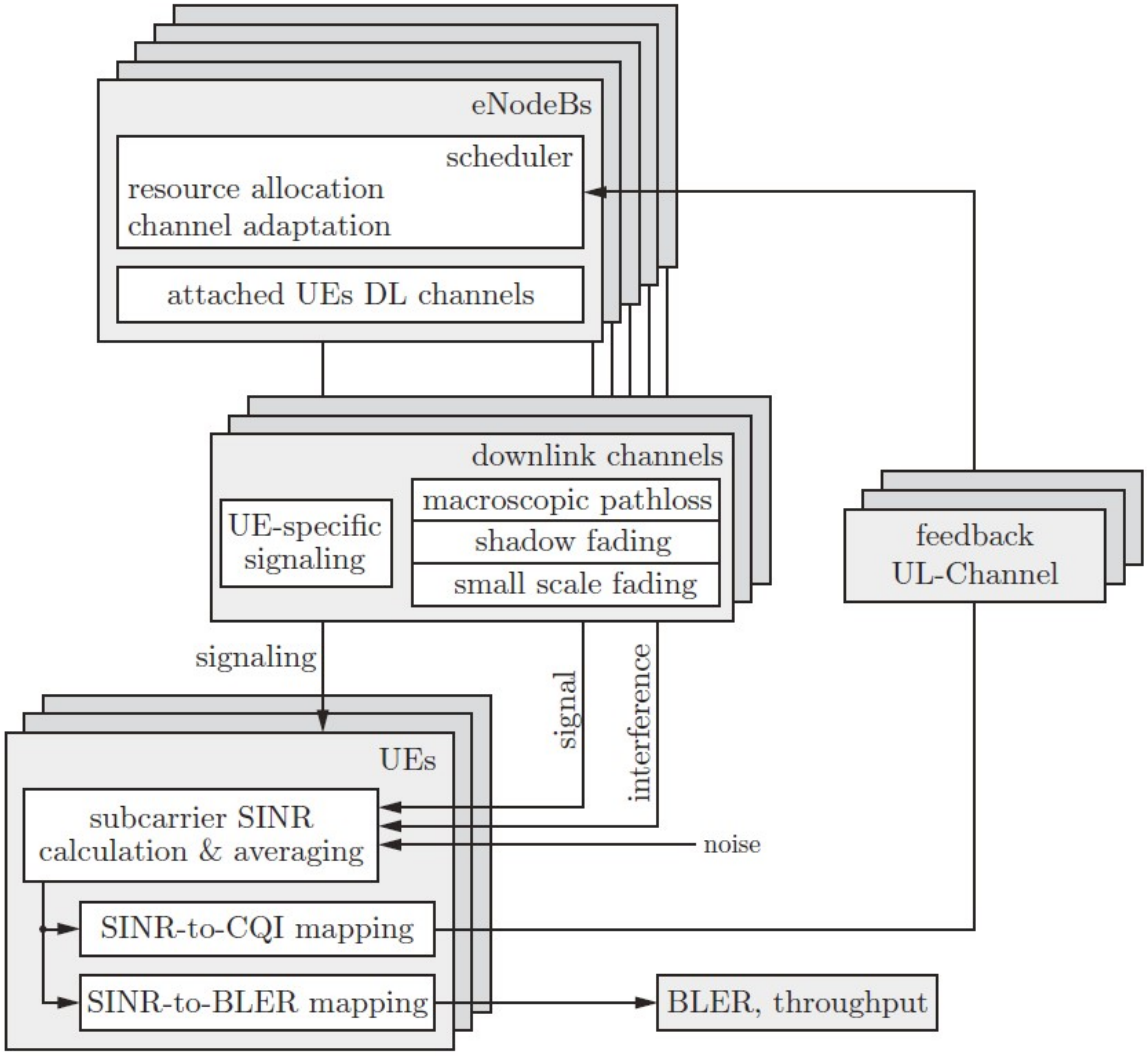

Figure 3.2: Implementation of the LTE system level simulator.

are shown in Figure 3.2.

At the beginning of the simulation, transmission sites made up of three sectors (Evolved Node B or eNodeB) are generated, each eNodeB containing a scheduler. The schedulers are responsible for assigning PHY resources, precoding matrices, and the appropriate MCS to each UE attached to the specific eNodeB.

Over at the UE side, the received SINR is calculated in the link measurement model based on the signal, interference, and noise power level. The SINR is dependent on the cell layout (eNodeB positions, macroscopic pathloss, macro-scale pathloss, and shadow

fading), as well as the time-variant small-scale (microscopic, micro-scale) fading. The UEs also generates channel quality indicator (CQI) feedback reports by an SINR-to-CQI mapping and send these reports to the eNodeB objects with adjustable delay. The transmitter can select the most suitable modulation and coding scheme (MCS) based on the CQI to achieve the target BLER during transmission. In the link performance model, the output of the link measurement model is mapped to an AWGN-equivalent SINR via Mutual Information Effective Signal to Interference and Noise Ratio Mapping (MIESM) [26], then the AWGN-equivalent SINR is mapped to BLER via AWGN link performance curves. The BLER, combined with the Transport Block Size are then used to compute the link throughput. The simulation output consists of traces, link throughput and error rates for each user, as well as a variety of other aggregate information, which can be used to determine statistical distributions of throughput and error.

The system level simulator contains several precalculated simulation parameters to reduces the computational load while carrying out a simulation and offers repeatability by loading an already partly precalculated scenario. The precalculations included in the simulator are the generation of eNodeB-dependent large-scale pathloss maps, site-dependent shadow fading maps, and time-dependent small-scale fading traces for each eNodeB-UE pair.

3.3 Overview of the NS-3 Network Simulator LTE Module

The ns-3 network simulator is a discrete-event network simulator targeted primarily for research and education use. The simulator has been developed since 2006 to provide an open, extensible network simulation platform. Simply, ns-3 provides a simulation engine for users to conduct simulation experiments to model how packet data networks perform [27].

Compared with other simulation tools, ns-3 particularly stands out for two main reasons. First of all, the modular design of the simulator means that its set of libraries can be combined with other external software libraries. For example, there are a variety of external data analysis and visualization tools that can be used with ns-3, compared to most other simulators that only comes with a single, integrated graphical user interface environment. Secondly, since ns-3 is open source and written entirely in C++ with optional python bindings, users have the option to write simulation scripts in C++ or in Python. There are also many new simulation modules, data analysis tools and visualization tools available or under development.

In ns-3, there are five key abstractions that makes up the network, these abstractions are the node, application, channel, net device, and topology helpers [28].

The node abstraction simulates the basic computing devices that connects to a network. This abstraction is represented in C++ by the class *Node*. The *Node* class provides methods for managing the representations of computing devices in simulations, allowing the user to define additional functionalities such as applications, protocol stacks and peripheral cards with their associated drivers.

In the real world, software applications run on computers to perform tasks, in ns-3, the application abstraction run on *Nodes* to generates activity to be simulated in the simulation world. This abstraction is represented in C++ by the class *Application*. The *Application* class provides methods for managing the representations "user-level" applications in simulations.

Similar to how a computer can connect to a network via a wired or wireless channel, in ns-3, the channel abstraction represents the communication channel and is represented in C++ by the class *Channel*. The *Channel* class provides methods for managing communication sub-network objects and connecting nodes to each other. *Channels* can be specialized to something as simple as a wire, or as complicated as a large Ethernet switch, or three-dimensional space full of obstructions for a wireless network.

The net device abstraction is represented in C++ by the class *NetDevice*. *NetDevice* acts as a network interface card and its network device drivers to be "installed" in a *Node* to enable the *Node* to communicate with other *Node* in the simulation via *Channels*. The *NetDevice* class provides methods for managing connections to *Node* and *Channel* objects.

Lastly, ns-3 provide a number of topology helpers to make the task of connecting a large number of *NetDevices* to *Nodes*, *NetDevices* to *Channels*, assigning IP addresses etc. as easy as possible. Some of these tasks include, creating a *Netdevice*, adding a MAC address, and installing that *Netdevice* on a *Node*, configuring the node's protocol stack and then connecting the *NetDevice* to a *Channel*. Many iterations of these operations would be required to connect multiple devices onto channels to complete a network, the topology helper objects combine these many distinct operations into an easy to use model for the user's convenience.

3.3.1 The LTE Module

The development of the LTE module for ns-3 started in 2010, the goal was to provide a comprehensive implementation of LTE devices.

The Physical Layer

The *UeLtePhy* and the *EnbLtePhy* classes represents the UE and eNodeB devices of the physical layer, respectively. The main task of the *EnbLtePhy* class is to handle the transmission and reception of signals by the eNodeB. At the end of the reception, the PHY interface first estimates the SINR of the received signal and then delivers the received packets to the eNodeB. On the other hand, the *UeLtePhy* class is allocated with a list of uplink sub-channels assigned by the uplink scheduler for transmitting packets through the uplink channel, as well as a list of downlink sub-channels assigned by the downlink packet scheduler for transmitting packets through the downlink channel.

The allocation is performed by the MAC scheduler at the eNodeB on a per-TTI basis, according to the scheduler. When the UE transmit a packet, it calls the method $UeLtePhy :: SendPacket()$ to delivers these packets to the uplink $LteSpectrumPhy$ object, which first creates the $SpectrumValue$ to describe the Power spectral density of the signal for each sub-channel, then the UE calls $SpectrumChannel :: StartTx()$ to transmit the signal over the channel. Similarly, the downlink $SpectrumPhy$ object is responsible for receiving packets. At the end of the reception procedure, the PHY interface first computes the SINR of the received signal, then transfers these values to the MAC layer for the creation of the CQI feedback and lastly delivers the received packets to the UE.

The $SpectrumModel$ class models the paired spectrum in which LTE operates according to the Frequency Division Duplex Mode. The class defines the set of frequencies to use by the devices and the signals to be transmitted through the channel, for both the uplink and downlink. During the simulation, the physical layer uses this class to create the $SpectrumValue$ instances to calculate the Power Spectral Density of both the signal and noise. Then the $SpectrumChannel$ class creates the channel propagation models and also handles the actual packet transmission process. The propagation loss model contains four different components: pathloss, shadowing, multipath and penetration loss, which are implemented respectively using the classes $PathLossModel$, $JakesFadingLossModel$, $ShadowingLossModel$, and $PenetrationLossModel$.

Lastly, the physical layer is also responsible for the transmission and the reception of control messages. The LTE module was designed with the intention of modeling user data transmission only. Therefore, the LTE module implements an ideal control channel to shorten the simulation time and limit the complexity of the simulator. In the simulator, the control messages are delivered to the destination nodes directly without being subjected to the channel object, therefore they are always received correctly.

Network Devices

The dedicated classes *UeLteNetDevice* and *EnbLteNetDevice* implement the functionality specific to the UE and eNodeB devices. In addition to performing all the common functionality of an ns-3 device, they contain and manage the main entities of the E-UTRAN protocol stack, i.e., the RRC, RLC, MAC and PHY. Since most of the functionalities are implemented in the eNodeB, the UE device only stores information about which eNodeB it is attached to. On the other hand, for the eNodeB, MAC entity hosts both the uplink and downlink packet scheduler components, which enables the eNodeB to perform Radio Resource Management.

The MAC entity, represented by the *MacEntity* class, hosts the Adaptive Modulation and Coding module and it is designed to deliver packets coming from the upper layer to the physical layer and vice-versa to provides an interface between the device and the physical layer for both the UE and the eNodeB. The Radio Resource Control entity implemented by the *RrcEntity* class and handles connection establishment and management, broadcast of system information, radio bearer management, mobility management, and paging. The interaction between the MAC and the Radio bearer is provided by the RLC entity, which is implemented by the *RlcEntity* class. With these tools, the eNodeB keeps track of all the UEs attached to it. For each UE, the eNodeB creates an UE Record to manage the UEs in various operations. For example, information such as the latest CQI feedbacks sent by the UE is stored and used by the packet scheduler to allocate resources to the UEs taking into account their channel conditions. the most important task of the eNodeB is the Radio Resource Management, which is performed by uplink and downlink packet schedulers [29].

3.4 Comparison of Vienna and NS-3 Against 3GPP Standard

This section presents the simulation results of a basic LTE scenario from the Vienna LTE-A Downlink System Level Simulator and ns-3 LTE module to the 3GPP reference scenario results. This is done to make sure the system level simulation results are close to those obtained by the industrial simulators and similar open source simulators.

3.4.1 The 3GPP Reference Scenario

The 3GPP technical report TR36.8143 [30] provides a set of reference scenarios, along with performance results based on an aggregate of 17 industrial simulators. This technical report is based on TR 25.814 [31], which provides parameters for a baseline macro-cell system in 2-D. TR 36.814 builds on TR 25.814 with additional details on 3D antenna patterns. In this work, the reference scenario chosen for validation is 3GPP Case 1, an urban LTE macro cell setup, as it is the only case that contains detailed information regarding SINR and throughput CDFs for full buffer traffic in graphical format. Detailed descriptions of the system can be found on Tables A.2.1.1-2 in TR 36.814 and A.2.1.1-3 in TR 25.814.

For the simulation, 3GPP technical report TR36.814 Case 1 assumes a hexagonal grid setup, with 19 cell sites and 3 sectors per site, and a total of 1425 UEs (25 UEs x 19 sites x 3 sectors/site) uniformly placed in a rectangular area as can be seen in Figure 3.3. This implies one central site, surrounded by 2 rings of additional sites (the inner ring comprises 6 sites, the outer ring comprises 12 sites).

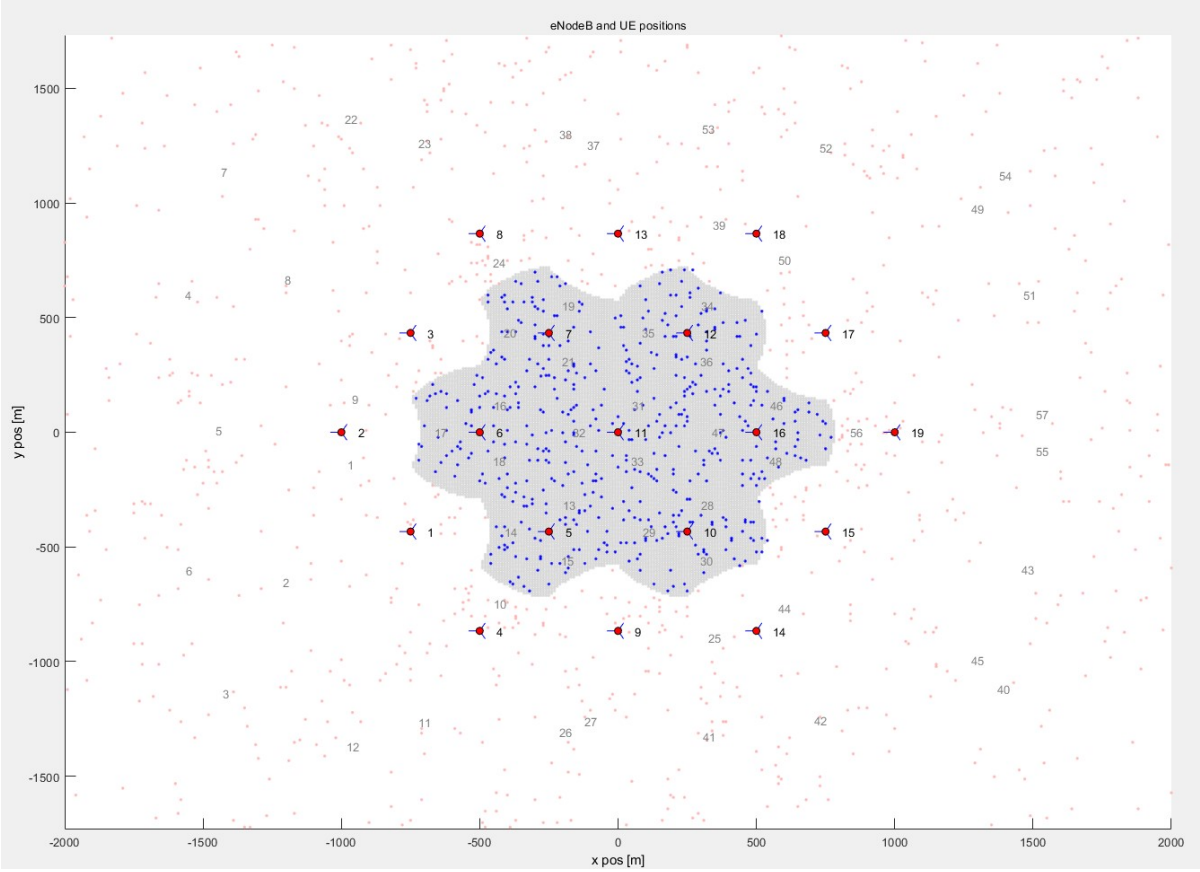

Figure 3.3: 3GPP case 1 cell and UE positions.

3.4.2 Replicating 3GPP Reference Scenario in NS-3 LTE Module

NS-3 already has its components within the LTE module individually validated and its system level LTE module validated in [32] against the 3GPP reference scenario. The ns-3 system level validation code are shared on GitHub, and will be used to compare with the results obtained from the Vienna system level simulator.

3.4.3 Replicating 3GPP Reference Scenario in Vienna System Level Simulator

The Vienna LTE-A Downlink System Level Simulator can be launched through the $sim\_main\_launcher\_files$ folder, which contains a set of pre-configured scenarios ready for use. *demo_basic* scenario was selected for adaptation to the 3GPP scenario, as its configuration was the most similar to the 3GPP scenario and did not have any unnecessary features such as RRH or femto-cells. The simulation type was set to $tri\_sector\_tilted\_traffic$ in order to simulate full buffer traffic as specified by the 3GPP technical report. The parameters that must be configured to replicate 3GPP Case 1 are found within the LTE_config structure. This structure can be set in the $hex\_grid\_tilted\_traffic$ file found in the $simulation\_config$ folder. LTE_config can be used to configure parameters including but not limited to: the center frequency, bandwidth, transmission mode, random number seed, simulation time, eNodeB layout, pathloss model, eNodeB transmission power, channel model, number of UEs and their distribution, antenna, and scheduler. Further specifications for the 3GPP reference scenario can be found in Table 3.1. For simulation, a total of 30 different iterations was performed, each iteration had a different independent UE placement, and the evaluation was performed only on the UEs attached to the inner 7 sites (21 eNodeBs). The outer ring was used only for interference purposes.

3GPP Reference Scenario Parameters	Vienna Configuration
Carrier Frequency = 2 GHz	LTE_config.frequency = 2e+09;
Bandwidth = 20 MHz	LTE_config.bandwidth = 20e+06;
Transmission Type = 1x2 SIMO FDD	LTE_config.nTX = 1; LTE_config.nRX = 2; LTE_config.tx_mode = 1;
UE speed = 3km/h	LTE_config.UE_speed = 0.8333; LTE_config.keep_UEs_still = 0;
Simulation Time = 100 ms	LTE_config.simulation_time_tti = 100;
Simulation layout = Hexagonal grid	LTE_config.network_geometry = 'regular_hexagonal_grid';
Number of Cell Sites = 19	LTE_config.nr_eNodeB_rings = 2;
Distance Between Cells = 500 m	LTE_config.inter_eNodeB_distance = 500;
Pathloss Model = $128.1 + 37.6 \cdot \log_{10} R$	LTE_config.macroscopic_pathloss_model = 'TS325814';
Cell Transmission Power = 40 W	LTE_config.eNodeB_tx_power = 40;
UE Distribution = 25 uniformly per cell	LTE_config.UE_per_eNodeB = 25; LTE_config.UE_distribution = 'constant UEs per cell';
Antenna Height = 32 m	LTE_config.site_height = 32;
Antenna downtilt = 15 degrees	LTE_config.antenna.mechanical_downtilt = 15;
UE Height = 1.5 m	LTE_config.rx_height = 1.5;
Downlink Scheduler = Round Robin	LTE_config.scheduler = "round robin traffic";
Traffic Model = full buffer	LTE_config.traffic_models.type = 'fullbuffer';
Number of Sites to Compute = 7	LTE_config.compute_only_center_users = 1;

Table 3.1: Vienna configurations of the 3GPP reference scenario.

3.4.4 Results and Comparison

Figures 3.4, 3.5, 3.6, 3.7, 3.8 3.9 present the simulation results from the 3GPP technical report TR36.8143 [30], ns-3 simulator [32] and Vienna LTE-A Downlink System Level Simulator. The system performance metrics to evaluate these results are based on Section A.2.1.4 of TR 36.814: UE average SINR cumulative distribution function (CDF), cell average SINR (median UE average SINR), cell edge SINR (95^{th} percentile UE average SINR), UE throughput CDF, cell average throughput (median UE throughput), and cell edge throughput (95^{th} percentile UE throughput). Table 3.2 presents the numerical system performance metrics.

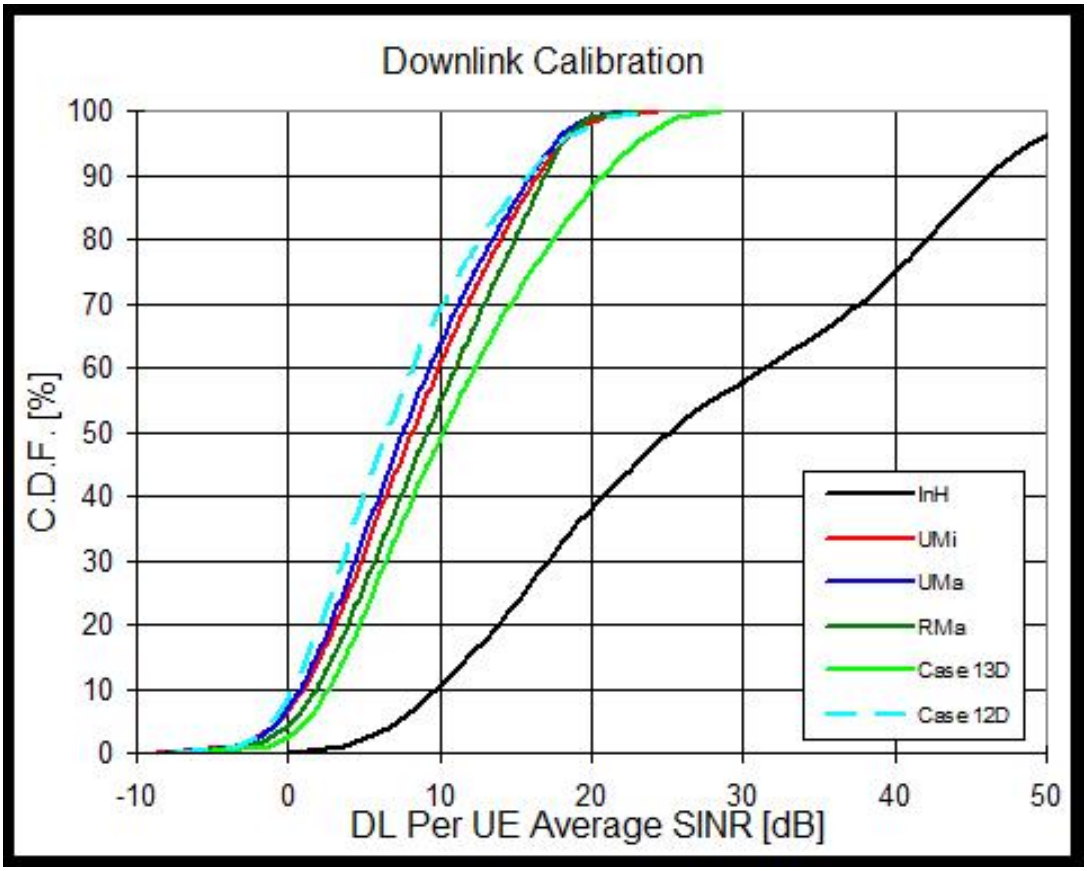

Figure 3.4: 3GPP TR36.8143 case 1 UE average SINR CDF.

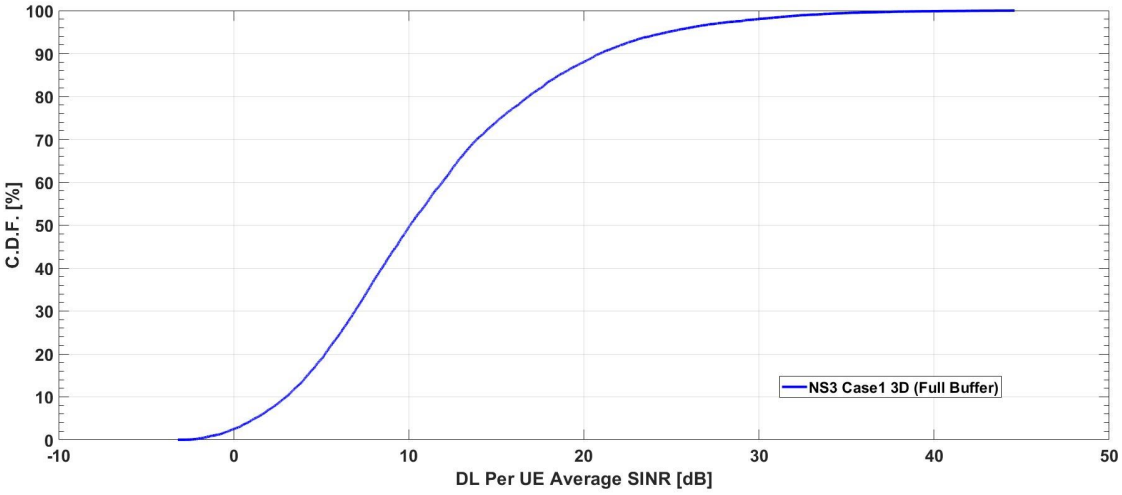

Figure 3.5: NS-3 UE average SINR CDF.

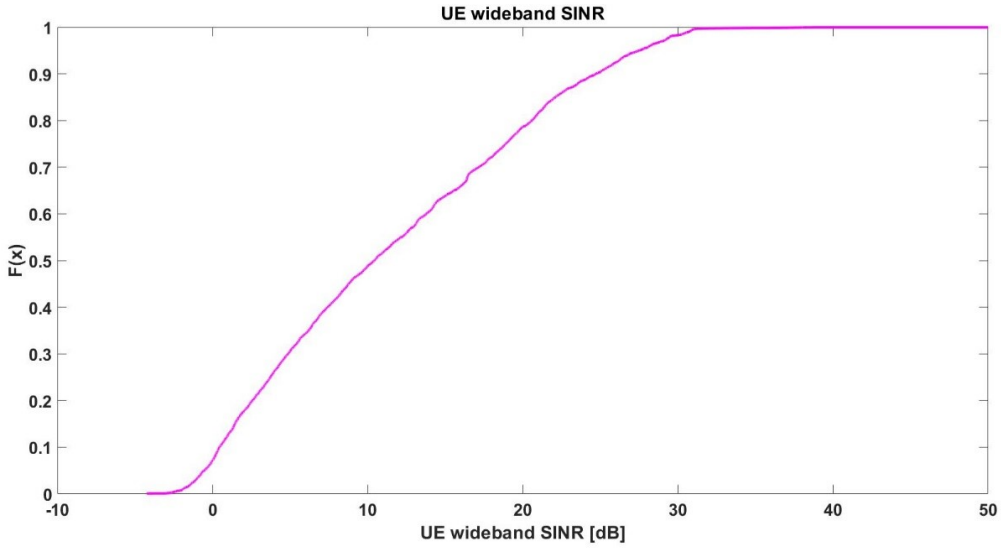

Figure 3.6: Vienna LTE-A downlink system level simulator UE average SINR CDF.

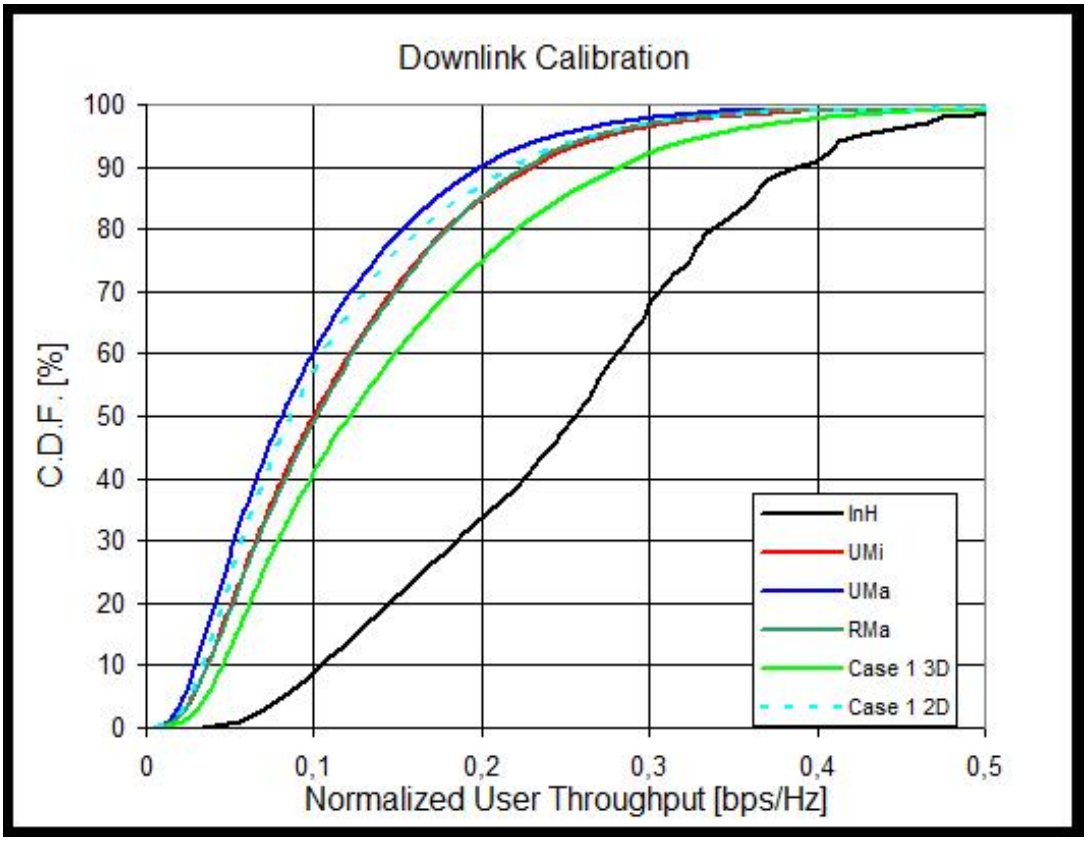

Figure 3.7: 3GPP TR36.8143 case 1 UE throughput CDF.

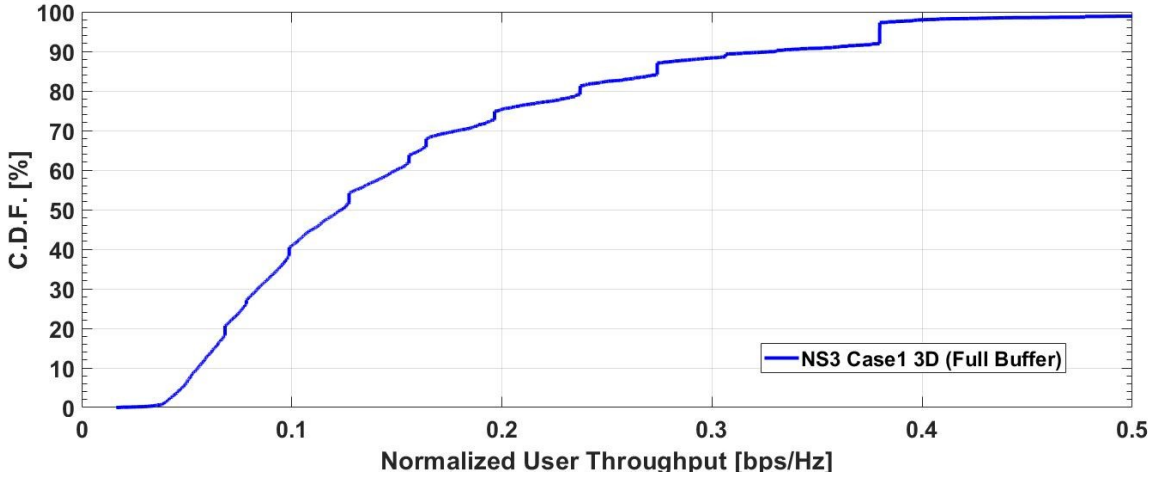

Figure 3.8: NS-3 UE throughput CDF.

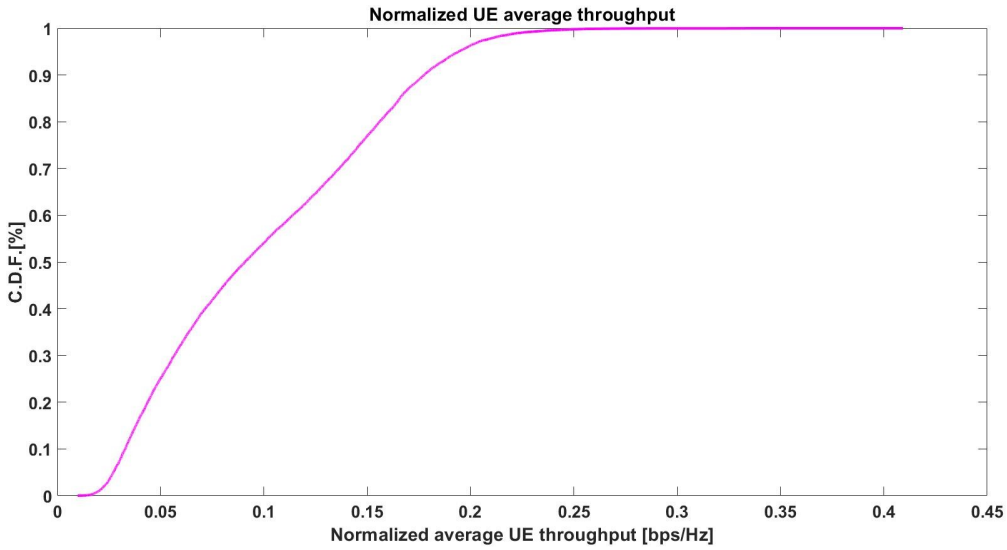

Figure 3.9: Vienna LTE-A downlink system level simulator UE throughput CDF.

Since the 3GPP results were only available through graphical format, the values were read off the graph as best as possible. SINR and throughput metrics for the Vienna and ns-3 simulations were extracted using the built in MATLAB Data Tips feature.

	3GPP	NS-3	Vienna
Cell Average SINR [dB]	10	10.08	10.44
Cell Edge SINR [dB]	2	1.21	-0.5072
Cell Average Throughput [bps/Hz]	0.1228	0.1235	0.09094
Cell Edge Throughput [bps/Hz]	0.037	0.0479	0.02719

Table 3.2: Verification system performance results.

Figures 3.4, 3.5, and 3.6 plot the 3GPP, ns-3, and Vienna UE average SINR CDFs. It can be noticed that the results from the Vienna system level simulator closely matches the 3GPP Case 1 3-D CDF (light green), with the exception for the bottom 10% UEs in terms of SINR. The bottom 10% UEs in the Vienna system level simulator experiences lower SINR than the ones in the 3GPP simulations. From Table 3.2, one can observe

that the Cell edge SINR from the Vienna system level simulator is lower than both ns-3 and 3GPP. One possible explanation could be from the antenna gain pattern used in the simulations. The antenna pattern used in Vienna system level simulator has a slightly narrower radiation pattern compared to the one used in ns-3 and specified in the 3GPP document, also the antenna gain value was not specified so it was left as default in the Vienna simulator. Therefore, at the cell edge, more UEs would have worse SINR due to the narrower antenna gain pattern. In the mid range of the CDF, results from both simulators are very close to the 3GPP reference scenario results. In the top range of the SINR CDF, the Vienna simulator produces results that matches the 3GPP reference results much closer than ns-3. The inaccuracy of the ns-3 results can be attributed to the fact that ns-3 does not have the function to allow the minimum distance between the UE and eNodeB to be set correctly.

Figures 3.7, 3.8, and 3.9 plot the 3GPP, ns-3, and Vienna UE throughput CDFs. It can be noticed that the CDFs produced by both the Vienna system level simulator and ns-3 network simulator has a very similar shape compared to the 3GPP reference results. However, for the Vienna system level simulator, the exact throughput values are consistently lower by about 30%. a closer look at the code determines that ns-3 multiplies the UE throughput values by 1.27 (14/11) to add the control bits on top of data bits, however the Vienna System Level simulator does not have such operation. On the other hand, the ns-3 simulator produces throughput CDF with similar value compared to 3GPP, however the plot shows a stepped pattern, this is due to the limited combinations of modulation and coding scheme and code block size; the plot produced by the Vienna system level simulator did not show this stepped pattern.

3.5 Simulator Comparison

Both simulators produced results that are close to the 3GPP reference scenario results. The Vienna simulator was slightly mismatched for the edge users, while ns-3 provided results that were slightly inaccurate with the UEs in the upper range of the CDF. For the purpose of this project, where the main concerns are the average and edge UEs, the results from ns-3 are more suitable for further analysis.

In terms of implementation, the Vienna simulator is more user-friendly since it is a simulator dedicated for the broadband system. The code is organized in a neat and clear way, with all the different objects sorted neatly in different folders. The code also includes a number of pre-configured examples that can be easily modified to match the 3GPP reference scenario. On the other hand, ns-3 is a much more complex network simulator that is not specific to the broadband system. Although there are a number of LTE specific examples, the actual code is much more involved and complex than Vienna, thus more time is required to configure the parameters. Secondly, since Vienna is written in MATLAB whereas ns-3 is written in C++, the code is much easier to understand and manipulate. In addition, the MATLAB environment also makes debugging quite simple compared to the Eclipse IDE used by ns-3.

Perhaps the biggest difference is in the performance of the two simulators. The Vienna simulator implements a very precise model of the physical layer, whereas ns-3 uses correspondence tables provided by the 3GPP LTE specification [33]. Therefore Vienna has to perform many more calculations that slows down the simulation. During the simulator validation process, it was noticed that the same simulation ran on the same computer would take Vienna approximately seven hours to complete, whereas ns-3 can finish the simulation within an hour and half with much less memory usage as well.

The final decision is to use ns-3 as the simulator for the evaluation of the additional opportunistic EL unicast service because of its more accurate results and faster simulation time. The project required simulating 154 different cases, thus using ns-3 would save

almost 900 hours of computation time. The implementation difficulty is also not an issue since the validation against the 3GPP reference scenario is already available and it can provide a good foundation to implement the opportunistic EL unicast service for this project.

Chapter 4

Simulation Set-up, Benchmark Scenarios, and Results

4.1 Simulation Environment and Assumptions

In this work, the effect of splitting transmission power on the unicast service is evaluated by computer simulations using the ns-3 LTE module. For the two-layer LDM system under consideration, the total transmission power is set to 40 Watts (46.0 dBm), power allocation between the broadcast and unicast services are controlled by the EL signal injection level. Tables 4.1 and 4.2 summarizes the power allocation of each layer under the considered injection levels. Note that when the injection level is expressed in dB scale, the convention is to omit the negative sign for simplicity. As an example, a injection level of 0.25 will be referred to as 6 dB instead of -6 dB.

Injection Level [dB]	CL Power Allocation [W]	EL Power Allocation [W]
4	28.61	11.39
5	30.39	9.61
6	31.97	8.03
8	34.53	5.47
10	36.36	3.64
13	38.09	1.91
16	39.02	0.98
19	39.50	0.50
22	39.75	0.25
26	39.90	0.10

Table 4.1: Power allocation of each layer, in watts.

Injection Level [dB]	CL Power Allocation [dBm]	EL Power Allocation [dBm]
4	44.57	40.57
5	44.83	39.83
6	45.05	39.05
8	45.38	37.38
10	45.61	35.61
13	45.81	32.81
16	45.91	29.91
19	45.97	26.97
22	45.99	23.99
26	46.01	20.01

Table 4.2: Power allocation of each layer, in dBm.

Simulations on the EL unicast network are based on the 3GPP reference scenarios specified in 3GPP TR36.814 [7], TR25.814 [8] and TR36.942 [9], two scenarios are considered: an urban macro set-up and a rural set-up. In both cases, the network consists of 19 cell sites arranged in a hexagonal grid set-up with three sectors at each site, as shown in Figure 4.1. The sites are arranged such that there is a single site in the center, one inner ring of 6 sites, and an outer ring of 12 sites, as shown in Figure 4.1, with the more detailed system configuration shown in Table 4.3.

Parameter	Value
Carrier Frequency	700 MHz
Uplink Bandwidth	10 MHz
Downlink Bandwidth	10 MHz
Downlink Transmission Scheme	1 x 2 SIMO FDD
Pathloss Model (Distance R in km)	Urban: $118.57 + 37.6 \cdot \log_{10}(R)$ Rural: $93.6 + 34.1 \cdot \log_{10}(R)$
Antenna Beamwidth	70°
Antenna Downtilt	Urban: 15° Rural: 6°
Antenna Height	Urban: 32 m Rural: 45 m
UE Height	1.5 m
UE Distribution	25 UEs/cell uniformly
UE speed	3 km/h
ISD	Urban: 500 m, 1 km, 2 km, 5km Rural: 5 km, 10 km, 15 km

Table 4.3: Simulation parameters.

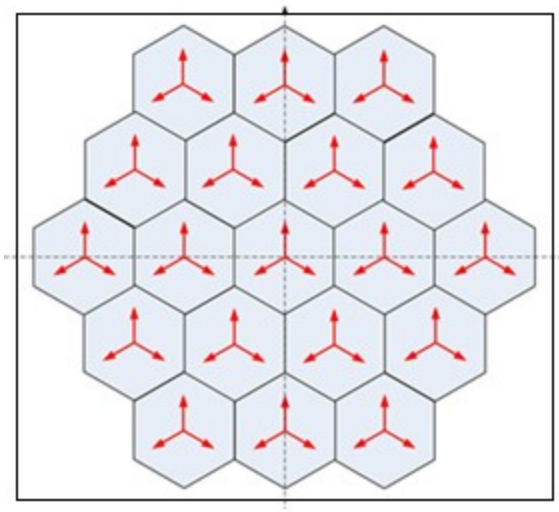

Figure 4.1: Cell layout for mixed unicast-broadcast simulations.

4.2 Configuring the ns-3 LTE Network Simulator

The simulation code was modified from the "System Level Evaluation and Validation of the ns-3 LTE Module in 3GPP Reference Scenarios" by [32]. Their program adapted the lena-dual-stripe example of the ns-3 LTE module to closely match the 3GPP TR36.814 reference scenarios and achieved very similar results in terms of users SINR and spectral efficiency.

A portion of the configurations for simulating the EL of an LDM scheme has already been done by the original lena-dual-stripe example and the adapted system validation code. For example, the location of the 19 cells have been configured in a 3-4-5-4-3 row setup in the rectangular region of interest (ROI) based on the cartesian coordinate system. The respective coordinates can easily scale to accommodate different ISD requirements for the urban and rural cases. The lena-dual-stripe example drops UEs uniformly in the ROI by specifying the number of UEs per square meter. For the simulation, a total of 1425 UE (25 UE/sector $\cdot$ 3 sectors/site $\cdot$ 19 sites) are dropped in the ROI with a uniform distribution, which will ensure an average of 25 UEs per sector. A number of

other parameters can also be configured using the LteHelper class, such as the antenna type, antenna beamwidth, scheduler, and the pathloss model parameters. The carrier frequency and uplink/downlink bandwidth can be set directly using the command line of the program by adjusting the Earfcn value and the ulBandwidth/dlBandwidth expressed in number of resource blocks.

Each power level and ISD combination is simulated using a total of 30 iterations, with independent random UE drops between each iteration. At the end of each iteration, data on the UEs from the within the inner ring are collected (7 sites, 21 sectors), while the outer 12 sites are only used for interference purposes. At the end of the simulation, the SINR and throughput information from the $25 \cdot 3 \cdot 7 \cdot 30 = 15{,}750$ independent UEs are collected and plotted as CDFs. This chapter will only present and discuss these plots. The cell average SINR, cell edge SINR, cell average throughput, cell edge throughput, as well as the average total cell throughput (total average of an entire cell, measured in Mbps) will be extracted from the plots and analyzed in the following chapters.

4.3 Results of Benchmark Scenarios

In order to properly assess the capacity gain of the lower powered additional opportunistic EL unicast service, a suitable benchmark is defined as the performance metrics of a typical single layer unicast-only service with full transmission power (46.0 dBm or 40 W). Simulations of the benchmark is performed for the urban scenario with ISD of 500 m, 1 km, 2 km, and 5 km, as well as rural scenario with ISD of 5 km, 10 km, and 15 km. The remaining of this section presents the UE average SINR CDFs and UE throughput CDFs for the benchmark scenarios in graphical form. The cell average SINR, cell edge SINR, cell average throughput, cell edge throughput, as well as the average total cell throughput for the benchmark scenarios will also be presented in table form to be used in the next chapters.

4.3.1 Urban Benchmark scenario Results

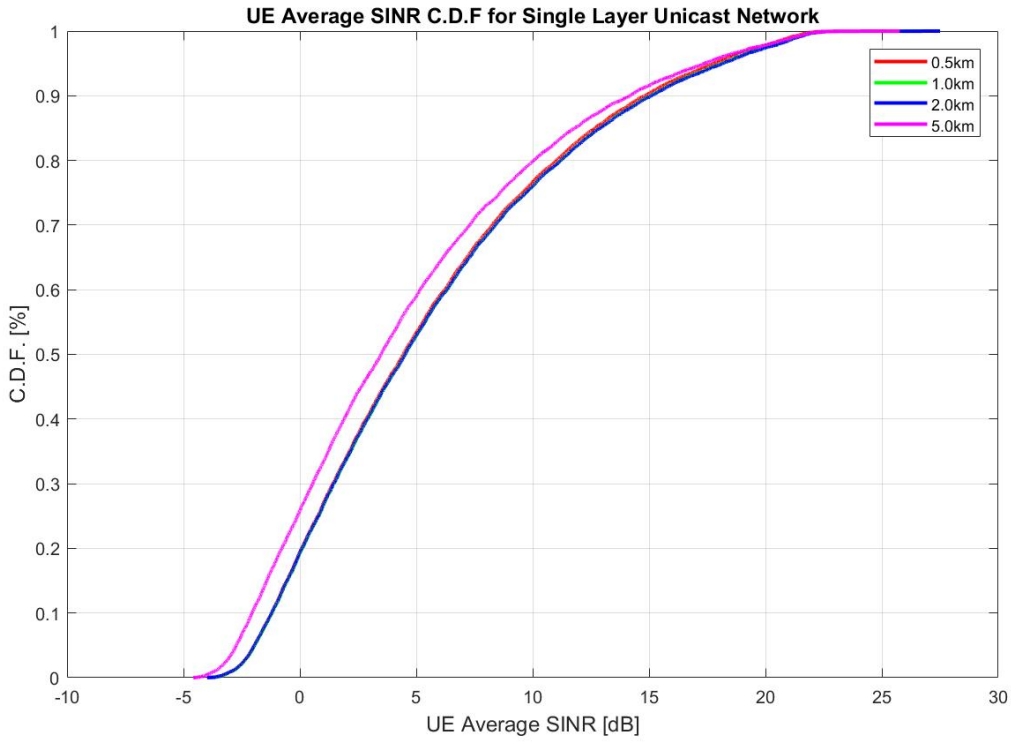

Figure 4.2: Urban UE average SINR for single layer unicast service.

Figure 4.2 plots the UE average SINR CDF for a benchmark single layer urban unicast service at ISD of 500 m, 1 km, 2 km, and 5 km transmitting at 46 dBm and configured according to Table 4.3. The plot shows that the benchmark unicast service performs consistently for ISD of 500 m, 1 km, and 2 km, however as the distance between base stations increases to 5 km, the SINR experienced by the UEs become worse. This can be observed from the plot since the UE average SINR CDF for ISD of 500 m, 1 km, and 2 km almost overlap each other, however at 5 km, the SINR shows slightly degraded values. The cell average SINR and cell edge SINR are read from the graph and summarized in Table 4.4. It can be observed that the cell average and cell edge SINR for cases with ISD of 500 m, 1 km, and 2 km are almost identical at 4.5 dB and -1.9 dB respectively, while for the 5.0 km case is only able to achieve 3.5 dB and -2.7 dB.

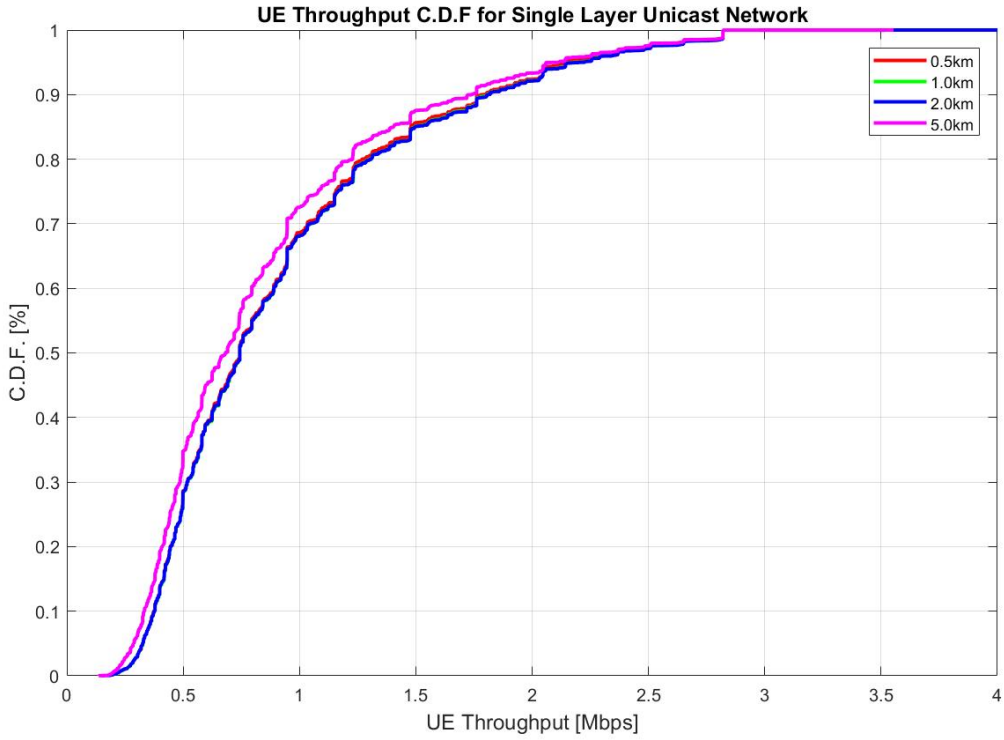

Figure 4.3: Urban UE throughput for single layer unicast network.

Figure 4.3 plots the corresponding UE Throughput CDF for a benchmark single layer urban unicast service at ISD of 500 m, 1 km, 2 km, and 5 km. For the 500 m, 1 km, and 2 km cases, since the SINR CDFs are mostly overlapping, their corresponding throughput CDFs are almost identical as well. On the other hand, the throughput CDF for when ISD is 5 km is slightly lower compared to the others, which is expected based on the SINR plot above. The cell average throughput and cell edge throughput are read from the graph and summarized in Table 4.4. The cell average and cell edge throughputs for cases with ISD of 500 m, 1 km, and 2 km are almost identical at 0.74 Mbps/UE and 0.33 Mbps/UE respectively, while the 5 km case is only able to achieve 0.68 Mbps/UE and 0.29 Mbps, approximately 90% of the capacity of the other case. For each of the 21 sectors that were evaluated, the average total cell throughput for the 500 m, 1 km, and 2 km cases are approximately 18.6 Mbps, whereas for the 5 km case decreases to

17.2 Mbps.

ISD	500 m	1 km	2 km	5 km
Cell Average SINR [dB]	4.448	4.533	4.522	3.477
Cell Edge SINR [dB]	-1.961	-1.935	-1.955	-2.722
Cell Average Throughput [Mbps/UE]	0.7433	0.7433	0.7433	0.6818
Cell Edge Throughput [Mbps/UE]	0.3258	0.3258	0.3258	0.2867
Average Total Cell Throughput [Mbps]	18.6347	18.6183	18.6239	17.2113

Table 4.4: Benchmark simulation results for urban EL unicast service.

4.3.2 Rural Benchmark scenarios Result

When the ISD is extended to beyond 5 km for the rural scenario, Figure 4.4 plots the UE average SINR CDF for a benchmark single layer rural unicast service at ISD of 5 km, 10 km, and 15 km transmitting at 46 dBm and configured according to Table 4.3. The plot shows that for the rural scenario, the single layer unicast service is able to provide consistent service for ISD ranging from 5 km up to 15 km as the UE SINR CDF for ISD of 5 km, 10 km, and 15 km mostly overlap each other. The cell average SINR and cell edge SINR are read from the graph and summarized in Table 4.5. It can be observed that the cell average and cell edge SINR for scenarios with ISD of 5 km, 10 km, and 15 km are almost identical at 3.6 dB and -2.3 dB respectively.

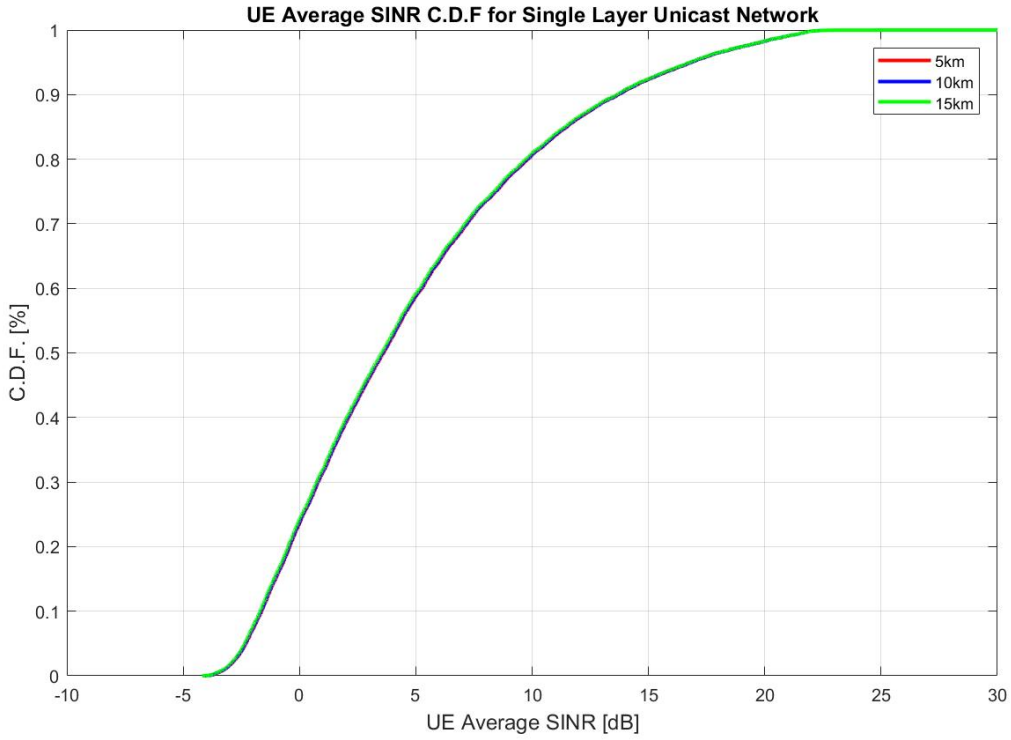

Figure 4.4: Rural UE average SINR for single layer unicast network.

Figure 4.5 plots the corresponding UE Throughput CDF for a single layer unicast service at ISD of 5 km, 10 km, and 15 km. For the rural cases, since their SINR CDFs are almost identical, it is within expectation that their throughput CDFs are almost identical as well. The cell average throughput and cell edge throughput are read from the graph and summarized in Table 4.5. These cell average and cell edge throughput values, for cases with ISD of 5 km, 10 km, and 15 km are almost identical at 0.7 Mbps/UE and 0.3 Mbps/UE respectively. For each of the 21 sectors that were evaluated, the average total cell throughput for the 5 km, 10 km, and 15 km cases are approximately 18 Mbps.

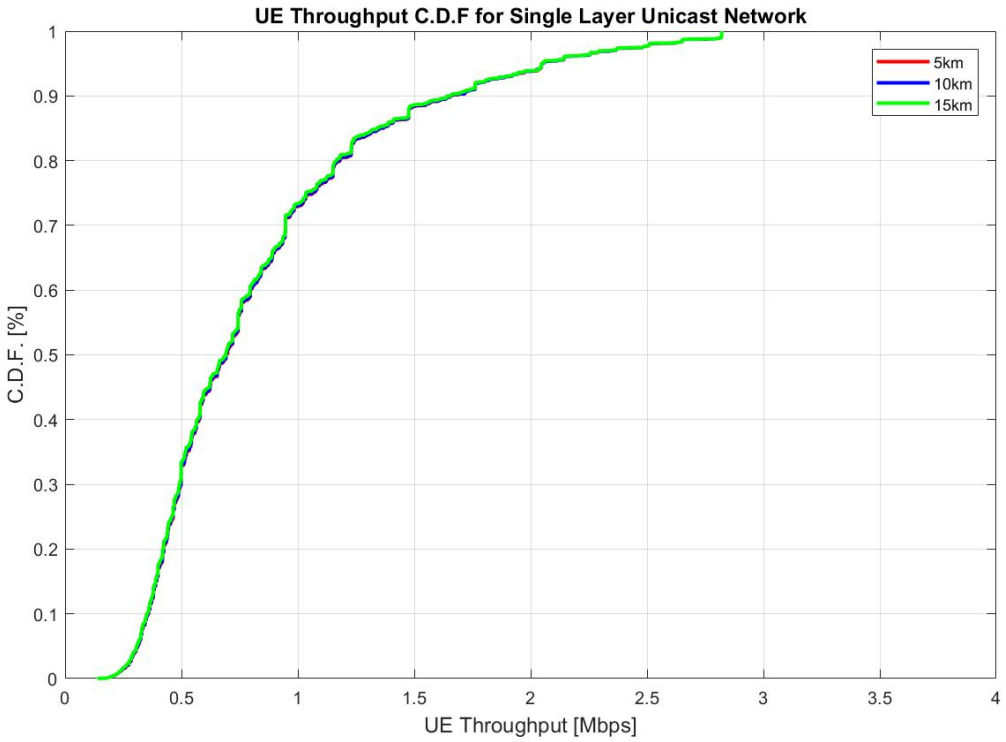

Figure 4.5: Rural UE throughput for single layer unicast network.

ISD	5 km	10 km	15 km
Cell Average SINR [dB]	3.632	3.607	3.521
Cell Edge SINR [dB]	-2.295	-2.312	-2.369
Cell Average Throughput [Mbps/UE]	0.6912	0.6912	0.6911
Cell Edge Throughput [Mbps/UE]	0.3134	0.3093	0.3076
Average Total Cell Throughput [Mbps]	17.1186	17.0877	16.9864

Table 4.5: Benchmark simulation results for rural EL unicast service.

Chapter 5

Simulation Results of the Opportunistic EL Unicast Service

This chapter presents the performance of the additional opportunistic EL unicast network. For each ISD, i.e. 500 m, 1 km, 2 km, and 5 km in the urban scenario, as well as 5 km, 10 km, and 15 km in the rural scenario, the UE average SINR CDF and UE throughput CDF of the EL unicast service at injection levels ranging from 4 dB to 26 dB are presented in graphical form. For each of the cases with different ISD, the impact of various injection levels on the capacity of the EL unicast service is observed and discussed.

5.1 UE Average SINR and Throughput of Urban Scenarios

5.1.1 UE Average SINR and Throughput for 500 m ISD

Figure 5.1 shows the UE average SINR CDF for the additional opportunistic unicast service delivered by the EL at injection levels between 4 dB and 26 dB where the ISD is set to 500 m. Injection levels up to 26 dB does not affect the SINR experienced by the

UE. The ability of the small ISD network to withstand strong injection levels can also be observed from Figure 5.2, where for injection levels from 4 dB up to 26 dB, the UE throughput CDF are also nearly identical, suggesting that increasing injection levels will not affect the UE's throughput in this specific case.

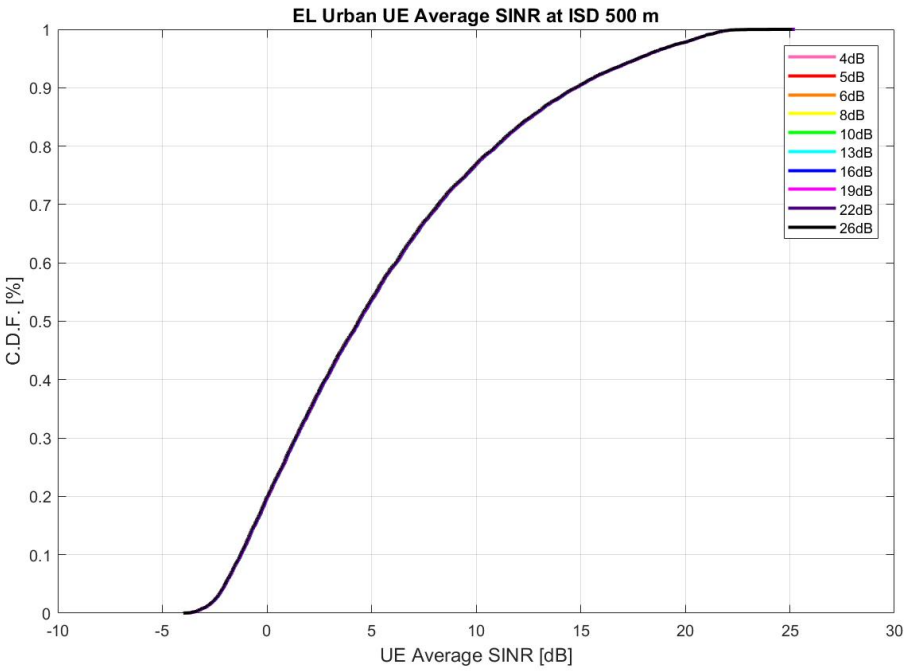

Figure 5.1: Urban UE average SINR for 500 m ISD at various injection levels.

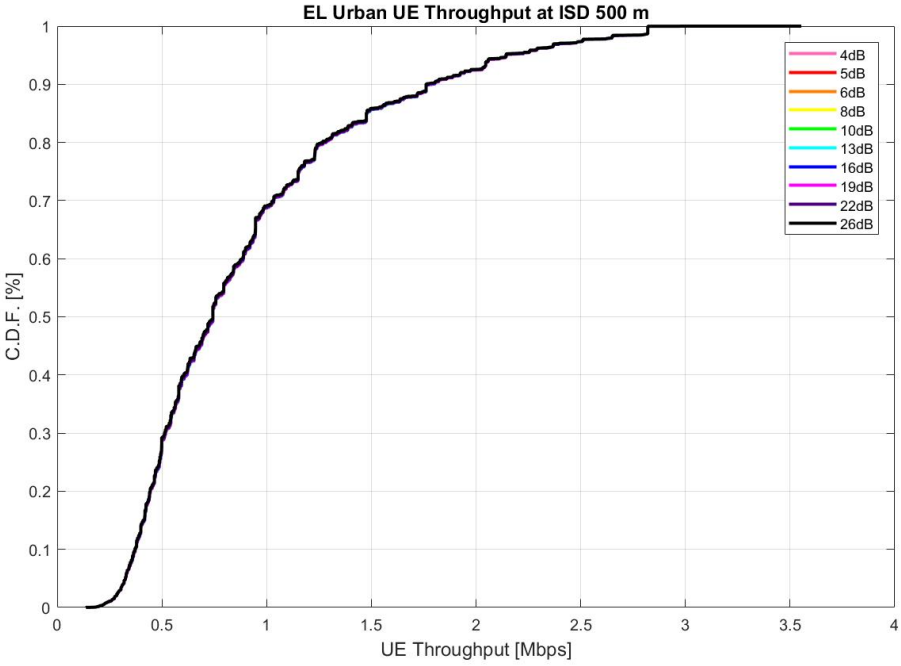

Figure 5.2: Urban UE throughput for 500 m ISD at various injection levels.

5.1.2 UE Average SINR and Throughput for 1 km ISD

Increasing the ISD to 1 km yields very similar results as the 500 m case. Figures 5.3 and 5.4 show the UE average SINR CDF and UE throughput CDF of the opportunistic EL unicast service. As a result of the increased ISD, performance degradation at extremely high injection levels begins to be evident. The plots reveal that the SINR and throughput experienced by the UE does not vary much for injection levels between 4 dB and 22 dB, however once the injection level reaches 26 dB, the UE average SINR and throughput shows a slight but visible decrease.

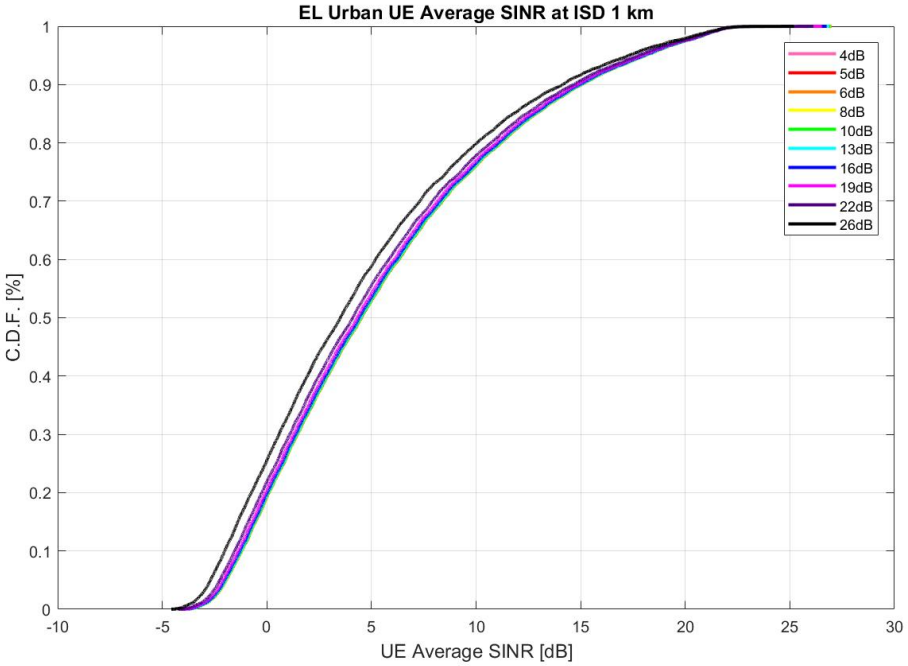

Figure 5.3: Urban UE average SINR for 1 km ISD at various injection levels.

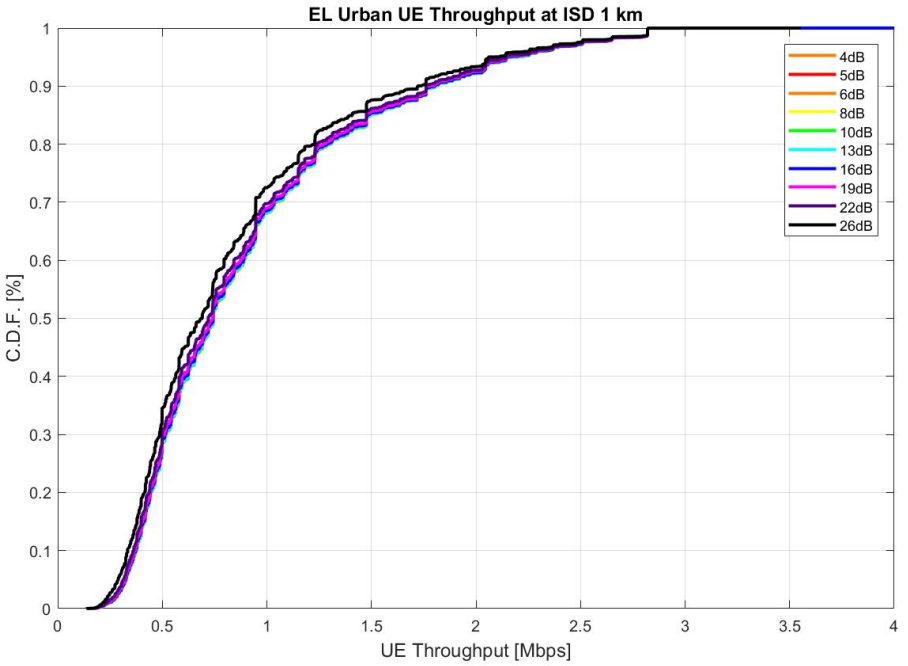

Figure 5.4: Urban UE throughput for 1 km ISD at various injection levels.

5.1.3 UE Average SINR and Throughput for 2 km ISD

The effect of increasing injection levels is more severe as the ISD becomes larger. Figures 5.5 and 5.6 show the UE average SINR CDF and UE throughput CDF of the EL unicast service when ISD is 2 km. Unlike previous cases where a relatively small ISD can provide a degree of robustness against high injection levels, in the 2 km ISD case, the SINR an throughput experienced by the UE decreases gradually as the injection level is increased. The UE average SINR and UE throughput stay fairly close to the benchmark for injection levels up to 16 dB, and then becomes visibly lower as the injection level increases to 19 dB and beyond.

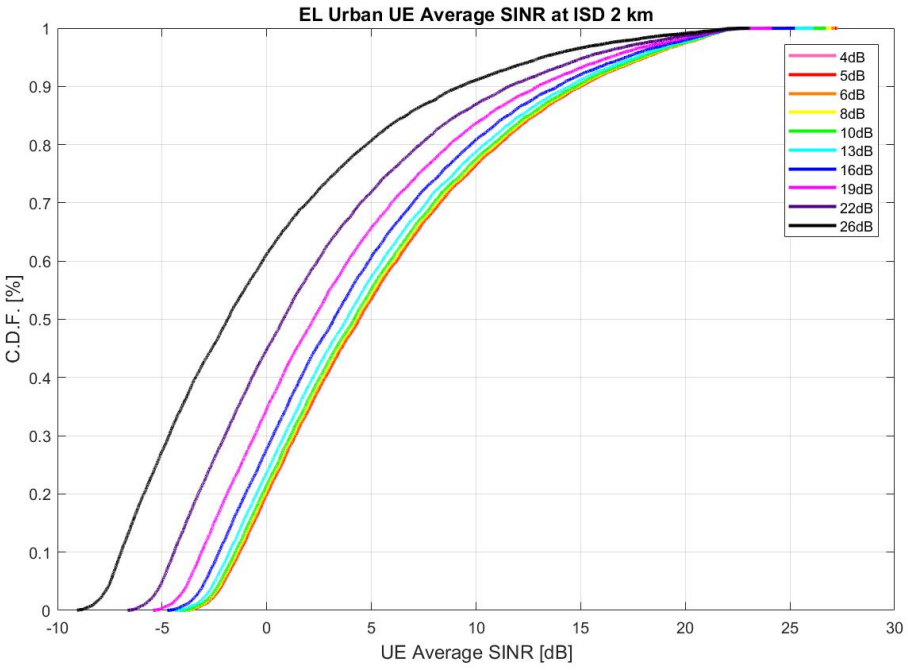

Figure 5.5: Urban UE average SINR for 2 km ISD at various injection levels.

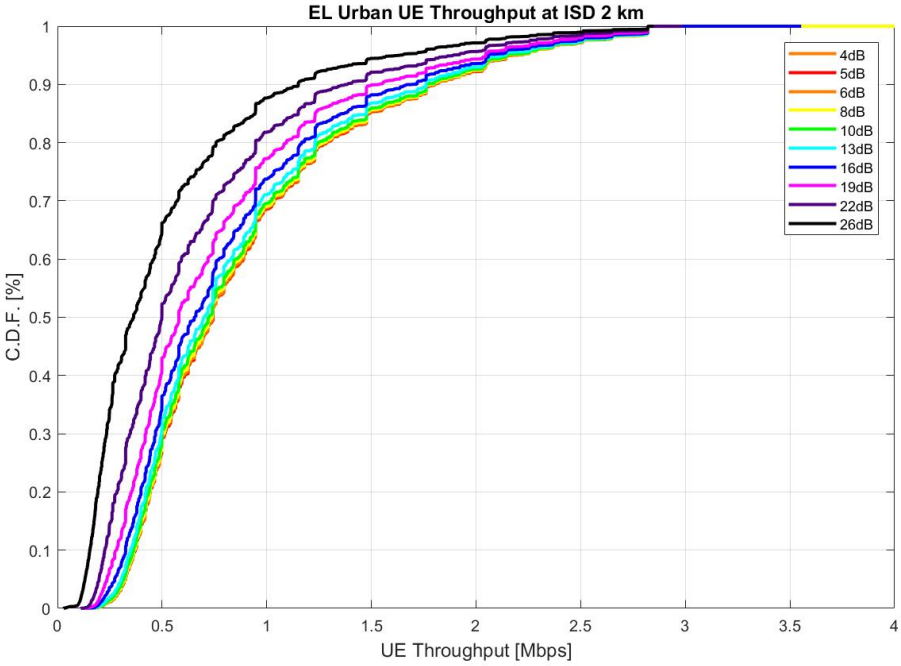

Figure 5.6: Urban UE throughput for 2 km ISD at various injection levels.

5.1.4 UE Average SINR and Throughput for 5 km ISD

When the ISD is even further increased to 5 km, simulation results suggest the EL is no longer suitable for delivering unicast service in an urban environment under strong injection levels. Figure 5.7 shows the UE average SINR CDFof the additional opportunistic EL unicast service for the case when ISD is 5 km. It is clear from the figure that the SINR experienced by the UE decreases dramatically as the injection level increases from 5 dB to 26 dB. The plot indicates that for injection levels 16 dB (blue), 19 dB (magenta), 22 dB (purple), and 26 dB (black), a significant number of UE are getting SINR values lower than -10 dB. The UE throughput CDF plotted in Figure 5.8 shows that for injection levels beyond 13 dB, i.e. 16 dB, 19 dB, 22 dB, and 26 dB lines, approximately 18%, 40%, 57%, and 73% of the UEs are not allocated with any throughput. This is expected as the transmission sites are further apart, the UEs located far from any base station will experience very poor signal reception.

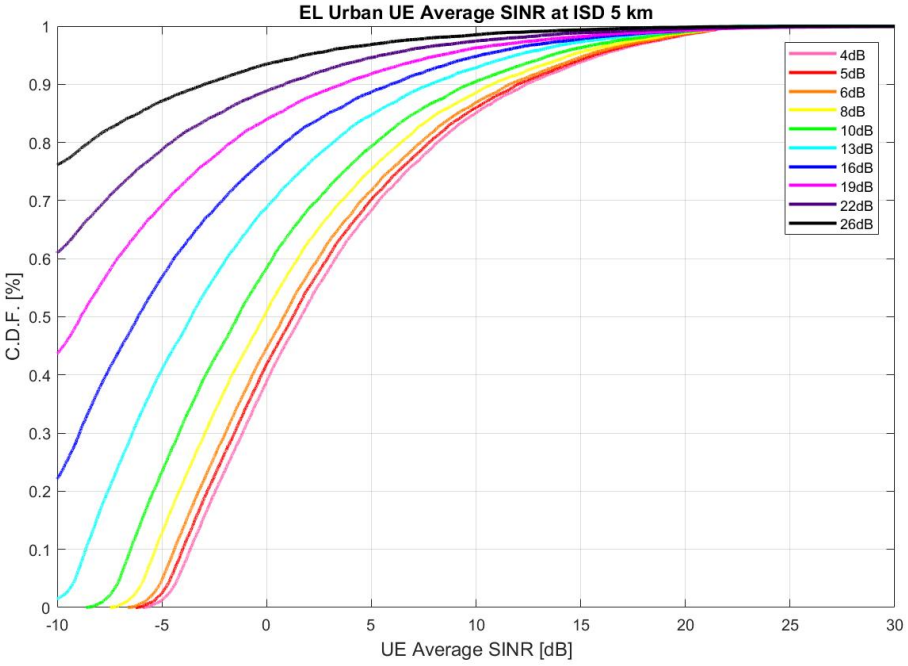

Figure 5.7: Urban UE average SINR for 5 km ISD at various injection levels.

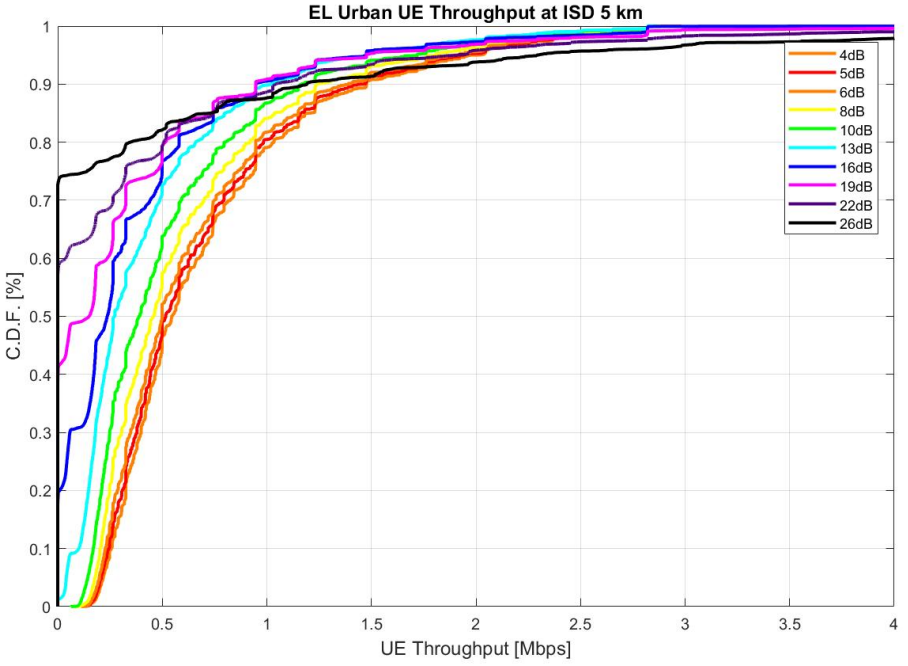

Figure 5.8: Urban UE throughput for 5 km ISD at various injection levels.

5.2 UE Average SINR and Throughput of Rural Scenarios

5.2.1 UE Average SINR and Throughput for 5 km ISD

Figures 5.9 and 5.10 show the UE average SINR CDF and UE throughput CDF for the additional opportunistic EL unicast service at injection levels between 4 dB and 26 dB for a rural case with 5 km of ISD. From the SINR and throughput CDF plots, it can be observed at an ISD of 5 km, unlike the urban case, the EL is able to provide unicast service in a rural environment at extremely high injection levels. The plots show that reduced transmission power due to the injection levels from 4 dB up to 22 dB has almost no effect on the SINR and throughput experienced by the UE as the CDFs are very closely together. Only when the injection level is increased to 26 dB does the UE average SINR and UE throughput decrease by a slight amount.

As previously mentioned, although the EL is only able to provide limited service in an urban scenario when the ISD is 5 km, in a rural scenario with the same ISD, the EL is much more robust against signal degradation due to increased injection levels. This is caused by the more favourable transmission conditions associated with the rural scenario such as the increase in antenna height, reduction of antenna down tilt, and less severe rural propagation pathloss.

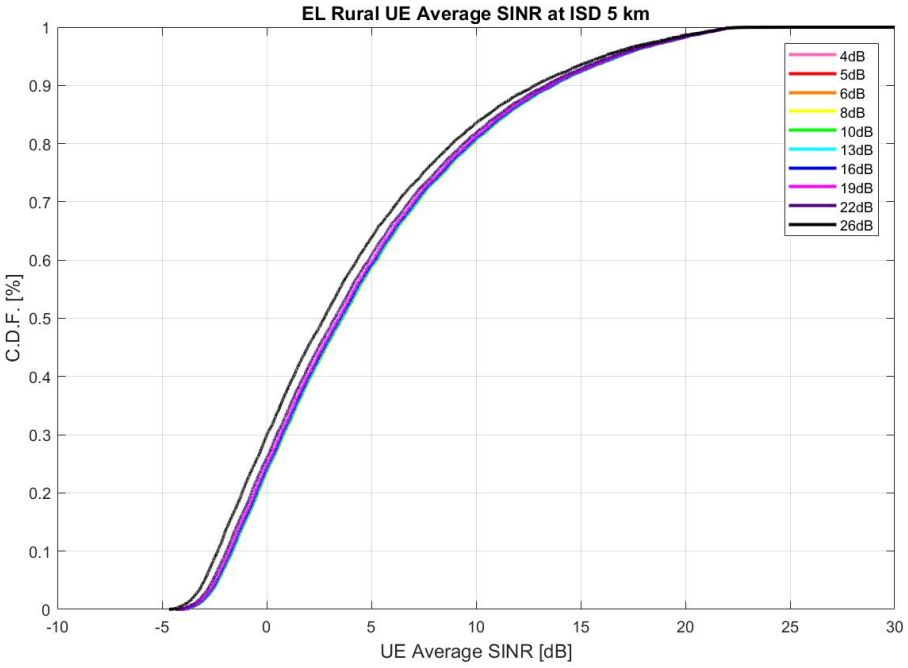

Figure 5.9: Rural UE average SINR for 5 km ISD at various injection levels.

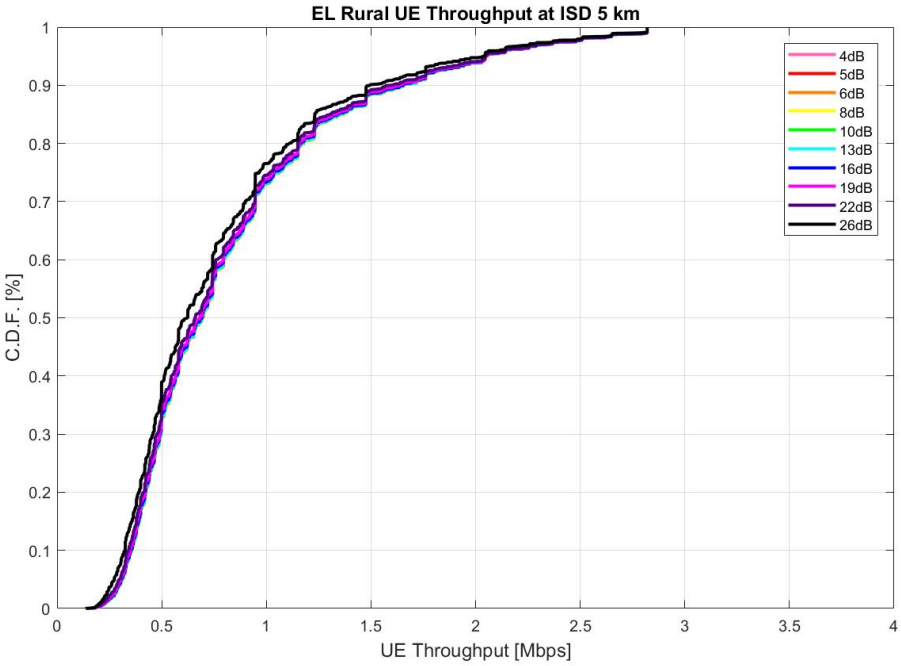

Figure 5.10: Rural UE throughput for 5 km ISD at various injection levels.

5.2.2 UE Average SINR and Throughput for 10 km ISD

When the ISD is increased to 10 km, the effect of increasing injection levels becomes more pronounced. Figures 5.11 and 5.12 show the UE average SINR CDF and UE throughput CDF of the opportunistic EL unicast service when the ISD is 10 km. As can be expected, the SINR and throughput experienced by the UE now decreases gradually as the injection level is increased. Injection levels under 16 dB yields similar SINR and throughput closely resembling the benchmark single layer service. However for injection levels 19 dB and above, a noticeable decrease can be observed.

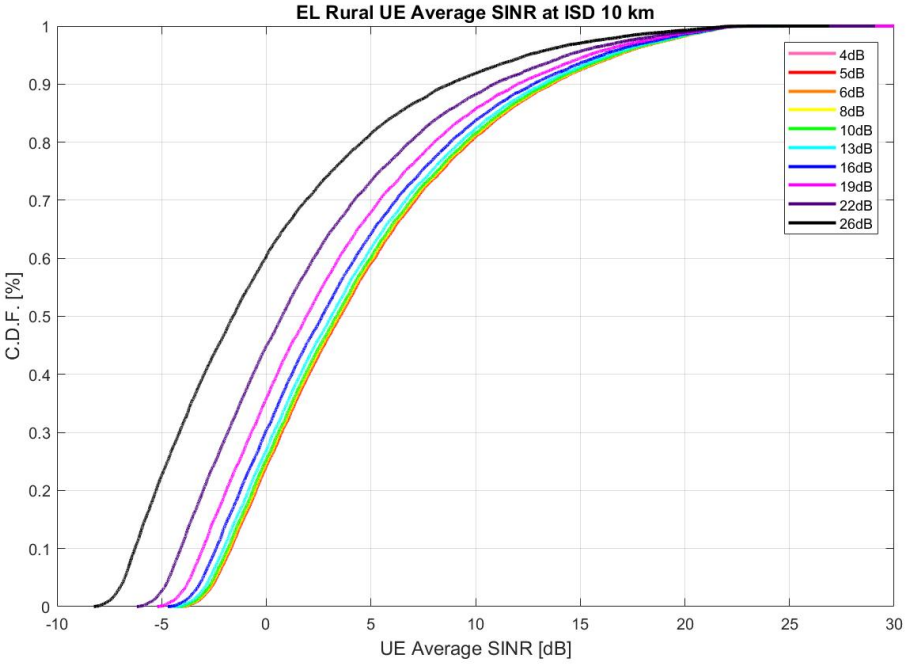

Figure 5.11: Rural UE average SINR for 10 km ISD at various injection levels.

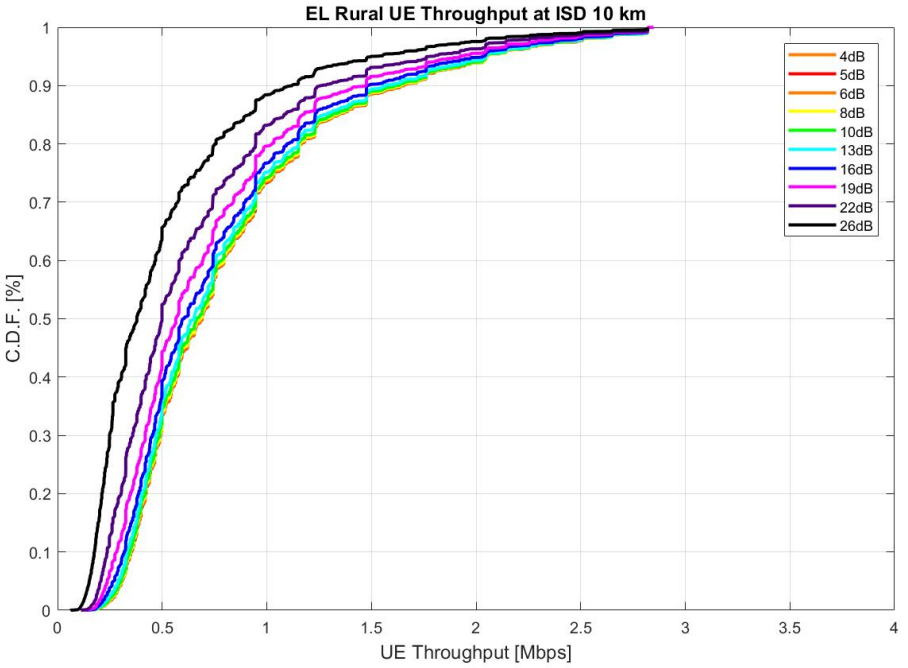

Figure 5.12: Rural UE throughput for 10 km ISD at various injection levels.

5.2.3 UE Average SINR and Throughput for 15 km ISD

When the ISD is even further increased to 15 km, simulation results indicate that the EL service is still suitable for unicast service delivery for injection level as high as 22 dB. Figure 5.13 shows the UE average SINR CDF of the EL unicast service, the SINR experienced by the UE strongly mimics the benchmark for injection levels up to 10 dB, then decreases dramatically as the injection level becomes stronger. The UE throughput CDF plotted in Figure 5.14 shows that as the injection level rises above 10 dB, the UE throughput suffers greatly. All injection levels are able to provide service to the entire system, with the exception of injection level 26 dB, where approximately 17% of the UE are not allocated with any throughput.

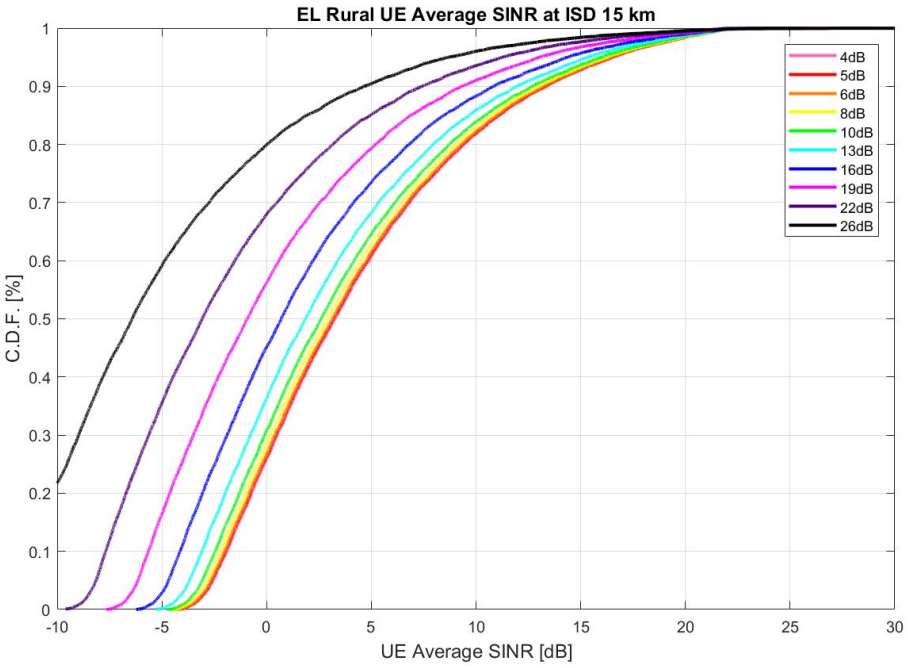

Figure 5.13: Rural UE average SINR for 15 km ISD at various injection levels.

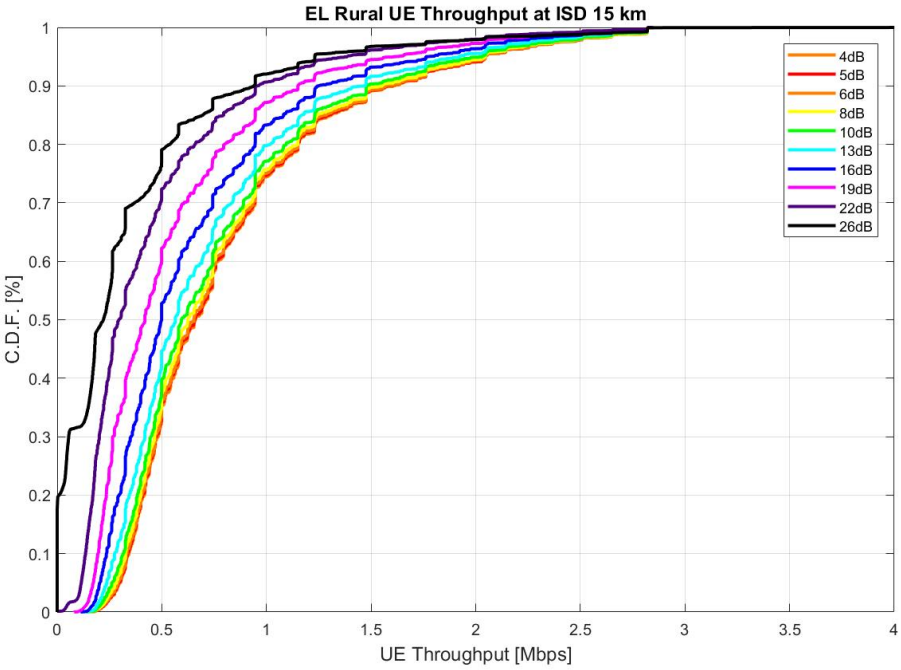

Figure 5.14: Rural UE throughput for 15 km ISD at various injection levels.

Chapter 6

Analysis and Discussion

In this chapter, the relevant performance metrics including the cell average SINR, cell edge SINR, cell average throughput, cell edge throughput, and average total cell throughput for each ISD and injection level combination are extracted from the plots shown in Chapter 5. These results are plotted and analyzed to determine the impact of various injection levels on the capacity of the additional opportunistic EL unicast service. Where applicable, trade-offs between higher injection levels and service capacity are discussed. Finally, recommendations are provided on suitable injection levels for each scenario.

6.1 Performance Analysis of Urban Scenarios

6.1.1 Performance Analysis for 500 m ISD

For the urban scenario with ISD of 500 m, Figure 6.1 shows the cell average and cell edge SINR of the opportunistic EL unicast service as a function of injection levels. The values on the y-axis are the cell average SINR and cell edge SINR of the benchmark single layer unicast service. The solid line illustrates the cell average SINR as a function of injection level from 4 dB to 26 dB, while the dashed line shows the cell edge SINR as a function of injection level from 4 dB to 26 dB. The plot shows that due to the small ISD

considered in this case, the cell average SINR and cell edge SINR of the opportunistic EL unicast service are essentially the same compared to the benchmark single layer unicast service. More specifically, injection levels of 4, 5, 6 and 8 dB cause no degradation in the cell average and cell edge SINR. As the injection level increases to 26 dB, the cell average SINR decreases by approximately 0.1 dB, whereas the cell edge SINR drops by only 0.05 dB.

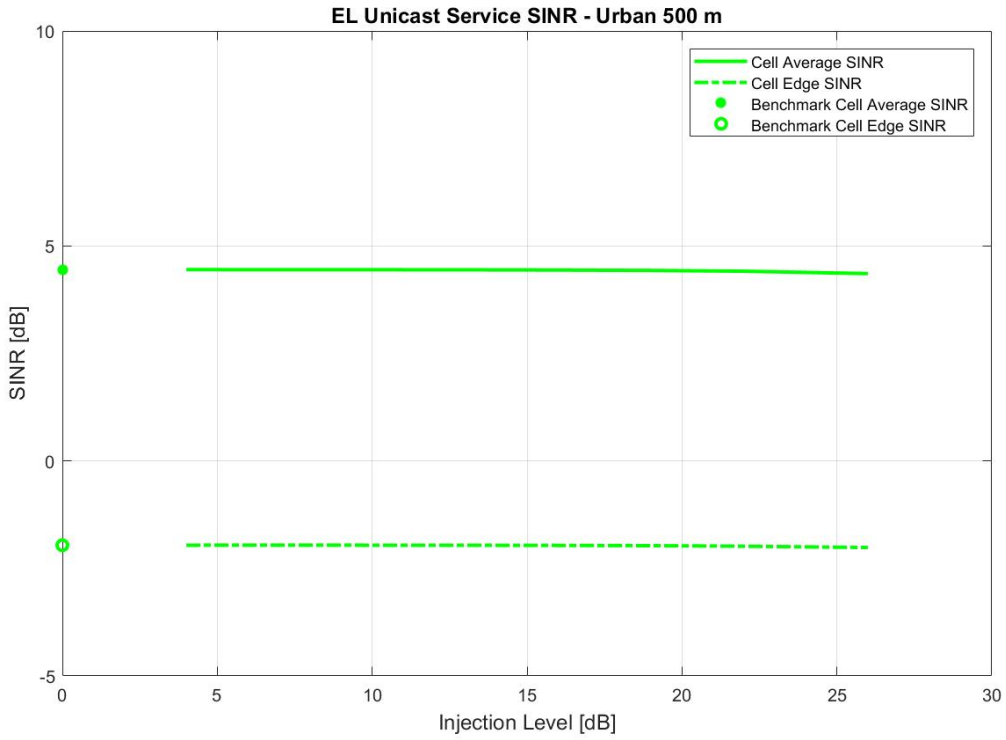

Figure 6.1: Urban 500 m ISD EL unicast service SINR.

Figure 6.2 show the cell average throughput and cell edge throughput for the range of injection levels of interest for the urban 500 m ISD case. The cell average and cell edge throughput values for the benchmark single layer unicast service is plotted on the y-axis. The solid line illustrates the cell average throughput as a function of injection level from 4 dB to 26 dB, while the dashed line shows the cell edge throughput as a function of injection level from 4 dB to 26 dB. The plot shows that the cell average throughput and

cell edge throughput is constant for the entire range of injection levels simulated for this report.

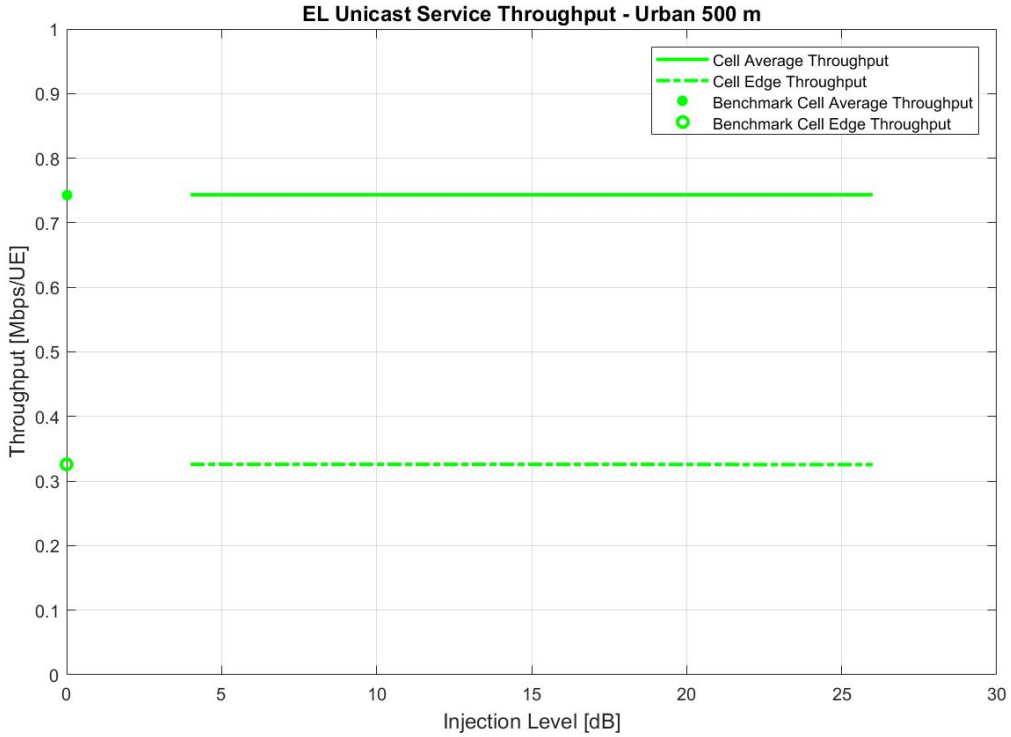

Figure 6.2: Urban 500 m ISD EL unicast service throughput.

The average total cell throughput for the EL unicast service at 500 m ISD confirms the finding. Figure 6.3 shows the average total cell throughput of the opportunistic EL unicast service as a function of injection levels. The values on the y-axis is average total cell throughput of the benchmark single layer unicast service, and the solid line shows the average total cell throughput as a function of injection levels from 4 dB to 26 dB. It can be observed that similar to the cell average and cell edge throughput, the average total cell throughput is almost constant with values almost identical the the benchmark single layer unicast service. More specifically, injection levels as high as 22 dB can still retain at least 18.381 Mbps of total cell throughput, corresponding to approximately 99% of the benchmark cell throughput capacity. Even for the highest injection level considered in

this investigation of 26 dB, the EL unicast network is still able to obtain more than 98% of the total cell throughput capacity compared to the benchmark single layer service.

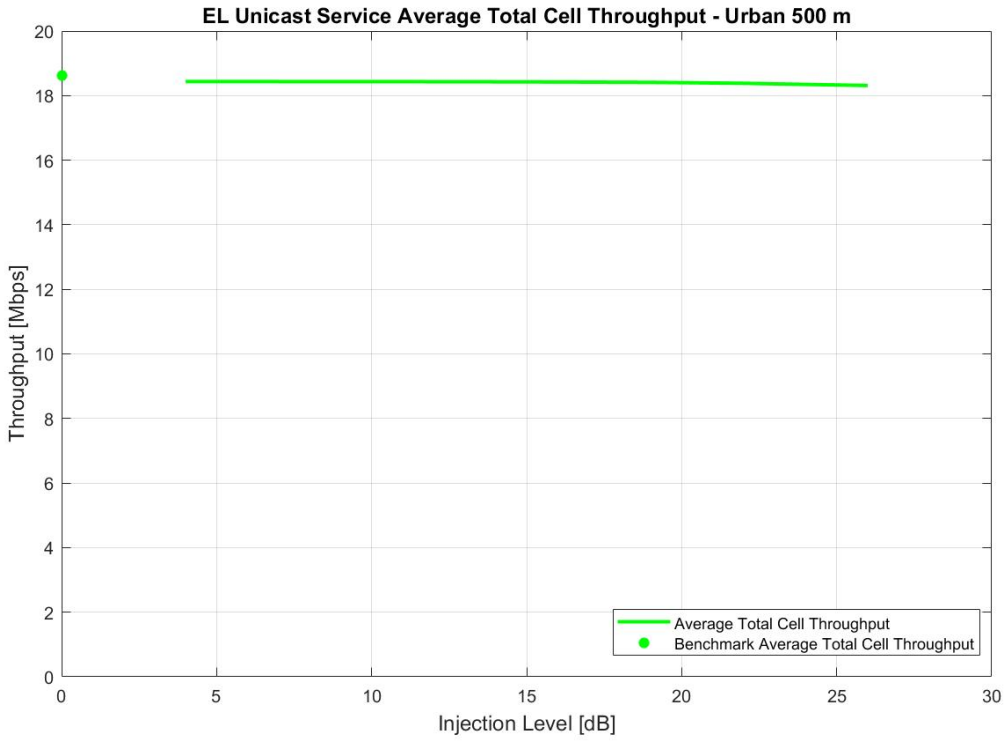

Figure 6.3: Urban 500 m ISD EL unicast service average total cell throughput.

These results suggest that in situations where the ISD is small such as the 500 m case, transmission power of 40 W is much higher than needed, 0.25 W can be used to sustain an additional EL unicast network with throughput that matches a single layer unicast network transmitting at full power. Therefore, injection levels up to 26 dB can be used for mixed unicast-broadcast service delivery in an urban environment where the ISD is 500 m.

6.1.2 Performance Analysis for 1 km ISD

The cell average SINR and cell edge SINR of the opportunistic EL unicast service for the case of 1 km ISD in an urban environment as a function of injection levels are plotted

in Figure 6.4. Again, the respective SINR values for the benchmark single layer unicast service is also plotted on the y-axis. It can be observed that the cell average SINR and cell edge SINR of the EL unicast service shows a similar behaviour as the 500 m case. Some typical injection levels of 4, 5, 6, 8, and 10 dB cause the cell average SINR to decrease by no more than 0.03 dB. The cell average SINR begins to decrease more visibly as the injection level increases further, at an injection level of 19 dB, the cell average SINR drops by 0.227 dB. The cell average SINR drops more rapidly as injection level increases to 26 dB, where the cell average SINR decreases by 1.022 dB to 3.511 dB. The cell edge SINR shows a similar trend, where it remains within 0.02 dB of the benchmark edge SINR for typical injection levels up to 10 dB. It only drops by 0.17 dB at injection level of 19 dB, and then starts to drop off more rapidly to -2.689 dB, for a total degradation of 0.75 dB.

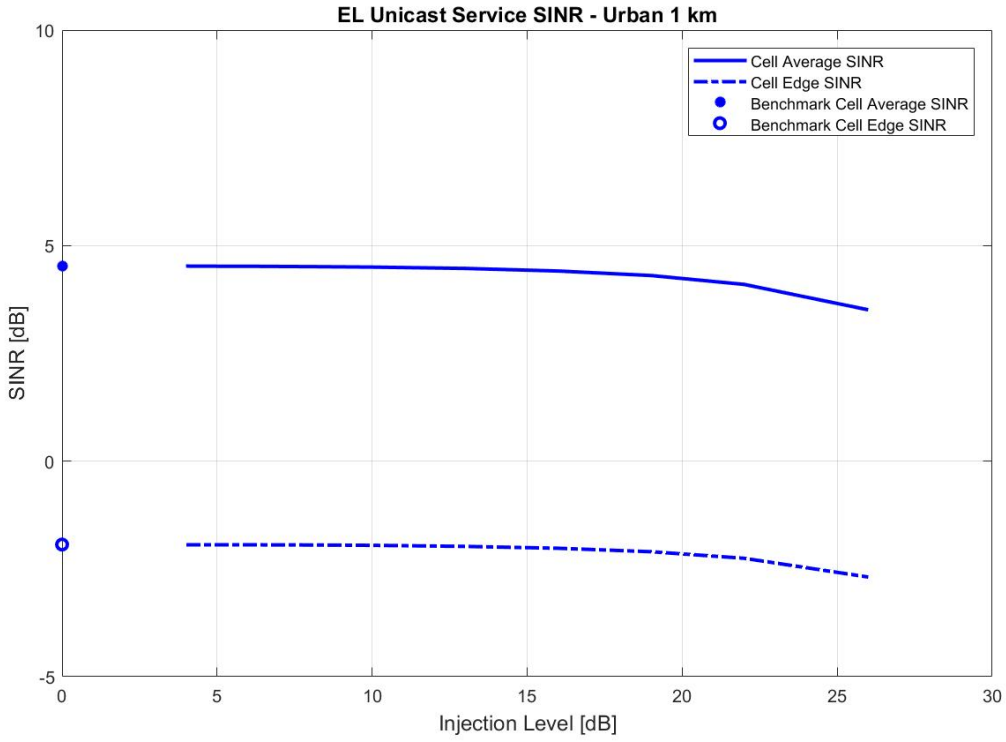

Figure 6.4: Urban 1 km ISD EL unicast service SINR.

For the urban 1 km ISD case, Figure 6.5 shows the cell average throughput and cell edge throughput with respect to the range of injection levels mentioned above. The respective throughput values for the benchmark single layer unicast service is also plotted on the y-axis. The plot shows that the cell average throughput is consistent with the benchmark single layer unicast service for injection levels up to 13 dB, and even at injection level of 19 dB, the EL is still able to keep more than 99% of the value. If the capacity requirement can be relaxed, then at an injection level of 26 dB, the EL can retain approximately 93% of the throughput. Similarly, the cell edge throughput also matches the benchmark case for injection levels up to 13 dB. At injection level of 19 dB, the EL is still able to retain 98% of the cell edge throughput. Finally at 26 dB, the EL then drops off to 89% of the benchmark edge throughput.

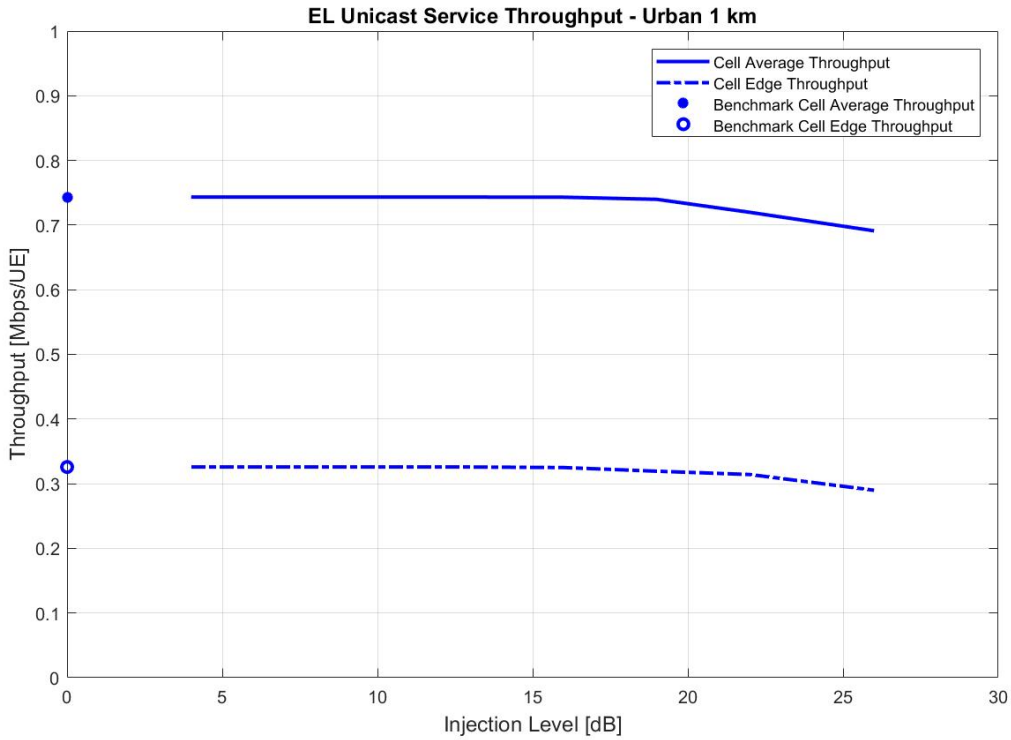

Figure 6.5: Urban 1 km ISD EL unicast service throughput.

The promising performance of the EL unicast service based on cell average throughput

and cell edge throughput can also be seen in terms of the average total cell throughput. Figure 6.6 shows the average total cell throughput as a function of injection levels for the additional opportunistic unicast service provided by the EL. From the plot, the EL can retain 100% of the total cell throughput for injection levels as high as 13 dB. Injection levels of 16, 19, 22, and 26 dB will reduce the total average cell throughput by 0.79%, 1.6%, 3.1%, and 7.5%, respectively.

These results indicate that for ISD of 1 km, injection levels of up to 13 dB can be used on the EL to support an additional unicast service with throughput that matches a single layer unicast service, or the injection level can be as high as 19 dB for very similar results. If the requirement on throughput can be relaxed, approximately 90% of the single layer unicast network throughput can still be achieved with 26 dB of injection level.

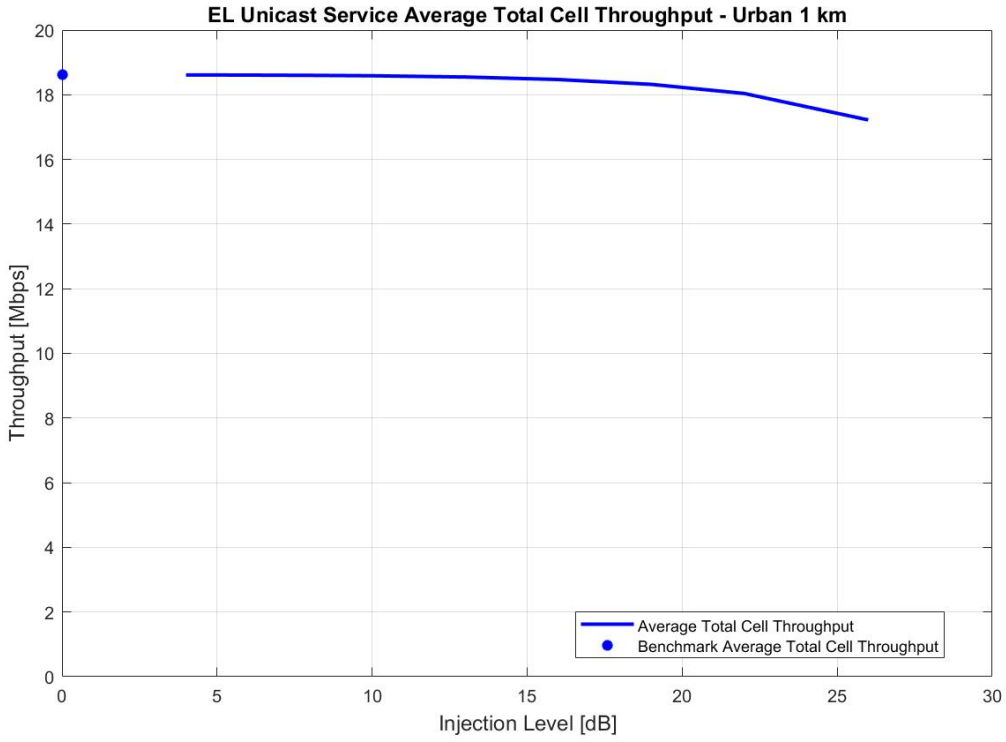

Figure 6.6: Urban 1 km ISD EL unicast service average total cell throughput.

6.1.3 Performance Analysis for 2 km ISD

For the urban scenario with ISD of 2 km, Figure 6.7 shows the cell average and cell edge SINR of the opportunistic EL unicast service as a function of injection levels. When the injection level is small, the cell average and cell edge SINR of the EL unicast service is comparable to those of the single layer unicast service. More specifically, injection levels of 4, 5, 6, 8 and 10 dB reduce the cell average SINR by only 0.10, 0.13, 0.16, 0.24 and 0.37 dB, respectively. The cell edge SINR data shows a similar trend, where the same injection levels cause the cell edge SINR values to decrease by 0.07, 0.09, 0.11, 0.17 and 0.27 dB, respectively. These small reductions indicate that for typical injection levels in an urban environment, the EL can provide unicast service to UEs without any significant signal degradation.

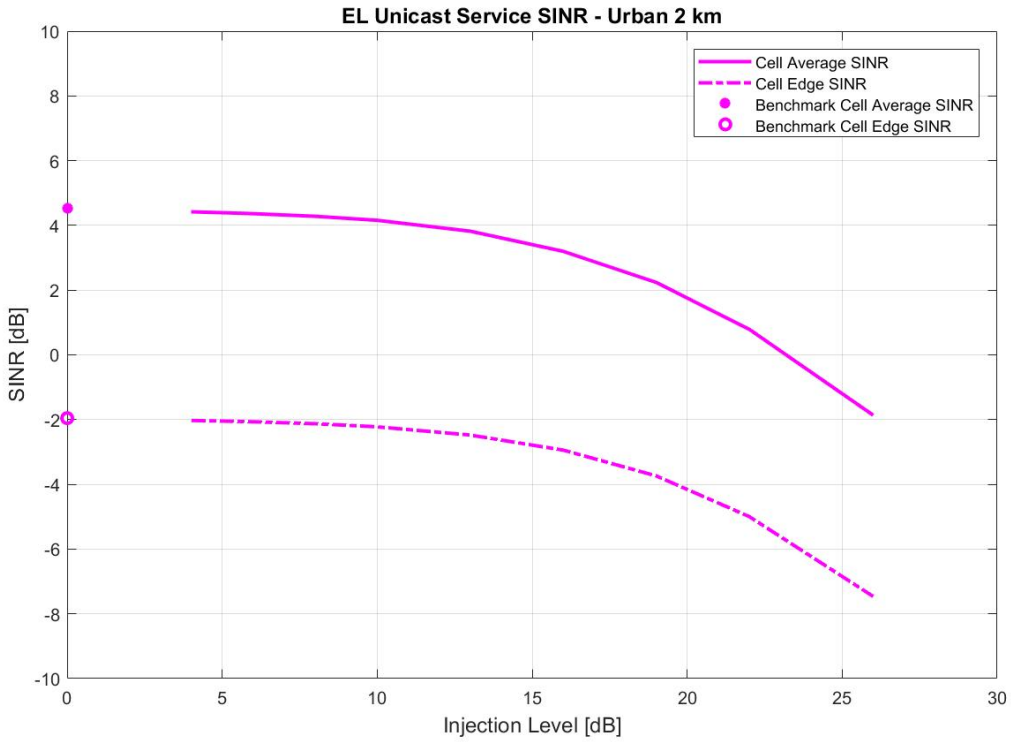

Figure 6.7: Urban 2 km ISD EL unicast service SINR.

The effect of injection levels on the EL unicast service is more apparent when ana-

lyzing the throughput rates. Figure 6.8 shows the cell average throughput and cell edge throughput as functions of injection levels. For the aforementioned injection levels, the cell average and cell edge throughput of the EL unicast service can achieve throughput that nearly matches the performance of a single layer unicast service provided at full power. For injection levels between 4 and 10 dB, the EL service can preserve at least 97% of the capacity in terms of cell average throughput, and 98% of the capacity in terms of cell edge throughput, offering a near full-capacity additional unicast service. If the requirement for capacity can be further relaxed, even if the injection level increases to 19 dB, the EL unicast service is still able to provide 78% and 73% of cell average and cell edge throughput rates, respectively. At the injection level 26 dB, then the EL unicast service can still provide 49% and 40% of cell average and cell edge throughput.

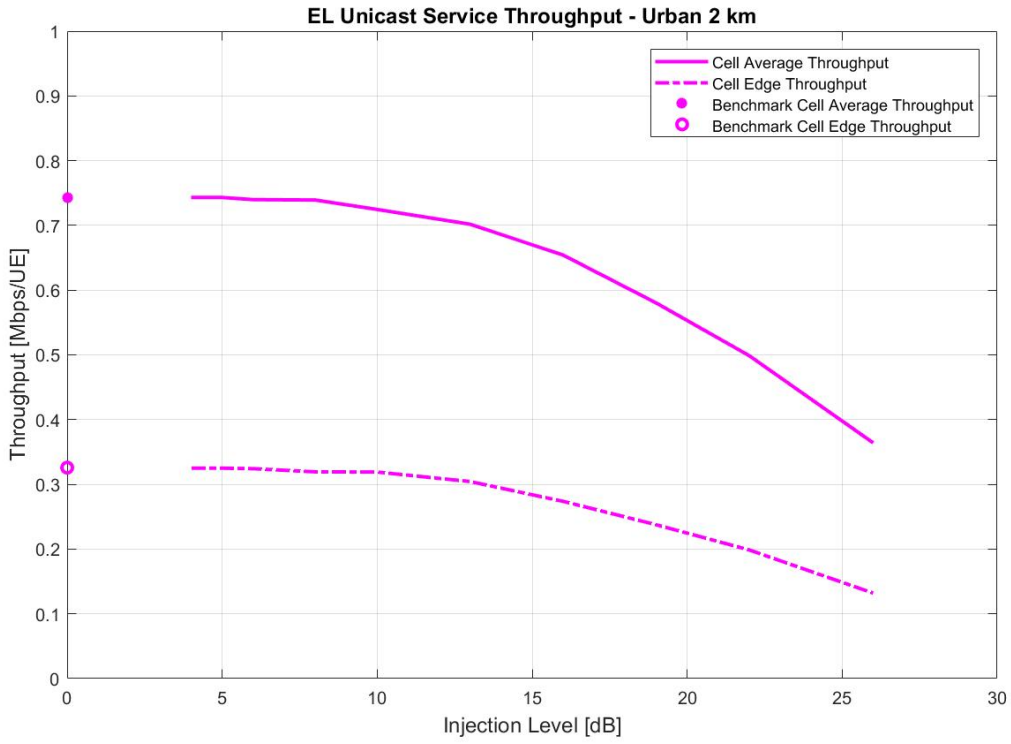

Figure 6.8: Urban 2 km ISD EL unicast service throughput.

Figure 6.9 shows the average total cell throughput as a function of injection levels for

the additional opportunistic unicast service provided by the EL. It can be observed that for injection levels of 4, 5, 6, 8, and 10 dB, the total cell throughput only decreases by 0.7%, 0.9%, 1.2%, 1.7%, and 2.7%, respectively. Thus once again showing that for typical injection levels, the EL is able to provide an additional unicast service with capacity that is comparable to a full network. As the injection levels continued to increase to 19 dB, the EL is still able to provide 15.5 Mbps of throughput per cell, corresponding to preserving 83% of the cell capacity. Even if the injection level is increased to 26 dB, the EL unicast network is still able to obtain a throughput 10.7 Mbps/cell, corresponding to approximately 58% of the original throughput capacity.

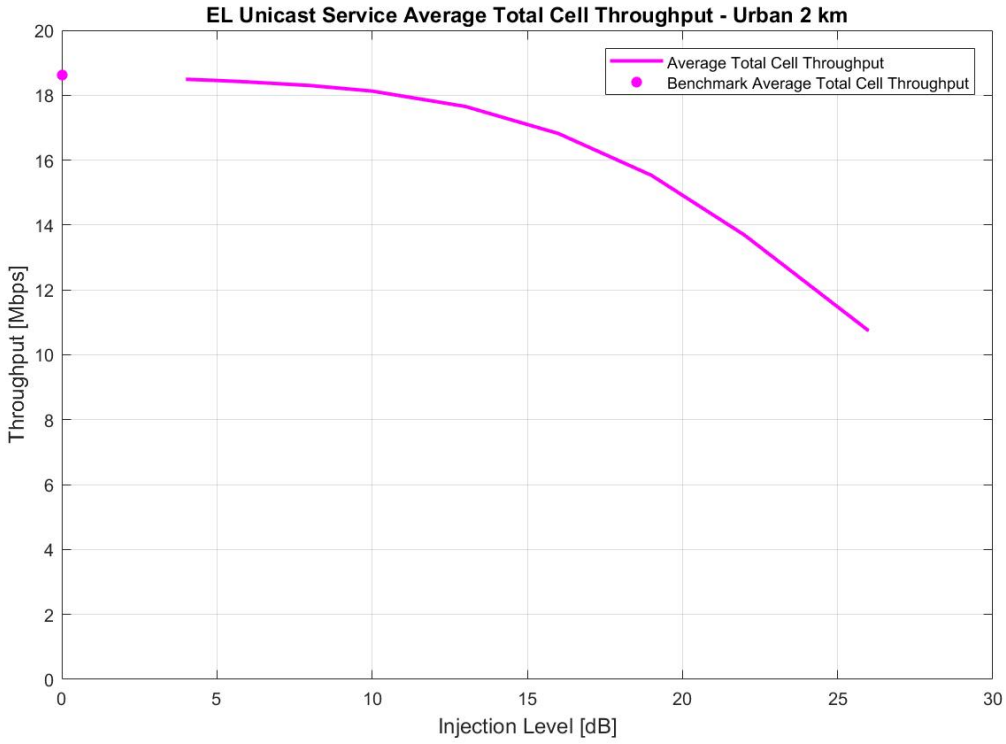

Figure 6.9: Urban 2 km ISD EL unicast service average total cell throughput.

6.1.4 Performance Analysis for 5 km ISD

For 5 km ISD case, the cell average SINR and cell edge SINR of the EL unicast service as a function of injection levels are plotted in Figure 6.10. As seen in the previous chapter, due to the extremely large ISD for an urban environment, the EL service suffers from significant signal degradation. Observations can be made that within the typical range, injection levels of 4, 5, 6, 8 and 10 dB cause the cell average SINR to decrease by 1.8, 2.2, 2.7, 3.6, and 4.9 dB, respectively. As the injection level increases beyond 19 dB, more than 50% of the UE are not being serviced by the base station due to the weak signal strength. A similar story can be said about the cell edge SINR, Injection levels of 4, 5, 6, 8 and 10 dB reduce the cell edge SINR by 1.5, 1.9, 2.3, 3.1 and 4.3 dB, respectively. If the injection level is increased beyond 13 dB, then the edge users cannot be serviced due to the weak signal. This suggests that in an urban environment, the EL can only provide reliable unicast service when the injection level is kept small.

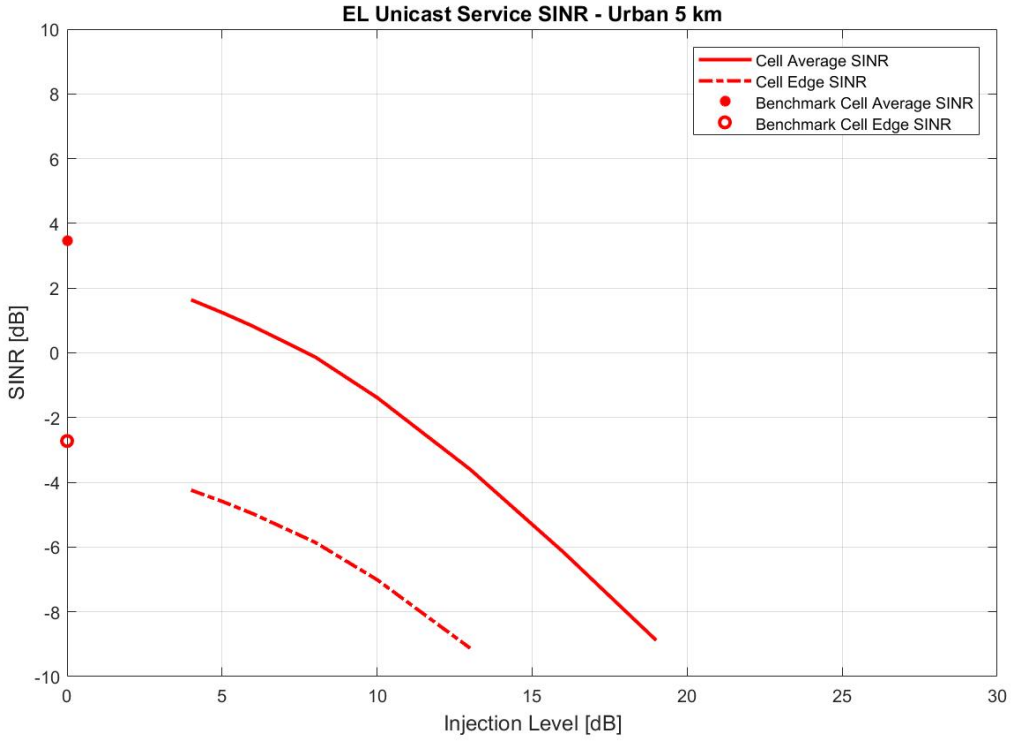

Figure 6.10: Urban 5 km ISD EL unicast service SINR.

The cell average and cell edge throughput as a function of injection levels for an urban environment at 5 km ISD is shown in Figure 6.11. The plot confirms the observation earlier. For selected typical injection levels of 4, 5, 6, 8 and 10 dB, the EL can achieve cell average throughput 80%, 76%, 73%, 67%, and 57% of the benchmark cell average throughput. At the same time, the same injection levels causes the cell edge throughput to only reach 76%, 73%, 69%, 62%, and 50% of the benchmark service. The highest feasible injection level for the 5 km case is 13 dB, where the system can still provide service to the edge users. The cell edge throughput at 13 dB injection level is only 0.04134 Mbps/UE, approximately 15% of the throughput capacity compared to the benchmark network.

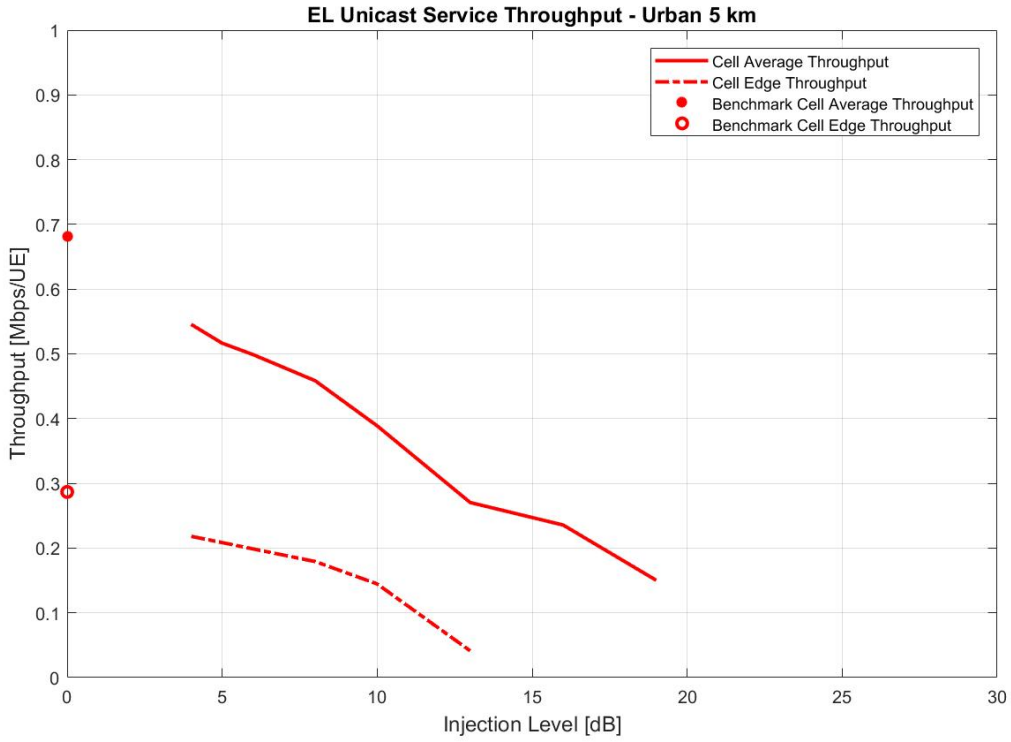

Figure 6.11: Urban 5 km ISD EL unicast service throughput.

The average total cell throughput as a function of injection levels for the additional opportunistic EL unicast service is shown in Figure 6.12. For the feasible injection levels of 4, 5, 6, 8, 10 and 13 dB, the EL can only achieve 86%, 83%, 80%, 73%, 65%, and 53% of the benchmark single layer unicast service, respectively. A conclusion can be made that for the urban case with 5 km ISD, the EL can no longer provide a near full capacity network due to the large ISD and relatively low signal strength. If full capacity is not a requirement, then the EL can provide service with throughput that is as high as 86% of a single layer network, or only half the capacity for a maximum injection level of 13 dB if the injection level must be kept high.

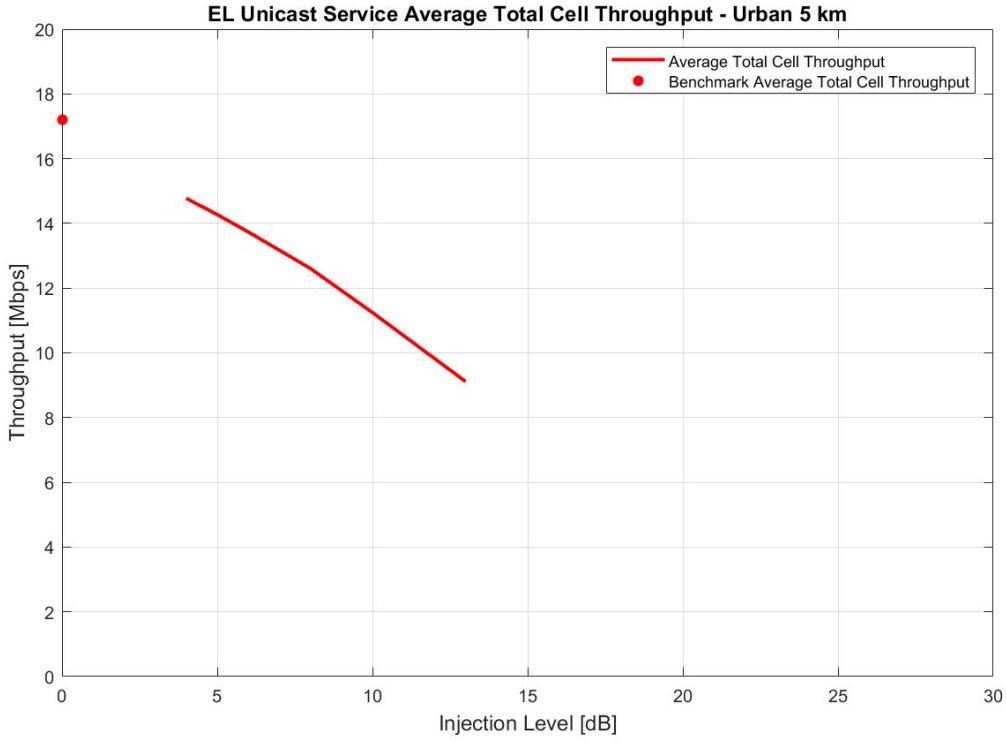

Figure 6.12: Urban 5 km ISD EL unicast service average total cell throughput.

6.2 Performance Analysis of Rural Scenarios

6.2.1 Performance Analysis for 5 km ISD

As illustrated previously, Figure 6.13 shows the cell average and cell edge SINR of the additional opportunistic EL unicast service as a function of injection levels for a rural case with an ISD of 5 km. The values on the y-axis are the cell average SINR and cell edge SINR values of the benchmark single layer unicast service. The solid line illustrates the cell average SINR as a function of injection level from 4 dB to 26 dB, while the dashed line shows the cell edge SINR as a function of injection level from 4 dB to 26 dB. It can be observed that the system indeed performs much better than an urban scenario with the same ISD. Typical injection levels up to 10 dB cause the cell average SINR to decrease by up to 0.027 dB. Even when the injection level is increased to 19 dB, the cell average SINR only drops by 0.205 dB to 3.427 dB. Beyond this point, the cell average SINR decreases more visibly, at injection level 26 dB, the cell average SINR becomes 2.731 dB, a total of 0.901 dB lower than the benchmark case. The cell edge SINR shows a similar trend, where it remains within 0.018 dB of the benchmark edge SINR for typical injection levels up to 10 dB, it stays fairly constant until an injection level of 19 dB where the value only drops by 0.143 dB, and then starts to drop off more visibly to -2.972 dB, for a total degradation of 0.66 dB.

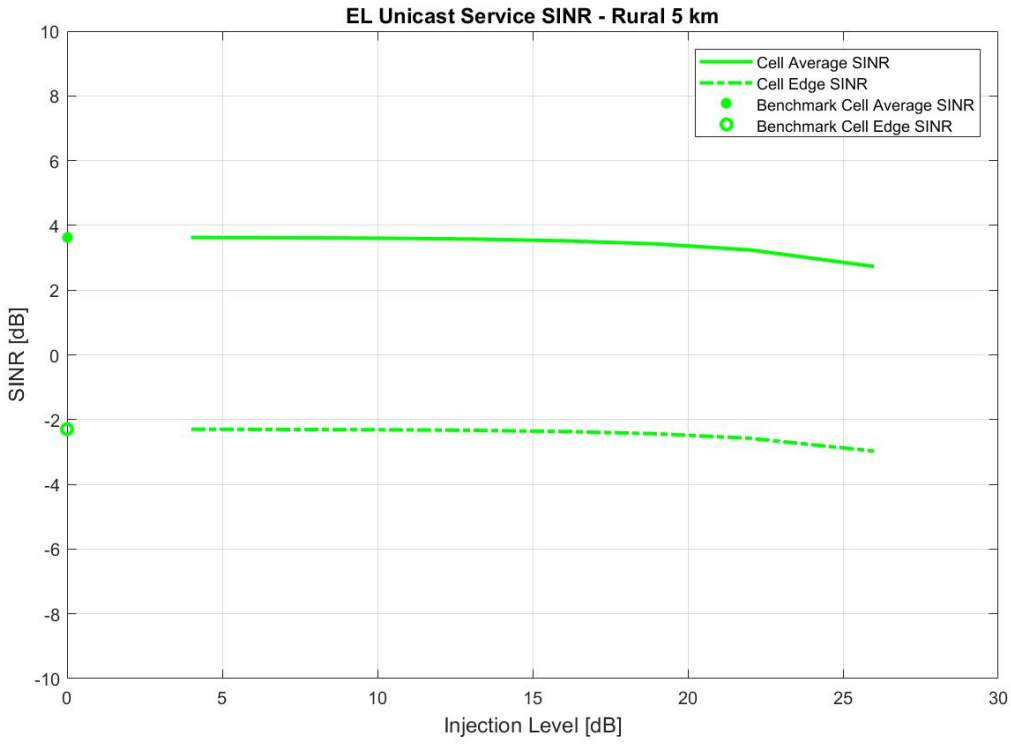

Figure 6.13: Rural 5 km ISD EL unicast service SINR.

Figure 6.14 shows the cell average throughput and cell edge throughput with respect to the range of injection levels mentioned above for the 5 km ISD rural case. Same as before, the respective throughput values for the benchmark single layer unicast service is plotted on the y-axis, the solid line illustrates the cell average throughput as a function of injection level from 4 dB to 26 dB, while the dashed line shows the cell edge throughput as a function of injection level from 4 dB to 26 dB. The plot shows that the cell average throughput is consistent with the benchmark single layer unicast service for injection levels up to 13dB, and even at injection level of 19 dB, the EL is still able to keep more than 98% of the capacity. Beyond this point, the cell average throughput decreases more visibly, at an injection level of 26 dB, the EL service can only retain approximately 90% of the throughput. Similarly, the cell edge throughput stays above 98.7% of the benchmark case for injection levels up to 10 dB. At an injection level of 19 dB, the EL is still able to

retain 97% of the cell edge throughput. Finally at injection level 26 dB, the EL provides 87.3% of the benchmark single layer edge throughput.

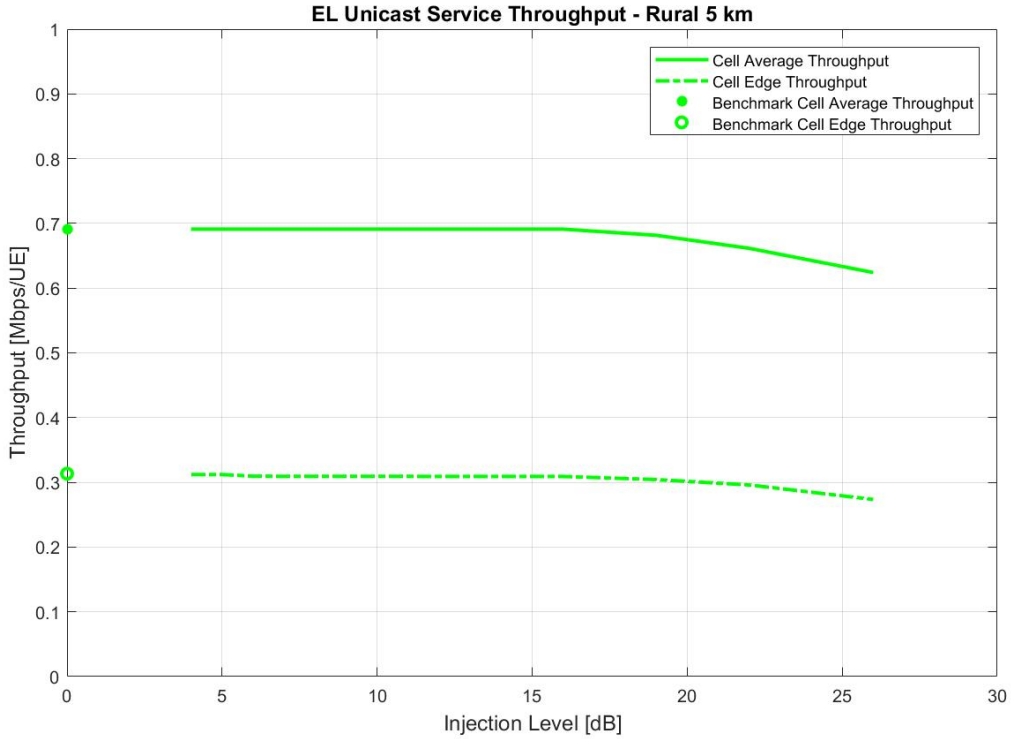

Figure 6.14: Rural 5 km ISD EL unicast service throughput.

The promising performance of the EL unicast service based on cell average and cell edge throughput can also be seen in terms of the average total cell throughput. Figure 6.15 shows the average total cell throughput as a function of injection levels for the additional opportunistic EL unicast service. The values on the y-axis is the average total cell throughput of the benchmark single layer unicast service, and the solid line shows the average total cell throughput as a function of injection levels from 4 dB to 26 dB. It can be observed that for typical injection levels within 10 dB, the EL can retain 99.8% of the total cell throughput. Injection levels of 13, 16, 19, 22, and 26 dB will reduce the total average cell throughput by 0.36%, 0.77%, 1.49%, 2.89%, and 7.01%, respectively.

These results indicate that in a rural environment with ISD of 5 km, the EL is more

than capable to provide an additional unicast service with throughput that matches a single layer unicast service for typical injection levels of up to 10 dB. In fact, the injection level can be increased to 19 dB for very similar results. If the requirement on throughput can be relaxed, approximately 90% of the single layer unicast network throughput can still be achieved with 26 dB of injection level.

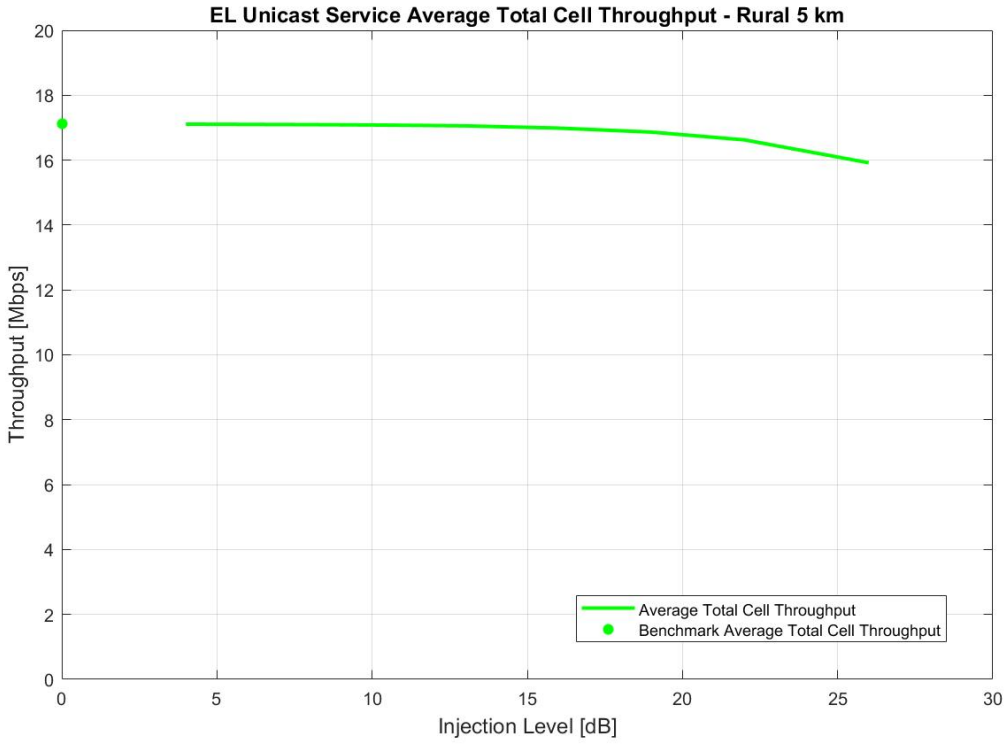

Figure 6.15: Rural 5 km ISD EL unicast service average total cell throughput.

6.2.2 Performance Analysis for 10 km ISD

Figure 6.16 shows the cell average and cell edge SINR of the opportunistic EL unicast service as a function of injection levels for a rural setting with an ISD of 10 km. It is clear from the plot that even though the ISD has increased, the cell average SINR and cell edge SINR of the EL unicast service are still comparable to a unicast network transmitted at full power. More specifically, injection levels of 4, 5, 6, 8, and 10 dB reduce the cell

average SINR by only 0.07, 0.09, 0.11, 0.17, and 0.26 dB, respectively, and the cell edge SINR degrades by 0.05, 0.06, 0.08, 0.12 and 0.19 dB, respectively. These results show that for the proposed injection level range, UEs in the network will not experience any significant signal degradation even in a rural environment where the ISD is much larger.

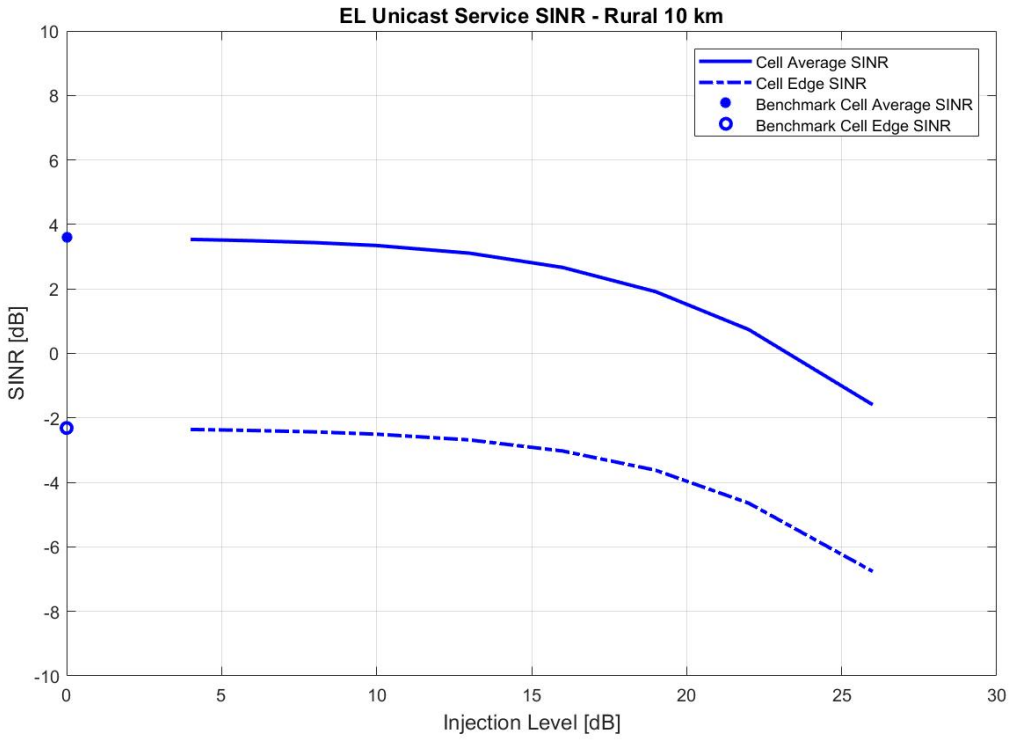

Figure 6.16: Rural 10 km ISD EL unicast service SINR.

In terms of throughput, Figure 6.17 shows the cell average throughput and cell edge throughput as a function of injection levels for the rural case with 10 km ISD. The plot shows the EL being capable of preserving more than 99% of the cell average and cell edge throughput for injection levels up to 6 dB. For injection levels of 8 and 10 dB, the EL achieves 98% and 96% of cell average throughput, and 98% of the cell edge throughput. Tolerating reduced unicast throughput rates, when the injection level is increased to 19 dB, the EL unicast service is still able to provide 82% and 77% of cell average and cell edge throughput, respectively. At an injection level of 26 dB, the EL unicast network

can provide 55% and 49% of cell average and cell edge throughputs.

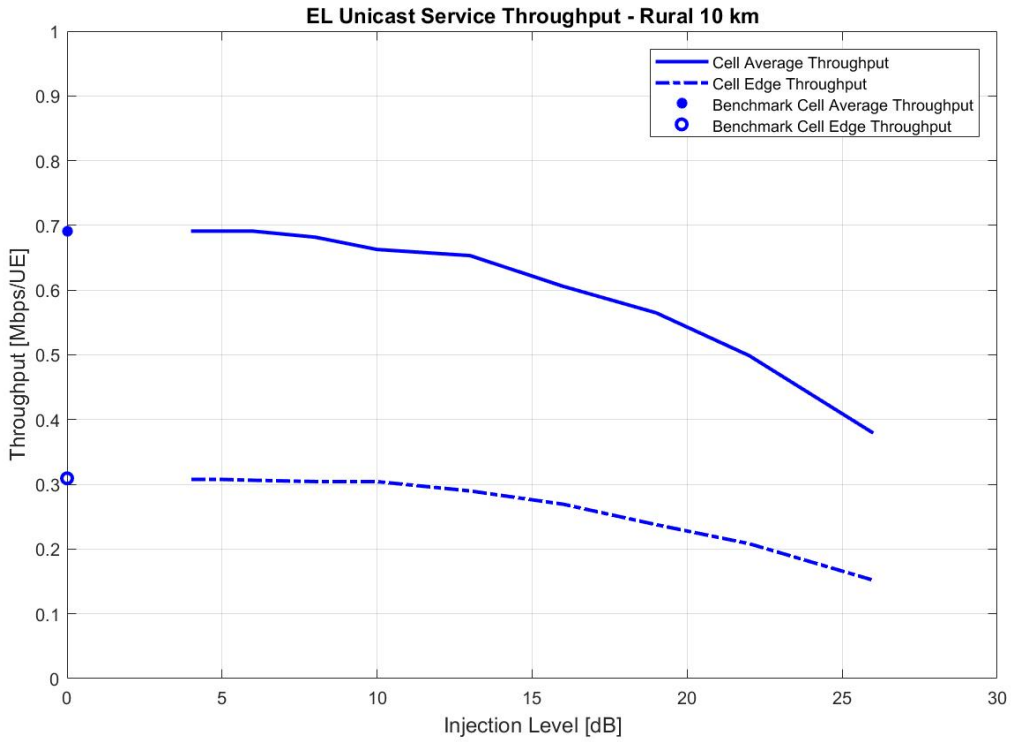

Figure 6.17: Rural 10 km ISD EL unicast service throughput.

Figure 6.18 shows the average total cell throughput as a function of injection levels for the additional opportunistic EL unicast service provided. It can be observed that for injection levels of 4, 5, 6, 8, and 10 dB, the total cell throughput only decreases by 0.7%, 0.9%, 1.2%, 1.7%, and 2.7%, respectively. Thus showing for typical injection levels, the EL is able to provide an additional unicast service with capacity that is comparable to a full network. As the injection levels continued to increase to 19 dB, the EL is still able to provide 15.5 Mbps of throughput per cell, corresponding to preserving 83% of the cell capacity. Even if the injection level is increased to 26 dB, the EL unicast network is still able to obtain a throughput 10.7 Mbps/cell, corresponding to approximately 58% of the original throughput capacity.

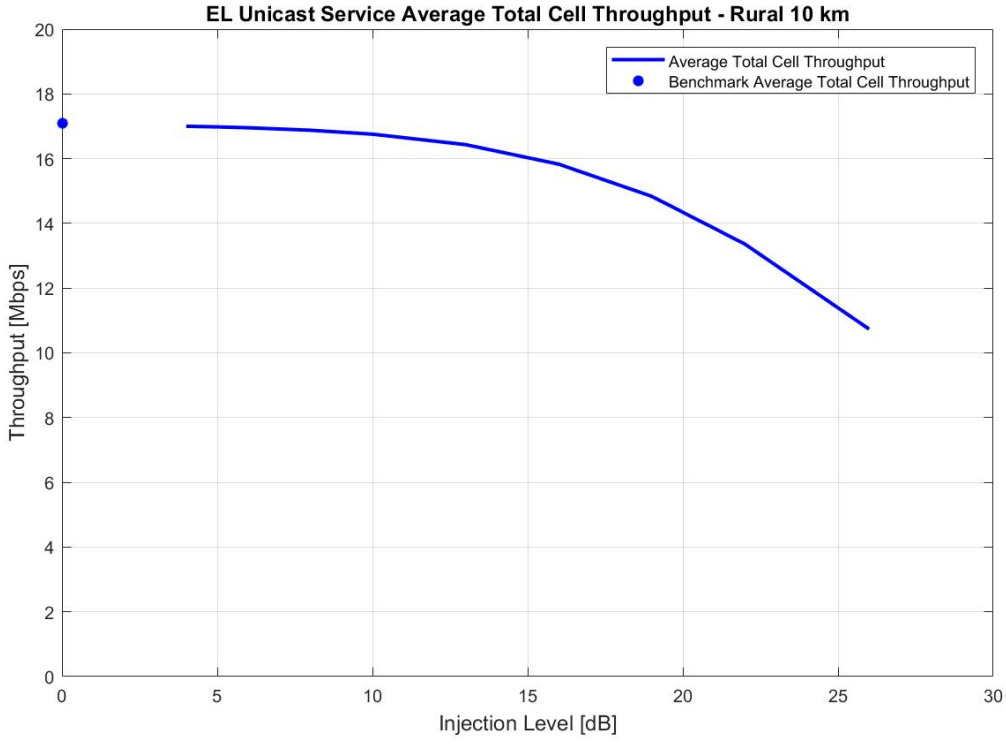

Figure 6.18: Rural 10 km ISD EL unicast service average total cell throughput.

6.2.3 Performance Analysis for 15 km ISD

Finally, the cell average SINR and cell edge SINR of the EL unicast network as a function of injection levels are plotted in Figure 6.19. In this case, the largest ISD considered for the rural case causes the EL to suffer from significant signal degradation due to the reduced transmission powers. Observations can be made that within the typical range, injection levels of 4, 5, 6, 8 and 10 dB cause the cell average SINR to decrease by 0.25, 0.32, 0.39, 0.60, and 0.91 dB, respectively, and the cell edge SINR degrades by 0.19, 0.24, 0.30, 0.46 and 0.71 dB, respectively. Although the SINR degrade more severely as the injection level continues to increase, the system is still able to provide service to all the UE in the network for injection levels up to 22 dB.

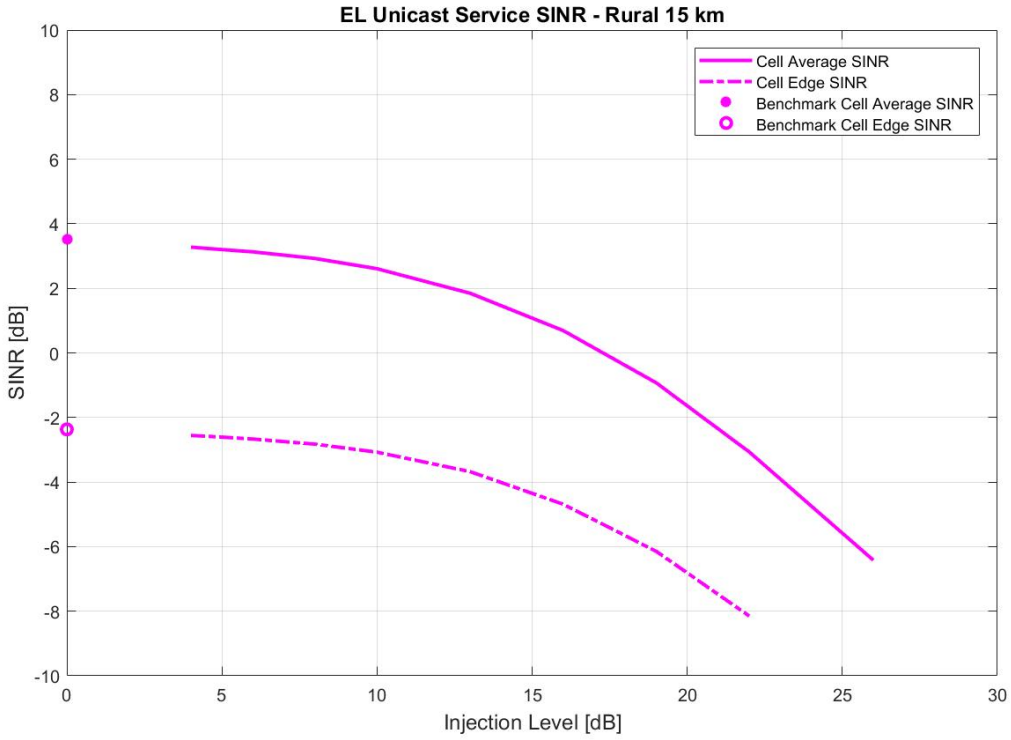

Figure 6.19: Rural 15 km ISD EL unicast service SINR.

The cell average throughput and cell edge throughput as a function of injection levels for a rural environment at 15 km ISD is shown in Figure 6.20. For selected typical injection levels of 4, 5, 6, 8, and 10 dB, the EL is capable of preserving 95.7%, 94.9%, 94.5%, 90.4%, and 86.0% of cell average throughput, respectively, and 98.0%, 95.7%, 94.3%, 92.4%, and 84.8% of cell edge throughput. If the throughput requirements can be further relaxed, when the injection level is increased to 19 dB, the EL unicast service is able to provide 60% and 56% of cell average and cell edge throughput, respectively. At the highest feasible injection level that the EL can still provide service to all the UEs, the system is able to preserve 43% and 38% of cell average and cell edge throughput.

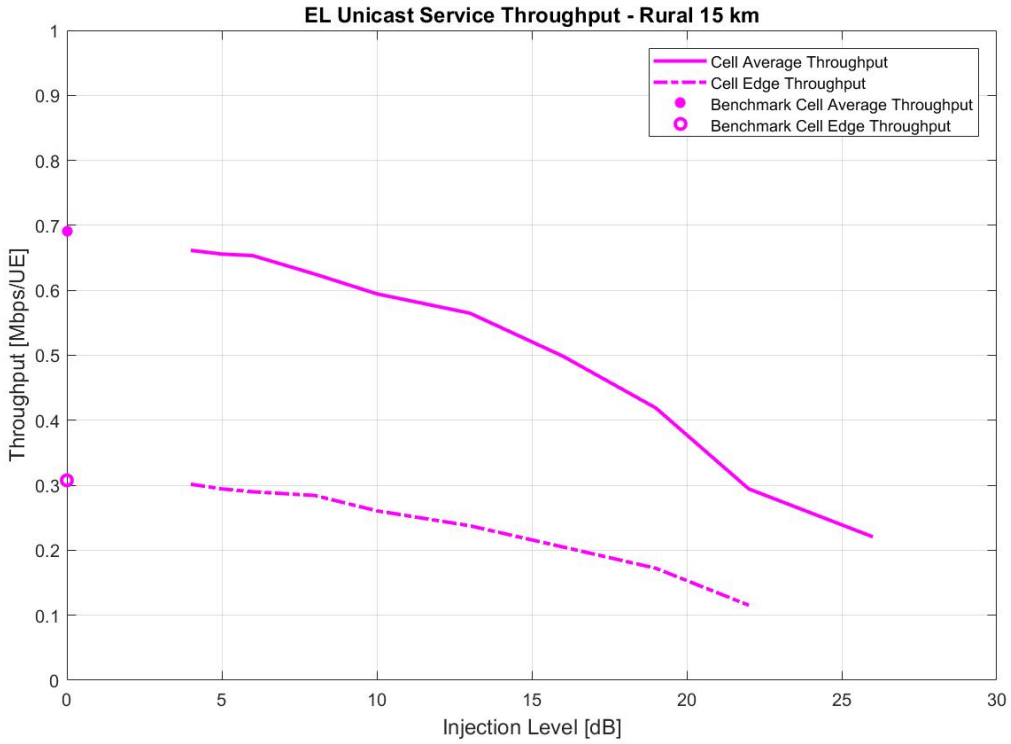

Figure 6.20: Rural 15 km ISD EL unicast service throughput.

Figure 6.21 shows the average total cell throughput as a function of injection levels of the additional opportunistic EL unicast service for the 15 km ISD rural case. It can be observed that for injection levels of 4, 5, 6, 8, and 10 dB, the total cell throughput decreases by 1.9%, 2.4%, 3.1%, 4.7%, and 7.3%, respectively. As the injection levels continued to increase to 19 dB, the EL is still able to provide 11.4 Mbps of throughput per cell, corresponding to preserving 67% of the cell capacity. At the highest feasible injection level that the EL can still provide service to all the UEs of 22 dB, the EL unicast service obtains a throughput 9.2 Mbps/cell, corresponding to approximately 54% of the original throughput capacity.

Even though the EL is not able to provide a completely full unicast service when the ISD is at its largest of 15 km, low injection levels can still allow the EL to provide more than 98% of the capacity compared to a typical single layer unicast service. Even for

injection levels of up to 10 dB, which is sufficiently high in practical system implementations, the EL is still able to offer more than 90% of service throughput capacity.

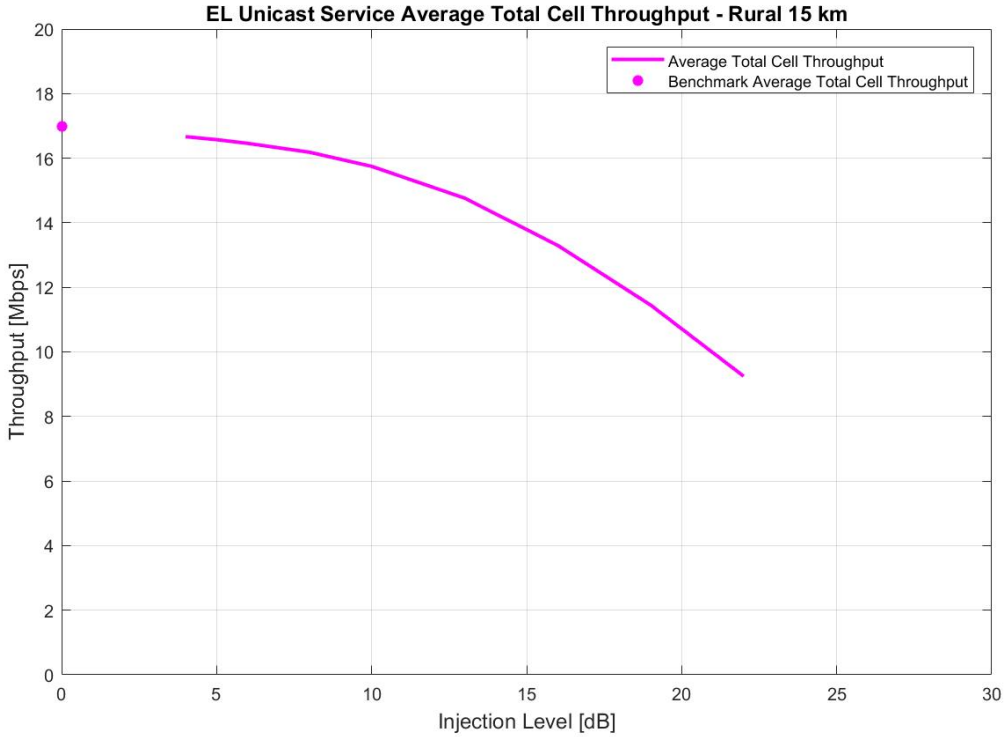

Figure 6.21: Rural 15 km ISD EL unicast service average total cell throughput.

Chapter 7

Conclusion

7.1 Summary and Conclusion

This thesis is the result of a joint project between Communication Research Center Canada and University of Toronto. The project goal is to explore the impact of LDM on the next generation broadband system. Previous research has demonstrated the capacity gain of using LDM to deliver broadcasting services with different quality requirements, however there is a lack of research into the capacity gain of using LDM for mixed broadcast-unicast service delivery. This work demonstrated the viability of having SFN broadcast and multi-cell unicast services efficiently and effectively delivered in a single RF channel using a two-layer LDM scheme. The result of this work was presented at the 2019 IEEE International Symposium on Broadband Multimedia Systems and Broadcasting, held in Jeju, Korea, and received " 2019 Best Student Paper Award" from the conference.

This thesis shows that in a broadband system, instead of splitting transmission capacity between broadcast and unicast services to provide MBMS, LDM has the capability to deliver in the core layer, a broadcast service with the same required quality of service as a dedicated broadcast network, plus in the enhanced layer, an additional opportunistic

unicast service with performance that can match a full power unicast network, essentially doubling the system performance.

Simulation results show that in an urban environment where the inter-site distance is small, the enhanced layer can provide full capacity unicast service with injection levels up to 19 dB. Even when applying more aggressive injection levels of 26 dB, acceptable unicast service could still be delivered with more than 90% of the cell throughput being preserved. For the case of larger inter-site distance of 2 km, the enhanced layer can provide near-full capacity unicast service for practical injection levels up to 10 dB. For rural deployment scenarios, the system exhibits higher tolerance to power reductions, where practical injection levels can support a near-full capacity unicast service for up to an inter-site distance of 10 km. At the inter-site distance of 15 km as required by 3GPP, only low injection levels around 4 dB can provide near-full capacity unicast service, whereas higher practical injection levels will support only approximately 90% of service throughput.

7.2 Future works

This collaborated work with CRC will be continued for the Ph.D program. Some potential research directions are: hybrid LDM-TDM structure to provide better service to UEs with unfavorable reception conditions and carrier aggregation (CA) mechanisms where the LDM 5G-MBMS is combined with a unicast-only band to accommodate the edge users. In addition, topics such as using machine learning for power allocation optimization and applications in connected vehicles are also being considered.

Bibliography

[1] Cisco public, "Cisco visual networking index: Global mobile data traffic forecast update, 2017-2022," Tech. Rep. 1486680503328360, Cisco, San Jose, CA, USA, February 2019.

[2] L. Zhang, Y. Wu, G. K. Walker, W. Li, K. Salehian, and A. Florea, "Improving LTE eMBMS with extended OFDM parameters and layered-division-multiplexing," *IEEE Transactions on Broadcasting*, vol. 63, pp. 32–47, March 2017.

[3] 3GPP Release 14: https://www.3gpp.org/release-14.

[4] J. J. Gimenez, J. L. Carcel, M. Fuentes, E. Garro, S. Elliott, D. Vargas, C. Menzel, and D. Gomez-Barquero, "5G new radio for terrestrial broadcast: A forward-looking approach for NR-MBMS," *IEEE Transactions on Broadcasting*, vol. 65, pp. 356–368, June 2019.

[5] Y. Liu, Z. Qin, M. Elkashlan, Z. Ding, A. Nallanathan, and L. Hanzo, "Nonorthogonal multiple access for 5G and beyond," *Proceedings of the IEEE*, vol. 105, pp. 2347–2381, Dec 2017.

[6] ETSI TR 138 913 v15.0.0, "5G; study on scenarios and requirements for next generation access technologies (3GPP TR 38.913 version 15.0.0 Release 15)." Sept.2018.

[7] Y. Xue, W. Li, A. Alsohaily, L. Zhang, E. Sousa, and Y. WU, "Using layered division multiplexing for mixed unicast-broadcast service delivery in 5G," in *2019*

IEEE International Symposium on Broadband Multimedia Systems and Broadcasting (BMSB), pp. 1–6, June 2019.

[8] L. Zhang, W. Li, Y. Wu, X. Wang, S. Park, H. M. Kim, J. Lee, P. Angueira, and J. Montalban, "Layered-division-multiplexing: Theory and practice," *IEEE Transactions on Broadcasting*, vol. 62, pp. 216–232, March 2016.

[9] L. Zhang, Y. Wu, W. Li, S. Park, J. Lee, N. Hur, and H. M. Kim, "Using layered-division-multiplexing to achieve enhanced spectral efficiency in 5G-MBMS," in *2019 IEEE International Symposium on Broadband Multimedia Systems and Broadcasting (BMSB)*, pp. 1–7, June 2019.

[10] Y. Wu, B. Rong, K. Salehian, and G. Gagnon, "Cloud transmission: A new spectrum-reuse friendly digital terrestrial broadcasting transmission system," *IEEE Transactions on Broadcasting*, vol. 58, pp. 329–337, Sep. 2012.

[11] J. Montalbn, L. Zhang, U. Gil, Y. Wu, I. Angulo, K. Salehian, S. Park, B. Rong, W. Li, H. M. Kim, P. Angueira, and M. Vlez, "Cloud transmission: System performance and application scenarios," *IEEE Transactions on Broadcasting*, vol. 60, pp. 170–184, June 2014.

[12] P. Bergmans and T. Cover, "Cooperative broadcasting," *IEEE Transactions on Information Theory*, vol. 20, pp. 317–324, May 1974.

[13] S. I. Park, J. Lee, S. Myoung, L. Zhang, Y. Wu, J. Montalbn, S. Kwon, B. Lim, P. Angueira, H. M. Kim, N. Hur, and J. Kim, "Low complexity layered division multiplexing for ATSC 3.0," *IEEE Transactions on Broadcasting*, vol. 62, pp. 233–243, March 2016.

[14] I. Eizmendi, M. Velez, D. Gmez-Barquero, J. Morgade, V. Baena-Lecuyer, M. Slimani, and J. Zoellner, "DVB-T2: The second generation of terrestrial digital video

broadcasting system," *IEEE Transactions on Broadcasting*, vol. 60, pp. 258–271, June 2014.

[15] D. Gmez-Barquero, C. Douillard, P. Moss, and V. Mignone, "DVB-NGH: The next generation of digital broadcast services to handheld devices," *IEEE Transactions on Broadcasting*, vol. 60, pp. 246–257, June 2014.

[16] L. Fay, L. Michael, D. Gmez-Barquero, N. Ammar, and M. W. Caldwell, "An overview of the ATSC 3.0 physical layer specification," *IEEE Transactions on Broadcasting*, vol. 62, pp. 159–171, March 2016.

[17] N. S. Loghin, J. Zllner, B. Mouhouche, D. Ansorregui, J. Kim, and S. Park, "Non-uniform constellations for ATSC 3.0," *IEEE Transactions on Broadcasting*, vol. 62, pp. 197–203, March 2016.

[18] K.-J. Kim, S. Myung, S. Park, J.-y. Lee, M. Kan, Y. Shinohara, J.-W. Shin, and J. Kim, "Low-density parity-check codes for ATSC 3.0," *IEEE Transactions on Broadcasting*, vol. 62, pp. 1–8, 02 2016.

[19] ATSC Digital Television Standard, ATSC Standard A/53 Parts 1-6, Jan. 2007.

[20] D. Gmez-Barquero, D. Vargas, M. Fuentes, P. Klenner, S. Moon, J. Choi, D. Schneider, and K. Murayama, "MIMO for ATSC 3.0," *IEEE Transactions on Broadcasting*, vol. 62, pp. 298–305, March 2016.

[21] D. Vargas, D. Gozalvez, D. Gomez-Barquero, and N. Cardona, "MIMO for DVB-NGH, the next generation mobile TV broadcasting [accepted from open call]," *IEEE Communications Magazine*, vol. 51, pp. 130–137, July 2013.

[22] D. He, L. Ding, Y. Guan, F. Yang, W. Zhang, and Y. Wu, "Dedicated return channel for ATSC 3.0," *IEEE Transactions on Broadcasting*, vol. 62, pp. 352–360, March 2016.

[23] W. Zhang, Y. Wu, N. Hur, T. Ikeda, and P. Xia, "FOBTV: Worldwide efforts in developing next-generation broadcasting system," *IEEE Transactions on Broadcasting*, vol. 60, pp. 154–159, June 2014.

[24] C. Mehlfuehrer, J. Colom Ikuno, M. imko, S. Schwarz, M. Wrulich, and M. Rupp, "The vienna LTE simulators-enabling reproducibility in wireless communications research," *EURASIP Journal on Advances in Signal Processing*, vol. 2011, p. 114, 01 2011.

[25] N. Baldo, M. Miozzo, M. Requena-Esteso, and J. Nin-Guerrero, "An open source product-oriented LTE network simulator based on ns-3," pp. 293–298, 10 2011.

[26] Lei Wan, Shiauhe Tsai, and M. Almgren, "A fading-insensitive performance metric for a unified link quality model," in *IEEE Wireless Communications and Networking Conference, 2006. WCNC 2006.*, vol. 4, pp. 2110–2114, April 2006.

[27] "ns-3 introduction." `https://www.nsnam.org/docs/tutorial/html/introduction.html`.

[28] "ns-3 conceptual overview." `https://www.nsnam.org/docs/tutorial/html/conceptual-overview.html`.

[29] G. Piro, N. Baldo, and M. Miozzo, "An LTE module for the ns-3 network simulator," *Proceedings of the 4th International ICST Conference on Simulation Tools and Techniques*, 01 2011.

[30] TR36.814. (2010), "3GPP evolved universal terrestrial radio access (e-utra); further advancements for e-utra physical layer aspects. rel-9 v9.0.0.." [online]. Available `http://www.3gpp.org/ftp/Specs/html-info/36814.htm`.

[31] TR25.814. (2006), "3GPP physical layer aspects for evolved universal terrestrial radio access (utra). rel-7 v7.1.0.." [online]. Available http://www.3gpp.org/ftp/Specs/html-info/25814.htm.

[32] A. Marinescu, I. Macaluso, and L. Dasilva, "System level evaluation and validation of the ns-3 LTE module in 3GPP reference scenarios," pp. 59–64, 11 2017.

[33] T. Abreu, B. Baynat, M. Gachouaoui, T. Jimnez, and N. Nya, "Comparative study of LTE simulations with the ns-3 and the vienna simulators," 08 2015.